CHARACTERIZATING THE EFFECTS OF EXPERIMENTAL GLAUCOMA AND AGE ON RETINAL GANGLION CELL FUNCTION

by

Delaney Catherine Marie Henderson

Submitted in partial fulfilment of the requirements
for the degree of Doctor of Philosophy

at

Dalhousie University
Halifax, Nova Scotia
August 2023

DEDICATION

This thesis is dedicated to my family.
With you, anything is possible.

TABLE OF CONTENTS

LIST OF FIGURES

ABSTRACT

Glaucoma is an optic neuropathy characterized by the progressive loss of retinal ganglion cells (RGCs). Clinical monitoring of disease progression uses gross structural changes as surrogate measures of RGC loss. Previous studies indicate structural imaging relates poorly to RGC axonal counts, due to inter-individual variability, and non-neuronal tissue remodelling that occurs during glaucoma. Moreover, clinical imaging does not provide information on the functional status of individual cells. Therefore, there is a need for tools to monitor longitudinal structural and functional changes to individual RGCs. In this study, we delivered the functional marker, GCaMP, using an intravitreal injection of AAV2-CAG-GCaMP6s viral vector to evaluate RGC structure and function. GCaMP labelling, monitored with *in vivo* imaging, increased weekly over 5-weeks, and plateaued by 8-weeks. Results showed GCaMP labelling persists for over 18-months following a single viral injection. Intact-isolated calcium imaging demonstrated robust GCaMP functional responses to chemical stimulation in adult (3-6 months) and aged mice (21-24 months). When compared to adult mice, aged mice showed more profound decreases in functional responses. Immunohistochemistry confirmed that the AAV2-CAG-GCaMP6s viral vector primarily transduces RGCs in the ganglion cell layer, and does not negatively impact RGCs when compared to non-injected control mice. Although intraocular pressure and age are the most significant risk factors for glaucoma development and progression, most experimental glaucoma (EG) research is performed in adult mice. Therefore, for our study, EG was induced in both adult and aged mice. Functional responses and RGC densities were decreased compared to controls following 4-, and 8-weeks of EG in adult mice, and to a significantly greater extent in aged mice. Interestingly, functional decline preceded structural loss in both adult and aged EG. Overall, our findings demonstrate that exogenous functional markers can be used to assess structural and functional changes over time and that age is a vital determinant of loss of RGC function.

LIST OF ABBREVIATIONS AND SYMBOLS USED

2P	2-Photon
AAV	Adeno-Associated Virus
AAV2	Adeno-Associated Virus Serotype 2
BDNF	Brain-Derived Neurotrophic Factor
Brn3a	Brain-Specific Homeobox/POU Domain Protein 3a
Ca^{2+}	Calcium
CAG	Cytomegalovirus Early Enhancer/Chicken β Actin Promoter
CFP	Cyan Fluorescent Protein
ChAT	Choline Acetyltransferase
CNS	Central Nervous System
CSLO	Confocal Scanning Laser Ophthalmoscopy
DCX	Doublecortin Promotor
EG	Experimental Glaucoma
ERG	Electroretinogram
F_0	Baseline Fluorescence
FG	Fluorogold
GABA	Gamma-Aminobutyric Acid
GCC	Ganglion Cell Complex
GCL	Ganglion Cell Layer
GECI	Genetically Encoded Calcium Indicator
GFAP	Glial Fibrillary Acidic Protein
GFP	Green Fluorescent Protein
HBSS	Hanks Balanced Salt Solution
IHC	Immunohistochemistry
ILM	Inner Limiting Membrane
iNOS	Inducible Nitric Oxide Synthase
IOP	Intraocular Pressure
IPL	Inner Plexiform Layer
IR	Infrared

KA	Kainic Acid
LC	Lamina Cribrosa
NHP	Non-Human Primate
NMDARs	N-Methyl-D-Aspartate Receptors
nSTR	Negative Scotopic Threshold Response
OCT	Optical Coherence Tomography
OH	Ocular Hypertension
ON	Optic Nerve
ONC	Optic Nerve Crush
ONH	Optic Nerve Head
ONT	Optic Nerve Transection
PACG	Primary Angle-Closure Glaucoma
POAG	Primary Open-Angle Glaucoma
PBS	Phosphate Buffered Saline
PFA	Paraformaldehyde
PhNR	Photopic Negative Response
pSTR	Positive Scotopic Threshold Response
RBPMS	RNA-Binding Protein with Multiple Splicing
RGC	Retinal Ganglion Cell
RNFL	Retinal Nerve Fiber Layer
ROI	Region of Interest
ROS	Reactive Oxygen Species
SA β-gal	Senescence-Associated β-Galactosidase
SASP	Senescence-Associated Secretory Phenotype
SC	Superior Colliculus
Thy1	Thymocyte Differentiation Antigen 1
TLR4	Toll-Like Receptor 4
TM	Trabecular Meshwork
YFP	Yellow Fluorescent Protein

ACKNOWLEDGMENTS

Without the mentorship, guidance, and friendship of many people, the work accomplished in this thesis would not have been possible.

First and foremost, I would like to thank my supervisor Dr. Balwantray Chauhan. Thank you for your support, encouragement, and the opportunity to be a part of your lab over the past 8 years. It has been a privilege to work with you and learn from you.

To my committee members Dr. William Baldridge, and Dr. Brennan Eadie, thank you for your time, expertise, and mentorship. Your questions, suggestions, and guidance have helped me become a better researcher.

To Michele Hooper, thank you for your expertise and technical advice, but even more so for your friendship. You have helped me more than you know, and I am so grateful for everything you have done for me.

To Dr. Spring Farrell, thank you for your mentorship, never-ending amazing advice, friendship, and feedback on drafts of this thesis. I would not have made it this far without you, and I am forever grateful for you.

Thank you to my friends and colleagues in the Retina and Optic Nerve Laboratory, both past and present, especially Dr. Tareq Yousef, Aliénor Jamet, Ryan Matthews, Dr. Johnny Di Pierdomenico, and in the Department of Medical Neuroscience. I consider myself lucky to have been surrounded by such wonderful scientists.

Finally, to my parents, Lana and Dave, and to my partner, Jack. A thank you just doesn't seem like enough for everything you have done for me. You are my people. Your unwavering love and support give me strength to do things that seem impossible. Thank you for reminding me to take things one step at a time. Without you none of this would have been possible.

CHAPTER 1. INTRODUCTION

1.1. The Retina and Optic Nerve

The transmission of visual signal and processing begins in the eye (Figure 1.1). Photons of light enter the eye and are converged onto the retina by the refractive power of the cornea and crystalline lens. The retina is a thin, laminated tissue composed of three nuclear layers, and two plexiform layers (Figure 1.2).

Photons are first captured by rod and cone outer segments embedded within the retinal pigment epithelium, where phototransduction occurs. Rod and cone photoreceptors contain specialized photopigments, rhodopsin and cone opsins, respectively, that initiate phototransduction cascades in response to specific wavelengths of light within the visible spectrum. Rods are highly sensitive to light and operate in scotopic or dim light conditions. In contrast, cones are active in photopic or bright light conditions contributing to daytime vision, and are also responsible for colour vision. Generally, the initiation of phototransduction within the photoreceptors causes changes in membrane potentials and the release of glutamate, one of the main neurotransmitters in the retina, onto bipolar cells, beginning the vertical visual pathway (Kolb et al., 2001; Masland, 2001).

There are two main classes of bipolar cells, ON bipolar cells and OFF bipolar cells, which depolarize and hyperpolarize in response to light, respectively. Bipolar cells synapse with retinal ganglion cells (RGCs) within the inner plexiform layer (IPL). RGC somata reside in the ganglion cell layer (GCL), the innermost neuronal layer, and their

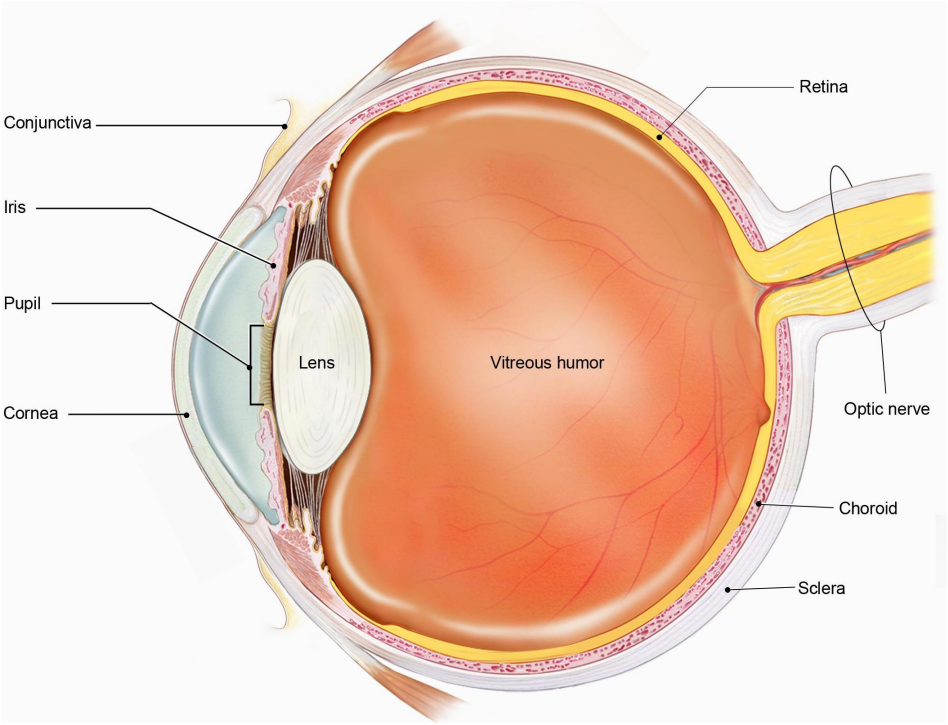

Figure 1.1. Anatomical structure of the human eye. Schematic of a cross section of the human eye showing major anatomical structures and landmarks. Figure was adapted with permission from the National Eye Institute Media Library.

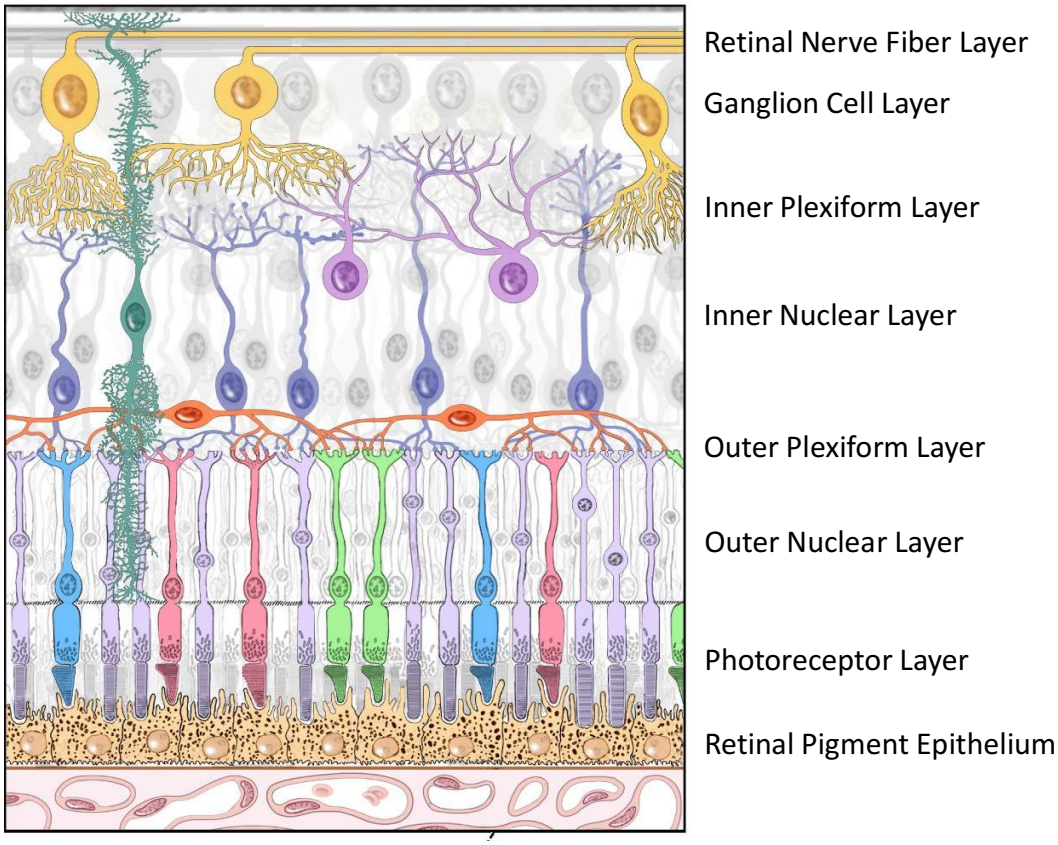

Figure 1.2. Retinal anatomy. Schematic of a cross section of the mammalian retina showing neuronal layers and their synaptic connections. Figure was adapted with permission from the National Eye Institute Media Library.

dendrites extend into various sublamina of the IPL. The sublamina in which the RGCs extend gives rise to different ON, OFF, or ON/OFF directionally sensitive RGCs, each with morphological and physiological differences. OFF RGCs synapse with bipolar cells in sublamina a of the IPL, ON RGCs in sublamina b, and ON-OFF RGCs are bistratified in both sublamina (Amthor et al., 1984; Kolb et al., 2001). Additionally, input from horizontal and amacrine cells modify and fine tune visual information primarily through lateral inhibition by releasing the inhibitory neurotransmitter, GABA. Visual information is sent along RGC axons to various brain regions for further processing (Sanes & Zipursky, 2010).

The region where RGC axons exit the eye and begin forming the optic nerve (ON) is called the optic nerve head (ONH). In humans, the ONH is approximately 1.5 mm in diameter but can have up to sevenfold variation in diameter among individuals (Weinreb & Tee Khaw, 2004). The ONH is considered as being comprised of 4 major regions, from anterior to posterior: the retinal nerve fiber layer (RNFL), the prelaminar region, the lamina cribrosa (LC), and the post-laminar or retrobulbar ON (Levin & Kaufman, 2011). Axons within the peripapillary RNFL form bundles and follow a distinct pattern as they travel towards the ONH, with axons of RGCs within the peripheral retina residing more peripherally within the ON (Levin & Kaufman, 2011).

The LC is composed of a series of fenestrated, collagenous, connective tissue sheets derived from the sclera, that extend the diameter of the ONH (Anderson, 1969). The connective tissue plates are lined with astrocytes and microglia, and the fenestrations are aligned sequentially to allow passing of unmyelinated axon bundles

through the LC. Axon bundles become myelinated in the retrobulbar nerve and are separated further by septa, or widely spaced collagen and pia mater fibers (Morrison, 2006).

There are anatomical differences in the structure of the LC among animal species that have a bearing on models of glaucoma. For example, mice do not have a structural LC, but a highly dense region of glial cells which provide structural support, creating a structure that has been referred to as a *glial lamina* (Howell et al., 2007). The LC in rats is strain dependent, with certain rats such as the Brown Norway (Morrison et al., 1995) and Long Evans rats (Hildebrand et al., 1985) having a LC composed of connective tissues and glial cells, whereas the Wistar rat (May, 2003) has sparse LC structure (Chen et al., 2017; May, 2008). In contrast, non-human primates (NHPs), and humans have a LC that is composed of multilayered connective tissue, with laminar support beams through which the RGC axon bundles and capillaries pass (Morrison, 2006).

1.2. Glaucoma

1.2.1. Clinical Glaucoma

Glaucoma is one of the leading causes of irreversible blindness worldwide (Tham et al., 2014). It is a family of optic neuropathies characterized by the progressive loss of RGCs and damage to the inner retina and ON structures. The two main types of glaucoma are primary angle-closure glaucoma (PACG), and primary open-angle glaucoma (POAG), and are primarily differentiated by the anatomy of the iridocorneal angle, the angle formed by the anterior iris and posterior corneal surfaces. It is

estimated that over 75 million people are affected by glaucoma, not including individuals being followed as glaucoma suspects or those with manifest undiagnosed glaucoma.

PACG is characterized by an anatomically closed iridocorneal angle, resulting in poor aqueous humour drainage from the anterior chamber (Weinreb et al., 2014). As aqueous humour accumulates, the intraocular pressure (IOP) increases and can result in glaucomatous damage to RGCs and their axons. PACG is typically caused by disorders of the lens, iris, or pupillary block, where there is a functional blockage of aqueous flow caused by the close proximity of the posterior surface of the iris to the anterior lens surface, increasing IOP. Moreover, patients with PACG are at risk for acute angle-closure attacks, where there is a rapid and significant increase in IOP leading to an ocular emergency. Individuals of Asian descent are at greater risk for the development of PACG, primarily due to anatomical differences, such as shallower iridocorneal angle and shorter axial length (Lavanya et al., 2008; Nongpiur et al., 2011; Sakai et al., 2005; Tham et al., 2014). PACG is typically diagnosed by gonioscopy, and treated using laser iridotomy, a procedure where a hole is created in the iris to facilitate aqueous outflow, and IOP lowering topical medications.

POAG is the most common form of glaucoma (Quigley & Broman, 2006; Tham et al., 2014). In contrast to PACG, POAG is characterized by an increased resistance of aqueous humour outflow through the trabecular meshwork (TM), despite a structurally unobstructed iridocorneal angle. POAG is characterized by loss of RGCs, resulting in changes to ONH structure such as thinning of the neuroretinal rim (indicative of RGC

axonal loss), posterior displacement and structural changes at the level of the LC, an excavated appearance of the optic disc, and thinning of the RNFL. There are numerous identified risk factors associated with POAG development and progression, including IOP, age, race, myopia and family history. To date, IOP remains the only modifiable risk factor.

Although IOP reduction slows disease progression (Gaasterland et al., 2000; Heijl et al., 2002; Kass et al., 2002; Lichter et al., 2001) the relationship between IOP and glaucoma remains very complex. For example, while some patients with elevated IOP, or ocular hypertension (OH), develop glaucoma, there are patients with OH that never clinically manifest glaucomatous pathology, even over long follow-up periods (Weinreb & Tee Khaw, 2004). Moreover, about 30% of patients with glaucoma have statistically normal pressures, and experience progressive, characteristic loss of their visual field, thinning of their RNFL and peripapillary neuroretinal rim, or changes in optic disc morphology. Interestingly, like in patients with higher IOP, lowering IOP in glaucoma patients with statistically normal IOP also reduces the rate of glaucomatous progression (Anderson et al., 1998) indicating that irrespective of the degree of elevation, IOP is an important factor.

In addition to IOP, age is another important risk factor in glaucoma pathogenesis. POAG disease prevalence increases with age, from approximately 2% in those aged 40 years and above, increasing to over 10% in those aged 75 and above (Allison et al., 2020; Klein & Klein, 2013; Tham et al., 2014). Each decade adds additional risk of both disease development and risk of progression (Coleman et al., 2004; Coleman & Miglior, 2008).

Due to the complex multifactorial nature of glaucoma, researchers have been exploring underlying mechanisms of the disease.

1.2.2. Mechanisms of RGC Death in Glaucoma

There are several cellular stressors and molecular pathways that may contribute to RGC death in glaucoma. These include biomechanical stress, neurotrophic deprivation, dysfunctional glial responses and inflammation, excitotoxicity, and mitochondrial dysfunction. It is probable that a combination of these insults, working in tandem, contributes to RGC apoptosis.

IOP-related force is thought to contribute to glaucomatous pathophysiology by direct biomechanical stress to RGC axons in the retina and ONH (Burgoyne, 2011). It is hypothesized that the load-bearing connective tissues, neural tissues (RGCs and their axons), and support cells in the ONH, such as astrocytes, glial cells, and endothelial cells, are influenced by biomechanical pressures, resulting in physical deformation and biochemical cascades that contribute to RGC death (Burgoyne, 2011; Quigley et al., 1980). IOP-induced compression on RGC axons and connective tissues within the LC can result in decreased blood supply and axoplasmic flow of nutrients along the RGC axons causing further insult through growth factor deprivation (Causin et al., 2014; Li & Song, 2020). Alterations in axonal transport and disruption within the LC have been noted in NHP (Bellezza et al., 2003; Burgoyne et al., 2004), and rodent (Cepurna et al., 2005; Danias et al., 2003; Jakobs et al., 2005; Schlamp et al., 2006)experimental glaucoma (EG).

Transport of nutrients and trophic factors along RGC axons from the brain is critical for the normal functioning and survival of RGCs. Neurotrophic deprivation of critical molecules and proteins from the brain to RGCs due to axonal damage or elevated IOP can lead to RGC death. In EG, elevated IOP impairs or blocks axonal transport of Brain-Derived Neurotropic Factor (BDNF), leading to neurotrophic deprivation at the level of the RGC somas (Pease et al., 2000; Quigley et al., 2000). Delivering exogenous BDNF is neuroprotective in models of ON damage (Chen & Weber, 2001), however, its effects are transient because of downregulation of the BDNF receptor, TrkB (Di Polo et al., 1998). For this reason, gene therapy approaches where BDNF is delivered exogenously in combination with the TrkB receptor, provides a more sustained neuroprotective effect (Osborne, Khatib, et al., 2018; Osborne, Wang, et al., 2018).

Alongside retinal neurons, both macroglia, and microglia provide support and regulate retinal homeostasis. Macroglial cells, namely Müller cells and astrocytes, maintain retinal homeostasis by regulating ion exchange, glucose and neurotransmitter transport (Bringmann et al., 2006). Microglia play important roles in responses to retinal injury and have a key function in mediating neuroinflammation (Seitz et al., 2013). Immediately following injury, glial cells may be neuroprotective, producing antioxidants and trophic factors (Di Polo et al., 1998). In later stages of disease and injury, they enter a phase of reactive gliosis and release harmful factors such as TNF-α, NFκB, and nitric oxide which can lead to RGC apoptosis through caspase activation (Tezel & Wax, 2000). Increased glial fibrillary acidic protein (GFAP) expression, a marker for increased

astrocyte activity and gliosis, has been observed in glaucomatous retinas (Tezel et al., 2003). Additionally, elevated levels of TNF-α and receptor, TNF-R1, were found in both the retina and surrounding the ONH of glaucomatous donor eyes (Tezel et al., 2001; Yuan & Neufeld, 2000), and in culture (Tezel & Wax, 2000; Tezel & Yang, 2004). Microglia also enter a reactive state in EG, where they secrete pro-inflammatory cytokines like TNF-α, inducible nitric oxide synthase (iNOS; which leads to increased production of nitric oxide and reactive oxygen species), and interleukin-1 (Hanisch, 2002; Taylor et al., 2005). These molecules can be neurotoxic and lead to damage to RGCs and their axons (Almasieh et al., 2012; Johnson et al., 2011; Yuan & Neufeld, 2000).

There is evolving evidence of the contributions of microglia in RGC degeneration through toll-like receptor 4 (TLR4) and P2X7 mediated responses (Dong et al., 2017; Takano et al., 2012; Ishikawa et al., 2023). TLR4 is found on microglial membranes and when activated can mediate immune responses. A stressed or damaged neuron can secrete intracellular substances known as damage associated molecular patterns (DAMPs), that can bind to TLR4. TLR4 activation leads to downstream NF-kB signalling and subsequent activation of the NLRP3 inflammasome within the cytoplasm. The NLRP3 inflammasome has critical roles in cytokine release, propagation of inflammatory cascades, and can activate caspases, leading to RGC damage (Yerramothu et al., 2018). Additionally, P2X7 receptors on microglial membranes can directly bind ATP that has been released into the extracellular space by damaged neurons in response to IOP-induced mechanical strain (Li et al., 2011; Lu et al., 2015; Rodrigues-Neves et al., 2018).

ATP binding promotes increases in K^+ efflux, increased ROS, and activation of the NLRP3 inflammasome, in addition to rapid changes in microglial morphology (Campagno et al., 2021). Increased levels of ATP have been found in the anterior chambers of patients with PACG when compared to controls, and ATP levels appear to increase in an IOP-dependent manner (Li et al., 2011). Interestingly, P2X7 receptors antagonists may preserve RGC function as shown in murine experimental glaucoma (Romano et al., 2020), and have been shown to decrease effects of NMDA-induced injury in rats (Sakamoto et al., 2015).

Glutamate is the primary excitatory neurotransmitter in the retina, and its transmission between neurons plays a critical role in signal transduction (Lukasiewicz, 2005). Glutamate re-uptake and clearance is achieved in part by retinal glial cells. It is possible that in addition to playing a role in inflammation, glial dysfunction can contribute to glutamate excitotoxicity. Excess glutamate binds to ionotropic glutamate receptors, namely N-Methyl-D-Aspartate receptors (NMDARs) and triggers a large influx of calcium (Ca^{2+}) into the cell. Moreover, inhibitors of NDMARs have been shown to be neuroprotective in models of EG (Almasieh et al., 2012a; Dong et al., 2008; Hare et al., 2001). Increased intracellular Ca^{2+} can trigger pro-apoptotic signalling pathways in neurons and may underlie some pathological mechanisms in glaucoma (Seki & Lipton, 2008). Elevated levels of calcineurin and calpains, Ca^{2+}-dependent phosphatases and proteases, respectively, can act downstream by cleaving and activating caspase 3, and apoptotic cell death pathways, and have been observed in models of EG (Huang et al., 2005; Huang et al., 2010).

The retina is highly susceptible to oxidative damage through its constant exposure to light and production of free radicals and reactive oxygen species (ROS). ROS are produced as a bioproduct of cellular metabolism and ATP production through the electron transport chain. ROS can also be produced during other cellular processes such as enzymatic degradation of proteins and neurotransmitters, and reduction/oxidation reactions (Halliwell, 2006). Under normal conditions, antioxidants neutralize and remove ROS, and cells maintain an equilibrium between levels of ROS and antioxidants. Accumulation of ROS can lead to mitochondrial dysfunction and association with neurodegenerative diseases (Almasieh et al., 2012) through metabolic deficiency and abnormal protein folding (Andersen, 2004). There is evidence that oxidative damage occurs in the TM in both models of EG and in patients with POAG (Babizhayev & Bunin, 1989; Izzotti et al., 2003; Ko et al., 2005; Tezel et al., 2005).

In summary, there are numerous theories on the pathophysiology of RGC death and degeneration in glaucoma, with critical research that has elucidated purported mechanisms and pathways (for detailed review see: Almasieh et al., 2012; Kuehn et al., 2005; Nickells, 2012). It is likely that the mechanism of RGC loss is multifactorial, with different pathways activated at various stages in glaucoma progression. Additionally, there is likely a large degree of inter-individual variability in the susceptibility of RGCs to these pathways. For example, one individual may experience increased inflammation, or oxidative stress compared to another individual depending on their genetic predisposition, or environmental factors. These considerations are highly important

when developing treatments for glaucoma, or when attempting to model glaucoma in experimental animals.

1.3. Experimental Models of Retinal Ganglion Cell Degeneration and Glaucoma

Modelling glaucoma has been conducted in a variety of animal species, including rodents (mice and rats), cats, dogs, rabbits, pigs, and NHPs (Bouhenni et al., 2012). Although glaucoma models in NHPs most closely relate to human disease, this research is uncommon because of the requirements for specialized staff and facilities, cost, and ethical issues. Rodents, specifically mice, remain the most utilized for EG research because they are readily available, less expensive and can be group-housed, all contributing to their cost-effectiveness. The broad knowledge on cell biology of rodent neurons and wide availability of reagents makes these approaches attractive. Finally, the ability to create transgenic mice to address the gamut of mechanistic, diagnostic, and therapeutic questions has significantly advanced the field.

Developing a model of EG that accurately mimics human disease has been a challenge for researchers. There are many methods, both acute and chronic, that have been used to induce RGC death which will be elaborated upon in this section. Some methods include direct injury to the ON which causes rapid RGC death, while others involve either mechanical damage to anterior chamber structures or utilize an intracameral injection of different agents into the anterior chamber to inhibit aqueous humour outflow.

1.3.1. Models of Acute Retinal Ganglion Cell Degeneration

Over the past decades, several methods have been used to induce rapid RGC degeneration and death (Almasieh & Levin, 2017). Most involve direct damage to the ON, either by crushing (optic nerve crush; ONC) the nerve with specialized forceps, or completely transecting (optic nerve transection; ONT) the nerve. Both models produce rapid RGC death with a high degree of reproducibility (Galindo-Romero et al., 2011; Sánchez-Migallón et al., 2018; Vidal-Sanz et al., 2017). In these models, the visual axis remains clear so non-invasive *in vivo* longitudinal imaging can be performed to track loss of RGC structure and function as well as changes to overall retinal structure with techniques such as optical coherence tomography (OCT; Chauhan et al., 2012; Henderson et al., 2021; Leung et al., 2011). Although these models permit high quality imaging, the main limitation is the rapid and almost complete loss of RGCs which does not mimic glaucomatous damage in humans.

1.3.2. Genetic Models of Experimental Glaucoma

The most characterized and utilized genetic model of glaucoma is the DBA/2J transgenic mouse (Chang et al., 1999; John et al., 1997, 1998). The DBA/2J transgenic mouse exhibits a progressive, age-related increase in IOP that results in RGC loss (Schuettauf et al., 2002, 2004), in addition to ON and retinal degeneration (Schlamp et al., 2006). The RGC loss occurs in a characteristic manner, beginning in the peripapillary retina before progressive degeneration towards the peripheral retina (Jakobs et al., 2005; Schlamp et al., 2006).

Although the DBA/2J mouse is highly convenient as no interventional procedure is required, there are several important limitations. These mice invariably develop anterior segment abnormalities, atrophy of the iris, and peripheral anterior synechiae which are not characteristic of POAG. Furthermore, these anterior segment changes make it challenging to conduct procedures that monitor disease progression. For example, opacities that result from anterior segment pathology make it challenging, if not impossible, to obtain *in vivo* longitudinal images with confocal scanning laser ophthalmoscopy (CSLO) and OCT (Turner et al., 2017). Finally, there is evidence that a sub-strain of the DBA mouse does not have IOP elevation and shows RGC loss, suggesting that IOP elevation is not the cause of RGC loss and that significant confounding factors may be at play (Scholz et al., 2008).

1.3.3. Models of Experimental Glaucoma Induced by Damage to Aqueous Outflow Pathways

There are several models of EG which aim to increase IOP by directly damaging the aqueous outflow pathways. In mammals, the majority of aqueous exits the eye through the *conventional pathway*. Aqueous humour, produced in the ciliary body, moves from the posterior chamber and circulates in the anterior chamber through convection currents before draining through the TM into Schlemm's canal. From there, it is drained through episcleral veins and into the venous system (Langham, 2009).

Laser photocoagulation, or laser-induced OH, is a technique in which anterior chamber structures such as the limbal plexus, TM or episcleral veins are treated with an

argon laser. The physical damage caused to these structures impairs aqueous outflow and elevates IOP to model glaucoma in rodents (Cuenca et al., 2010; Valiente-Soriano et al., 2015) and NHPs (Burgoyne, 2015; Quigley & RM, 1983). Although laser photocoagulation is widely used, there are several limitations. The impact on IOP is frequently transient, requiring repeat treatment for a more sustained IOP elevation. Additionally, laser treatment can produce significant inflammation and edema in the anterior chamber and surrounding structures (Biswas & Wan, 2019). It has also been shown to cause corneal opacities and cataracts (Biswas & Wan, 2019) which greatly reduce the ability to perform longitudinal *in vivo* imaging to monitor cell structure and function over time.

Injecting hypertonic saline solution into episcleral veins, a model first described by Morrison and colleagues, causes scarring of anterior chamber structures and a subsequent increase in IOP (Morrison et al., 1997). Following injection, IOP can remain elevated for a few weeks to months (Chauhan et al., 2002; Guo et al., 2005; Johnson et al., 1996; Kipfer-Kauer et al., 2010; Morrison et al., 1997). The degree of IOP elevation has been reported as variable, potentially due to variability in the amount of scarring produced, or the difficulty in accessing the small episcleral vessels. Like the laser photocoagulation model, subsequent injections may need to be performed to achieve sustained IOP elevation (Chauhan et al., 2002; Kipfer-Kauer et al., 2010; Morrison et al., 2015). Episcleral venous injection results in RGC loss and in changes in the appearance of the ONH with CSLO and OCT (Chauhan et al., 2002; Cordeiro et al., 2004; Morrison et al., 1997).

1.3.4. Models Induced by Intracameral Injections of Materials

Intracameral injection of materials that occlude aqueous humour outflow through the TM are now routinely used to increase IOP. Materials used to induce IOP elevation can include polystyrene microspheres or microbeads, or other materials such as temperature sensitive polymer hydrogels that cross link to impair outflow.

One of the most widely used models to induce EG in mice is through intracameral injection of microbeads. Sappington and colleagues first described intracameral injection of microbeads to impede aqueous outflow through the iridocorneal angle, and increase IOP (Sappington et al., 2010). The microbead technique is widely used, however, the degree of IOP elevation has been shown to be variable and transient, with the effects lasting for 2-12 weeks before returning to baseline levels (Cone et al., 2010; Schaub et al., 2017). There is a frequent need for repeat injections to sustain IOP elevation and its impact on RGCs (Morgan & Tribble, 2015; Sappington et al., 2010). Repeat injection or an initial injection of a larger volume or concentration of microbeads runs the risk of a sudden IOP elevation, potentially causing corneal edema or ulcers. Due to the variability in the level and duration of IOP elevation, the resulting RGC somal and axonal loss have been variable. Studies have reported 5% to 40% loss over 3-8 weeks (Chen et al., 2011; Cone et al., 2010; Henderson et al., 2021; Ito et al., 2016; Samsel et al., 2011; Sappington et al., 2010; Urcola et al., 2006; Wei et al., 2011). Moreover, there doesn't appear to be a clear relationship between the volume of beads injected and RGC loss in both mouse and rat microbead models (Morgan & Tribble, 2015).

Another limitation of microbeads is obstruction of the visual axis which impedes longitudinal *in vivo* imaging. The use of magnetic microbeads has become a better alternative for *in vivo* imaging studies because the beads can be displaced into the iridocorneal angle with the use of a magnet (Abbott et al., 2014; Henderson et al., 2021). Maintaining a clear visual axis limits the number of magnetic microbeads that can be injected into the eye, and as a result, the IOP elevation is often modest, resulting in only modest RGC loss (Henderson et al., 2021). Therefore, different models of elevating IOP chronically while maintaining a clear visual axis are needed.

Intracameral injection of temperature-sensitive cross-linking hydrogel polymers resolves many of the limitations of microbeads. First described by Chan and colleagues (Chan et al., 2019), the gel polymer is a mixture of two components that when injected into the anterior chamber, gelate, and impair aqueous flow through the iridocorneal angle. Chan and colleagues reported significant loss of RGC function, with electroretinograms (ERGs), and structure, with both *in vivo* fluorescence imaging and immunohistochemistry over four weeks of EG (Chan et al., 2019). The hydrogel model was subsequently used to study changes to individual RGC dendritic arbor structure following four weeks of elevated IOP (Di Pierdomenico et al., 2022). In summary, this model has numerous critical advantages. It produces sustained increases in IOP, and because the hydrogel is transparent, the visual axis remains clear so that longitudinal CSLO and OCT imaging can be performed with no obstructions or media opacities.

1.4. Age-Related Changes in the Eye

1.4.1. Tissue Level Changes

There are numerous age-related changes that occur in both anterior and posterior segments of the eye. Changes in the cornea and crystalline lens lead to alternations in refractive index and can alter the refractive power of the eye. For example, cataracts are the leading cause of reversible blindness and are strongly associated with aging (Cedrone et al., 1999; Hashemi et al., 2020). Most cataracts form due to the oxidation of proteins within the lens over time, which can be seen as cloudy or yellow pigments within the lens. Presbyopia, another age-related phenomenon characterized by the inability to focus on near objects, is due to loss of accommodative power caused by changes in the lens zonules, lens elasticity and weakened ciliary muscles (Glasser & Campbell, 1999; Heys et al., 2004).

The TM is also impacted by age and has been implicated in glaucomatous pathology. The TM in younger individuals holds a long wedge shape, permitting aqueous humour to flow out of the anterior chamber. With age, the TM becomes more rhomboidal, with the beams, or trabeculae, becoming thicker due to the accumulation of extracellular matrix proteins such as proteoglycans and collagen (McMenamin et al., 1986). Additionally, age-related reduction in giant vacuoles and pores within the TM, can impact the aqueous outflow pathways and potentially lead to an increase in IOP (Miyazaki et al., 1987).

The retina and ONH also undergo numerous age-related changes. Within the retina, changes in structure can lead to changes in visual function, and these occur in

both the outer and inner retina. In the outer retina, decreases in photoreceptor density has been shown, with approximately 30% loss of rod photoreceptors in the central retina between 34 and 90 years of age (Curcio et al., 1993). In contrast, the density of cone photoreceptors appears to remain more stable (Gao & Hollyfield, 1992). The age-related loss of rod photoreceptors has been hypothesized to be due to repeated oxidative damage and exposure to UV light that leads to mitochondrial DNA damage and metabolic dysfunction (Winkler et al., 1999).

There is also a steady attrition of RGCs and their axons with age (Calkins, 2013). It is estimated that there is approximately 0.3%-0.6% RGC loss per year between the second and eighth decades of life (Budenz et al., 2007; Harwerth et al., 2008). This loss can be seen *in vivo* using OCT to compare RNFL measurements in aged patients compared to normal individuals (Leung et al., 2012), and in patients with glaucoma compared to healthy age-matched controls (Vianna et al., 2015). Other retinal and ONH structures such as the macular ganglion cell layer and neuroretinal rim (Chauhan et al., 2020), have shown significant age-related decreases with OCT. Although structural changes occur in normal aging individuals and in glaucoma, patients with glaucoma experience greater magnitude of change over time. Interestingly, one study found no statistical difference between rates of change of RNFL and neuroretinal rim width between healthy controls and those being treated for glaucoma (Vianna et al., 2015), suggesting that effects of normal aging should be considered when estimating effects of glaucoma in disease progression.

Within the ONH, there is a corresponding decrease in the number of axons with age, and a thickening of the fibrovascular pial septa, or the connective tissue that separates axon bundles (Dolman et al., 1980). The thickening is caused, in part, by the increase in elastin (Dolman et al., 1980; Hernandez, 1992) and thickening of pia mater which form the septa, within the ON (Dolman et al., 1980). The septal thickening can cause impairment in the exchange of nutrients between capillaries and axon bundles (Dolman et al., 1980). The amount of elastic and collagen fibers in the LC and surrounding sclera also increase with age, resulting in increased stiffness (Morrison et al., 1989, 1990; Vannas & Teir, 1960). The increase stiffness can potentially lead to increased mechanical stress on the ON and the unmyelinated RGC axons within the LC (Caprioli, 2013), contributing to axonal damage.

Many of the age-related changes within the anterior and posterior segments can increase the susceptibility to glaucoma. Age-related changes to anterior segment structures such as the TM may cause increased resistance for aqueous outflow and elevated IOP, which can be modified through laser trabeculoplasty, or the creation of new outflow pathways, which are current common treatments for glaucoma. Posterior segment structures such as the retina and ONH are also highly impacted by age and glaucomatous pathology, but in contrast, they are not currently amenable to treatment. Therefore, research is actively being conducted to further our understanding of how aging impacts normal function and increases susceptibility to diseases, like glaucoma.

1.4.2. Cellular Senescence

Cellular aging, or cellular senescence, was first described by Hayflick and Moorhead in 1961 in cultured human fibroblasts (Hayflick & Moorhead, 1961). Cellular senescence refers to a permanent state of cell cycle arrest and has been shown to play a crucial role in driving and accelerating aging processes. DNA damage is one of the most influential causes of cell senescence (Flach et al., 2014; Hernandez-Segura et al., 2018; Van Deursen, 2014), with increases in chromatin alterations and lipofuscin accumulation. It is hypothesized that in addition to DNA damage (Mizi et al., 2020), senescence can be initiated by telomere shortening (Hayflick & Moorhead, 1961; McHugh & Gil, 2018), inflammation (Di Mitri & Alimonti, 2016), mitochondrial dysfunction, and metabolic dysfunction (McHugh & Gil, 2018; Van Deursen, 2014).

In senescent cells, there are widespread changes in cellular gene expression, which is accompanied with increased secretion of inflammatory mediators like chemokines, cytokines, and growth factors. Senescent cells enter a senescence-associated secretory phenotype (SASP) where they can produce and secrete interleukins, chemokines, growth factors, proteases, and extracellular matrix (ECM) components (Campisi & D'Adda Di Fagagna, 2007; Coppé et al., 2008, 2010).

Senescence was conventionally associated with mitotic cells, however, exogenous stressors can induce senescence in post-mitotic cells like neurons (Jurk et al., 2012). For example, due to their high oxygen consumption, neurons are more vulnerable to ROS accumulation, neuroinflammation and subsequent DNA damage, all of which can induce senescence (Si et al., 2021). In neurons of aged mice (32 months of

age) there are several senescence-associated features, such as increases in phosphorylated p38/MAPK, increased levels of IL-6, markers of oxidative stress, and an accumulation of lipofuscin (Jurk et al., 2012). Increases in senescence-associated β-galactosidase activity have been observed in brains of aged mice (SA β-gal; Geng et al., 2010; Ota et al., 2012). SA β-gal is a lysosomal enzyme that exhibits age-related increases in aging rodent brains (Geng et al., 2010). Additionally, Jurk and colleagues showed similar mechanisms in post-mitotic cortical neurons, which was previously only shown in actively proliferating cells (Jurk et al., 2012; Si et al., 2021).

Microglia, the resident immune modulating cell type in the eye and brain, remain relatively inactive unless stimulated by pathogens, infections, or injuries when they respond by releasing various cytokines. In aged mice, there are increased levels of TNF-α, IL-6, and IL-1, indicative of microglial activation (Bachstetter et al., 2011; Flanary et al., 2007). When neurons secrete SASP, there is microglial activation, increasing pro-inflammatory mediators, resulting in increased senescence of neighbouring neurons and microglia and subsequent promotion of neurodegeneration (Yu et al., 2012). Microglia and astrocytes have also been considered key players in aging and senescence through SASP because of their close association with neurons (Bhat et al., 2012; Salminen et al., 2011). Astrocytes undergo senescence by growth arrest, and increased SA β-gal activity (Bitto et al., 2010). Researchers have hypothesized that because astrocytes play critical roles of in neuronal homeostasis, and clearance of ROS (Chen et al., 2020), they may be more susceptible to oxidative stress, leading to premature senescence phenotypes (Bitto et al., 2010).

Cellular senescence has been a contributor to many neurodegenerative diseases such as Alzheimer's dementia (Musi et al., 2018), Parkinson's disease (Chinta et al., 2018) and glaucoma (Caprioli, 2013). Glaucoma is now considered a disease of cellular senescence because of the tissue and cellular environment that occurs with aging. Markers of age-related changes have been discovered within the retina, and TM. For example, increased levels of lipofuscin within the retina is one of the key observations with age. Lipofuscin is an intracellular fluorescent material, formed by the aggregation of non-degradable lipids and proteins that accumulate over time, and actively produce ROS (Călin et al., 2021). Lipofuscin is known to be stored in highly metabolic, post-mitotic cells which is why it is commonly found in CNS neurons and RPE cells within the retina (Călin et al., 2021). Although lipofuscin is not a direct marker of cellular senescence, it is associated with age-related changes, and regions with high levels of lipofuscin seem to be most susceptible to degeneration (Holz et al., 2007; Lois et al., 2002).

A current marker for cellular senescence is SA β-gal and has been found in aqueous outflow pathway structures like the TM in eyes of glaucoma patients and animals with EG (Caprioli, 2013; Rocha et al., 2020; Skowronska-Krawczyk et al., 2015). Moreover, Skowronska-Krawxzyk and colleagues demonstrated that removing senescent cells using senolytic drugs (drugs that target cells expressing senescent markers) leads to RGC protection following OH (Skowronska-Krawczyk et al., 2015), thereby emphasizing the negative impact senescent cells may have on neighbouring cells and the potential for neuroprotection strategies through targeting senescent cells.

1.5. Visualizing Retinal Ganglion Cells

1.5.1. Histology

There are numerous histological techniques used to label RGCs for quantifying change to RGC populations or RGC dendritic structures. Some common techniques include retrograde labelling, immunohistochemistry and labelling cells exogenously through viral injections.

Retrograde labelling of RGCs requires the fluorescent tracer to be applied directly to RGC projection sites in the brain and the ON stump. Applying fluorophores to the superior colliculus (SC) in rodents, is a reliable technique with a high degree of specificity to RGCs because the tracer is transported retrogradely along RGC axons to the somas within the retina. The durations for expression within RGCs in the retina differ depending on the fluorophore. For example, fluorogold (FG) is a widely used collicular label that labels RGC somas within one week. It is a reliable method of quantifying RGCs in normal retinas for relatively short periods, however, it has several limitations. FG cannot be used for longer term studies because it begins to be expressed in amacrine cells through transfer via gap junctions (Abdel-Majid et al., 2005). Additionally, FG can be taken up by activated microglia after RGCs undergo apoptosis and are phagocytosed. Hence, quantification of FG-positive cells following injury may not be specific to RGCs (Biermann et al., 2012; Chauhan et al., 2004). Finally, although approximately 96% of RGCs project to the SC, it is not the only projection site in the mouse brain, with some RGCs projecting to the suprachiasmatic nucleus, the lateral geniculate nucleus, and the olivary pretectal nucleus (Hattar et al., 2006; Quina et al.,

2005; Salinas-Navarro et al., 2009). Retrograde labeling through applying fluorophores directly to the ON stump is advantageous as it labels slightly more RGCs in murine retina than SC application (approximately 2-4% more RGCs; Salinas-Navarro et al., 2009). The main limitation of the technique is that ONT is required to expose the stump, therefore the cell loss from the primary injury cannot be accurately distinguished from the loss that occurred due to the transection itself (Nuschke et al., 2015).

Immunohistochemistry provides an alternative technique to stain the retina with cell specific markers, without invasive loading procedures or retrograde transportation of fluorophores. Brain-specific homeobox/POU domain protein 3a (Brn3a) and RNA-binding protein with multiple splicing (RBPMS) are routinely used to label RGCs with immunohistochemistry. Brn3a is a transcription factor expressed within the nucleus in the majority of adult RGCs (Wang et al., 2002), therefore automated quantification of Brn3a-positive cells can be performed reliably (Vidal-Sanz et al., 2012). However, depending on species, Brn3a only labels 80-95% of RGCs (Galindo-Romero et al., 2011; Nadal-Nicolás et al., 2009; Rodriguez et al., 2014). Moreover, Brn3a expression is reduced following ON injury in wholemounted retina, and Western blot showed significantly decreased expression at as early as 3-days following ON injury (Nuschke et al., 2015). For these reasons, Brn3a quantification following injury may lead to an overestimation of RGC loss.

RBPMS is an RNA binding protein, important in translation regulation, and post-translational modification of proteins (Kwong et al., 2010). RBPMS is highly expressed in the mammalian retina and is specific to RGCs, as demonstrated by colocalization with

FG labelled cells (Kwong et al., 2010, 2011). Additionally, RBPMS-positive cells were almost completely colocalized with FG-positive cells both before and after elevated IOP (Kwong et al., 2010, 2011) suggesting that even after injury, RBPMS remains a reliable marker for RGC quantification. In contrast to Brn3a which is a nuclear stain, RBPMS is expressed throughout the RGC cytoplasm (Rodriguez et al., 2014) which can cause some somal overlap between neighbouring cells, making automated quantification methods more difficult.

Histological techniques ensure a high degree of cell-type specificity, however, quantification is performed at a single timepoint resulting in cross-sectional data, and the need to infer longitudinal behaviour. In diseases such as glaucoma where progression occurs gradually, the ability to track the same individual cell or population of cells over time is critical, and advances in *in vivo* imaging techniques permit this investigation.

1.5.2. In Vivo Imaging of Retinal Ganglion Cells

Retinal imaging modalities and their use for both clinical examinations and basic science, have been advancing rapidly. Techniques such as OCT and CSLO are used to estimate RGC survival in clinical settings for disease diagnostics and to monitor disease progression and have been adapted for use in experimental research.

OCT is a light-interference-based technique that uses backscattered light to obtain high resolution images of the retina in cross-section (Wojtkowski et al., 2005). Thickness measurements of retinal layers can be quantified and are used as surrogate

measures of cell loss. For example, in glaucoma, changes in RNFL thickness are used as a surrogate measure of RGC loss in clinical (Bussel et al., 2014; Schuman, 2008) and experimental (Chauhan et al., 2012; Guo et al., 2010) glaucoma. In addition to the retina, OCT is capable of scanning and producing detailed images and three-dimensional reconstructions of the ONH with high axial resolution. 3-dimensional reconstruction of the ONH has improved the ability to visualize and quantify neuroretinal structures and ONH landmarks such as Bruch's membrane opening, longitudinally throughout disease progression.

CSLO is another non-invasive imaging technique that utilizes confocal optics to generate tomographic images of the retina with high axial resolution (Webb et al., 1987). Images acquired with CSLO imaging can be used to visualize and differentiate small and gradual changes in glaucomatous pathophysiology (Chauhan, 1996). CSLO imaging has been adapted for visualizing fluorescence at various wavelengths within the visible and invisible spectra for the purposes of quantifying individual RGCs. *In vivo* RGC visualization has been performed following collicular labelling, in transgenic mice that express fluorophores under the control of RGC specific genes (Chauhan et al., 2012; Di Pierdomenico et al., 2022; Henderson et al., 2021; Leung et al., 2011), and following intravitreal injection of fluorophores (Smith & Chauhan, 2015; Yin et al., 2014).

Current *in vivo* clinical ophthalmic imaging modalities have advanced disease monitoring and diagnostics. However, the data acquired through these imaging modalities typically uses gross anatomical structures as surrogate measures for RGC population changes. Measurements such as changes in RNFL thickness do not provide a

direct measure of RGC somal or axonal loss, because there is non-axonal tissue that also compose the RNFL. For this reason, experimental research has been utilizing fluorescent proteins to visualize changes to individual RGCs over time in attempts to better understand the underlying mechanisms of glaucomatous pathophysiology.

1.5.3. Experimental Single Cell Imaging Tools

Transgenic mice have been generated to express a variety of fluorophores under the control of RGC-specific genes for the purposes of studying both structure and function. For example, the Thy1-CFP mouse (Figure 1.3A) was engineered to express cyan fluorescent protein (CFP) through the Thy1 promotor which drives expression in central nervous system projection neurons (Feng et al., 2000). In this strain, CFP is expressed in approximately 90% of RGCs making it a valuable approach for assessing changes to pan-retinal RGC density (Wang et al., 2010). In contrast, in the Thy1-YFP-H strain (Figure 1.3B) yellow fluorescent protein (YFP) is expressed through the same Thy1 promotor in less than 0.5% of RGCs (Feng et al., 2013; Oglesby et al., 2012). The Thy1-YFP transgenic mouse can be utilized to study early changes to RGC dendritic structure *in vivo* following ONC (Leung et al., 2011) and EG (Di Pierdomenico et al., 2022; Henderson et al., 2021).

As transgenic manipulation in humans is not ethical, techniques have been developed to deliver exogenous proteins, or genes to the retina for diagnostic and therapeutic tools. The use of viral vectors such as adeno-associated viral vector (AAV) is an effective and relatively safe way to deliver agents to the retina. AAV is a small, single-

stranded DNA virus (Balakrishnan & Jayandharan, 2014; Colella et al., 2018). AAV is an episomal virus, therefore, it does not integrate into host DNA, and is currently being used in preclinical and clinical trials for the treatment of inherited blinding ocular diseases (Drag et al., 2023). For example, AAV2 vectors are currently being used for the treatment of Leber's Congenital Amaurosis (Bainbridge et al., 2008, 2015; Bennett et al., 2012, 2016; Le Meur et al., 2018; Keeler and Flotte, 2019; Russell et al., 2017).

AAV vectors have been used to deliver structural markers such as GFP to the inner retina for several years. Although there are several delivery techniques used in retinal research, intravitreal injections are preferred for targeting cells in the inner retina. Using *in vivo* CSLO fluorescence imaging, viral transduction efficacy and transduction rates can be determined, and the number of visible cells can be quantified *in vivo* in healthy control subjects and following injury. For example, Smith and Chauhan labelled RGCs with AAV2-GFP (Figure 1.3C) and reported a decrease in the number of cells labelled *in vivo* following ONT and co-localized those lost cells to baseline images (Smith & Chauhan, 2018).

Several groups have used AAV vectors to deliver functional proteins, genetically encoded calcium indicators (GECIs) such as GCaMP, to the inner retina (Figure 1.3D; (Borghuis et al., 2011; L. Li et al., 2022; Sharma et al., 2013; Weitz et al., 2013) to successfully elicit functional responses in intact-isolated retinal preparations. When performing *in vivo* 2-photon imaging experiments, GCaMP3 could only be utilized as a structural marker because of its high baseline fluorescence and small dynamic range (Ye et al., 2017). Other GCaMP variants with a larger dynamic range such as GCaMP6s have

been more successful in obtaining functional data from RGCs using optical stimuli (Bar-Noam et al., 2016; Cheong et al., 2018; Qin et al., 2020).

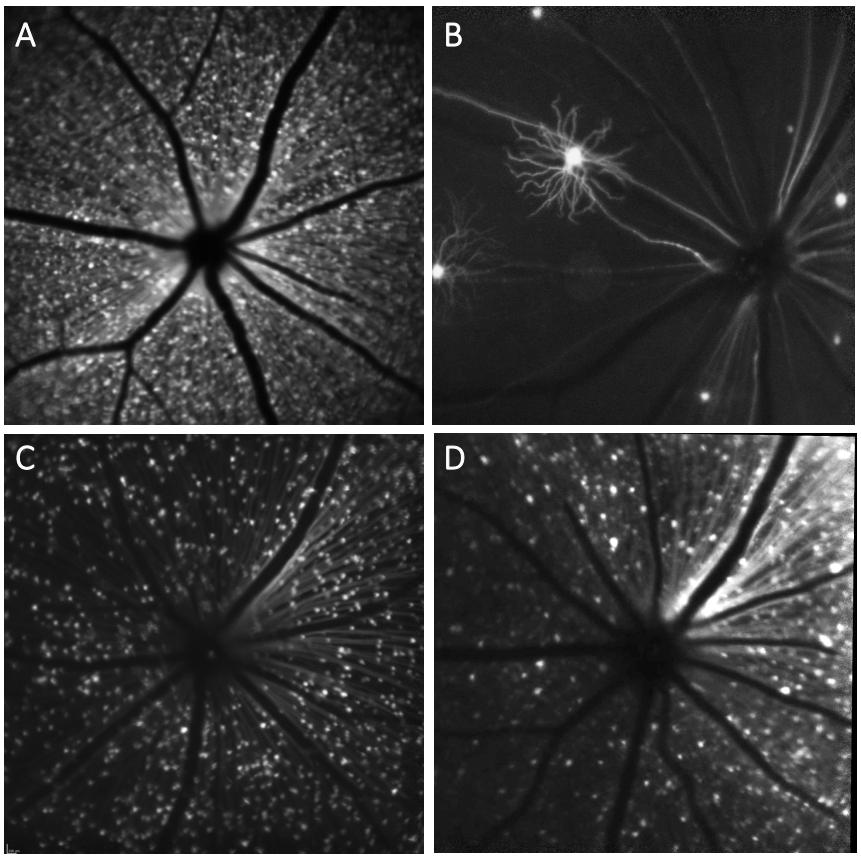

Figure 1.3. ***In vivo*** **fluorescence CSLO images of RGCs.** A) Thy1-CFP transgenic mouse expressing cyan fluorescent protein in approximately 80-90% of total RGCs in the mouse retina, B) Thy1-YFP line H transgenic mouse expressing yellow fluorescent protein in less than 0.5% of total RGCs permitting dendritic arbor visualization, C) AAV transduction of GFP delivered to RGCs through intravitreal injection, D) genetically encoded calcium indicator, GCaMP3, expression following AAV viral transduction.

1.6. *Thesis Objectives*

Much of the current literature in EG research has been performed in adult mice (3-6 months of age, the equivalent of 20-30 human years), with very little in old mice (2 years or older, the equivalent of 70-80 human years). Using models of EG in aged animals to study RGC degeneration is critical when modeling this age-related disease. Additionally, due to the degree of inter-individual differences in RGC number, and the amount of non-RGC tissue remodelling that occurs in structures like the RNFL and ONH in glaucoma, there is a need to develop methods to visualize structural and functional changes occurring at the single RGC level.

The aims of this research centre on validating the AAV2-CAG-GCaMP6s viral vector as a tool to visualize and monitor RGC function, and loss of function, longitudinally. The specific thesis objectives are:

1. To characterize the AAV2-CAG-GCaMP6s viral vector as a method to deliver an exogenous functional fluorescent marker for the purposes of visualizing cell function
2. To examine the ability of the AAV2-CAG-GCaMP6s viral vector to detect functional loss in acute and chronic models of ON damage
3. To investigate the role of age and EG on loss of RGC function

In **Chapter 3** of this thesis, I began by characterizing the use of AAV2-CAG-GCaMP6s viral vector as a tool to visualize functional responses of RGCs in adult mice. Additionally, I characterized the hit rate and specificity of the viral vector to RGCs within the GCL using

both *in vivo* imaging and immunohistochemical analyses. In **Chapter 4**, I explored the capability of the virus to detect loss of functional capacity of RGCs in both acute and chronic models of ON damage, specifically ONT and EG. Finally, in **Chapter 5**, I built upon the findings in the previous two chapters to explore the longevity of the expression of the viral vector, and the effects that age alone, and age in combination with EG have on the functional capacity of RGCs.

CHAPTER 2. MATERIALS AND METHODS

2.1. Animals

Animal procedures were conducted in accordance with the Canadian Council of Animal Care (CCAC) and animal ethics approval was obtained through the University Committee on Laboratory Animals at Dalhousie University. Adult male and female Thy1-GCaMP6s transgenic mice (C57BL/6J-Tg(Thy1-GCaMP6s)GP4.3Dkim/J,JAX^{TM} Stock Number: 024275, The Jackson Laboratory, Maine, US) and female wildtype C57Bl/6 mice (JAX^{TM} Mice Stock Number: 000664, Charles River Laboratories, Saint-Constant, QC, Canada), were used in this research. All mice were housed in an environment with a 12-hour light-dark cycle and had access to food and water *ad libitum*. Anesthesia for all procedures was performed using 2% isoflurane (Baxter Corporation, Mississauga, ON, Canada) and 1% O_2 administered at a flow rate of 1.5 L/min through a nose cone.

2.2. Intravitreal Injection

Mice were anesthetized with inhalant isoflurane and the left eye was topically dilated using 1% tropicamide (Alcon, Mississauga, ON, Canada) and 2.5% phenylephrine hydrochloride (Alcon). A 30-gauge needle was used to create a puncture in the sclera, 0.5 mm posterior to the limbus, the boarder between the cornea and sclera. The tip of a 33-gauge needle (Hamilton Company, Reno, NV, USA) was guided through the puncture site and 1.5 µL of the AAV vector (AAV2.CAG.GCaMP6s.WPRE.SV40, Penn Vector Core Lab, University of Pennsylvania, PA, USA), at a viral titer of $8.38x10^{12}$ GC/ml was slowly

injected into the vitreous body. Following the injection, topical antibacterial eye drops were applied, and the animals recovered on a heating pad overnight.

2.3. In Vivo Imaging

In vivo imaging was performed for the left eye only. Mice were first anesthetized, and the left eye was topically dilated with 1% tropicamide (Alcon, Mississauga, ON, Canada) and 2.5% phenylephrine hydrochloride (Alcon). An ophthalmic liquid gel (Tear-Gel, Novartis Pharmaceuticals Canada, Inc, Mississauga, ON, Canada) and a polymethyl methacrylate contact lens (Cantor and Nissel Limited, Brackley, UK) were placed on the cornea to maintain corneal hydration, prevent cataracts and corneal ulcerations, and to enhance image quality. A CSLO/OCT device, modified for use in mice (Spectralis Multiline, Heidelberg Engineering GmbH, Heidelberg, Germany), was used (Chauhan et al., 2012).

Images acquired with the CSLO were obtained with a 30-degree field of view, centered on the ONH and focused on the RNFL. For CSLO imaging, each image acquired was averaged 100 times to achieve high signal to noise ratio. Real-time eye tracking software was used during imaging to minimize motion artefacts due to respiration (Chauhan et al., 2012). For OCT imaging, a peripapillary OCT scan subtending 12 degrees was used. All follow-up images were acquired with image registered acquisition and eye-tracking software. Image registered acquisition was used to ensure all follow-up images are acquired in the same orientation as the baseline image so an accurate serial analysis could be performed. Baseline images and peripapillary OCT circle scans were

acquired with infrared light (IR; 820 nm) and fluorescence images of the GCaMP expressing cells were acquired with 488 nm excitation and emission bandpass filter of 500-550 nm (Chauhan et al., 2012).

2.4. Optic Nerve Transection

Mice were first anesthetized with inhalant isoflurane and their heads were secured in a stereotaxic frame to eliminate head movement. Using an operating microscope, an incision was made in the skin above the left eyelid to expose the supraorbital ridge. The superior rectus muscle was dissected, and the underlying tissue was carefully displaced to expose the optic nerve. An incision was made in the dura and the optic nerve was transected completely within the dural sheath using Vannas scissors 0.5 mm posterior to the globe. The incisions in the superior rectus and skin were sutured. ONT was performed in the left eye with the right eye being an internal control. Mice recovered on a heating pad for 24 hours.

2.5. Experimental Glaucoma

The induction of EG was performed using an intracameral injection of a crosslinking hydrogel polymer, first described by Chan and colleagues (Chan et al., 2019) and has been previously used in our laboratory (Di Pierdomenico et al., 2022). The hydrogel model was chosen because it causes a persistent IOP elevation with a single injection of the hydrogel without the need for subsequent injections. Furthermore, this approach permits longitudinal *in vivo* imaging as the ocular media remain transparent.

The cross-linking hydrogel polymer is composed of two hyaluronic acid mixtures, functionalized with vinyl-sulphone and thiol groups. Once mixed together and injected into the eye, the two materials gelate in a temperature-dependent process, thereby inhibiting aqueous outflow through the TM and increasing IOP.

In this procedure, mice were anesthetized and placed in a stereotaxic frame as described above. The left pupil was dilated and a topical anesthetic (proparacaine hydrochloride, Alcon Canada Inc) was instilled. 2.5 μL of each hydrogel was mixed and kept on ice until the mouse was correctly positioned and the eye was adequately dilated. The needle was inserted into the anterior chamber, approximately 2-3 mm from the corneal apex, taking care not to contact the cornea, lens, or iris. The gel was injected slowly towards the iridocorneal angle, with the needle remaining in the anterior chamber for 2-3 minutes. The procedure was performed in the left eye only, with the right eye as an internal control. Mice recovered on a heating pad overnight.

2.6. Intraocular Pressure Measurements

Prior to induction of EG, baseline IOP measurements were performed in both left and right eyes with a rebound tonometer (TonoLab, Tiolat, Inc., Helsinki, Finland), after five minutes of anaesthesia. Ten measurements were taken for each eye at each timepoint, and an average of these measurements was used to report the IOP in the data analysis. To minimize the variations that occurs with daily IOP fluctuations, the IOPs were performed between 12 pm and 2 pm.

2.7. Calcium Imaging

Following the final *in vivo* imaging timepoints for all control and experimental groups, retinas were dissected and prepared for Ca^{2+} imaging. Retinas were hemisected and mounted on filter paper before being submerged in oxygenated Hanks Balanced Salts Solution (HBSS; 100% O_2, 1 mM HEPES; Praxair, Dartmouth, NS) at a pH of 7.4 and placed in a microscope mounted superfusion chamber. The retinas were perfused with HBSS at a rate of 2 mL/minute for the duration of the Ca^{2+} imaging experiments.

A 40X water immersion objective (0.80W numerical aperture, Achroplan; Carl Zeiss Meditec, Oberkochen, Germany) connected to a charge-coupled device camera (Sensicam PCO, Kelheim, Germany) was used to image the retinas. The GCaMP6s fluorescence was stimulated with 488 nm excitation and collected at 516 nm emission. The microscope was focused on the GCL and experiments began with five minutes of baseline imaging at an acquisition rate of one image frame per 20 seconds. Following five minutes of baseline imaging, 15 second treatments of 50 µM kainic acid (KA; a glutamate receptor agonist), dissolved in oxygenated HBSS were performed followed by 15 minutes of KA washout with oxygenated HBSS solution. Each retina was treated 4 times with KA per experiment. Images were acquired at a rate of one frame per five seconds during KA application, and a rate of one frame per 20 seconds between treatments, during washout periods. All experiments were recorded using Axon Imaging Workbench 4 software (Molecular Devices, Sunnyvale, CA, USA).

2.8. Immunohistochemistry and Tissue Preparation

Immunohistochemistry was performed to quantify cell density and specificity of the viral vector to retinal cells. Retinas were carefully dissected and fixed at room temperature in 4% paraformaldehyde (PFA) for one hour. Following one hour of fixation, retinas were washed with phosphate buffered saline (PBS) and blocked in 10% normal donkey serum (Jackson ImmunoResearch Laboratories Inc., West Grove, PA, USA) in PBS with 0.3% Triton X-100 overnight at 4°C. Retinas were left to incubate in primary antibodies against RBPMS (1:1000 guinea pig anti-RBPMS, PhosphoSolutions #1832, Aurora, Colorado, USA) and choline acetyltransferase (ChAT; 1:100 goat anti-ChAT, PhosphoSolutions #315, Aurora, CO, USA) for five days at 4°C to label RGCs and cholinergic amacrine cells, respectively. Retinas were washed with PBS and incubated in Cy3 (1:1000 Cy3 conjugated donkey anti-guinea pig, Jackson Immuno Research Laboratories Inc., West Grove, PA, USA), Alexa Fluor® 633 (1:1000 Alexa Fluor® 633 conjugated donkey anti-goat, Invitrogen #A21082), and Alexa Fluor® 488 (1:400; Alexa Fluor® 488 conjugated rabbit anti GFP, Molecular Probes, Eugene, OR, USA) overnight. Retinas were washed with PBS, mounted on microscope slides with Vectashield® anti-fade fluorescent mounting medium (Vector Labs, Burlingame, CA) and cover-slipped in preparation for epifluorescence imaging.

2.9. Ex vivo Epifluorescence Imaging and Image Processing

Tiled images of retinal whole-mounts were obtained using a Zeiss Axio Imager M2 microscope (Carl Zeiss AG, Oberkochen, Germany) and a 20x Plan-Apochromat

objective (0.8 numerical aperture; Carl Zeiss). Using ZEN Software (Carl Zeiss), exposure times were set for each of the three channels and fluorescence images of cells expressing RBPMS, ChAT, and GFP (GCaMP) in the GCL were acquired.

2.10. Data Analysis and Statistics

Statistics were performed using Prism (version 9.5.0 for Macintosh, GraphPad Software, La Jolla, CA, USA) and statistical significance was assumed when $p < 0.05$. All data is reported as mean (standard deviation (SD)).

2.10.1. In Vivo Imaging

Fluorescence images acquired with CSLO were imported into ImageJ (Schneider et al., 2012). Using the cell counting tool, all fluorescently labelled cells within the field of view were manually counted for each timepoint and reported as a cell density (cells/mm^2). Repeated measures one-way ANOVA with Tukey's multiple comparisons tests were performed to determine significance by comparing means across timepoints.

To measure the Ganglion Cell Complex (GCC) thickness, circular peripapillary B-scans, acquired with OCT were manually segmented using Heidelberg Eye Explorer Software (Heidelberg Engineering). In mice, because the RNFL is too thin to reliably segment, the GCC thickness was segmented from the inner-limiting membrane (ILM; near the vitreous-retina interface) to the outer border of the IPL, thereby comprising the RNFL, GCL, and IPL. Repeated measures one-way ANOVAs with Tukey's multiple comparisons tests were used to determine significance between means across

timepoints. Pearson's correlation with two-tailed significance tests were also used to correlate *in vivo* measures with IOP following EG.

2.10.2. Calcium Imaging

Experiments were recorded and analyzed using Axon Imaging Workbench 4 (Molecular Devices, Sunnyvale, CA, USA). Retinal cells expressing GCaMP6s within the GCL were traced as individual regions of interest (ROI). Approximately 50-75 cells were selected and analyzed for the duration of the experiment. Data for each cell were reported as changes in arbitrary fluorescence units over time. Baseline fluorescence for each cell was measured as an average of the first 15 frames of the recorded experiment. Maximum fluorescence was determined for each cell for each of the KA treatments and averaged. KA-induced Ca^{2+} transient amplitudes were defined as the peak fluorescence change over the baseline fluorescence ($\Delta F/F_0$). Repeated measures one-way ANOVAs were used for intragroup analyses. For inter-group analyses, unpaired t-tests, and Brown-Forsythe one-way ANOVAs with Dunnett's T3 multiple comparisons tests, or Tukey's multiple comparisons tests were performed to determine significance between groups. Pearson's correlation with two-tailed significance tests were also used to correlate transient amplitudes with IOP following EG.

2.10.3. Immunohistochemistry

The image analysis for wholemounted retinas was performed using Zen2Lite software (Carl Zeiss Meditec, Oberkochen, Germany). From the tiled images of the

retinal wholemounts, 316 µm x 316 µm ROIs were selected. ROIs were selected from central, mid-peripheral and peripheral retina, at distances of 0.5, 1.0 and 1.5 mm from the ONH, respectively. For each region, the number of cells labelled with RBPMS, ChAT, and GFP (GCaMP) were quantified and reported as cell densities. Additionally, in control retinas, the number of GFP-positive cells that colocalized with RBPMS-positive cells, and ChAT-positive cells was also quantified. Ordinary one-way ANOVAs with Tukey's multiple comparisons test were performed to determine significance between groups. Pearson's correlation with two-tailed significance tests were also used to correlate RBPMS-positive cell density with IOP following EG.

CHAPTER 3. CHARACTERIZATION OF GCaMP6s IN ADULT MICE

3.1. Chapter Objectives

The experiments performed aimed to characterize GCaMP6s expressed in wildtype C57Bl/6 mice through viral transduction using the AAV2-CAG-GCaMP6s viral vector and compare its structural and functional properties to the commercially available Thy1-GCaMP6s transgenic mouse. The specific objectives in this chapter were:

i) Characterize GCaMP6s expression with *in vivo* CSLO imaging in wildtype mice injected with AAV2-CAG-GCaMP6s and Thy1-GCaMP6s transgenic mice

ii) Compare the functional properties of GCaMP6s in both wildtype and transgenic mice using Ca^{2+} imaging in intact-isolated retinal preparations

iii) Examine the specificity and hit rate of the GCaMP6s to RGCs in retinas from wildtype mice injected with AAV2-CAG-GCaMP6s

3.2. Experimental Design

Adult (3-6 months of age) female C57Bl/6 mice (n= 10) and adult (male and female Thy1-GCaMP6s mice (n= 11) were used in this study. Prior to intravitreal injection in wildtype mice, baseline *in vivo* CSLO IR images and peripapillary OCT circle scans were acquired. Following intravitreal injection, viral transduction was monitored with weekly *in vivo* imaging over eight-weeks. The transgenic Thy1-GCaMP6s mice were imaged with *in vivo* imaging (IR and fluorescence CSLO) once prior to being euthanized.

In both groups, manual quantification of fluorescent cells from the *in vivo* images was performed using the Cell Counter plug-in in ImageJ.

After eight-weeks, mice injected with the viral vector were euthanized and retinas were dissected and prepared for Ca^{2+} imaging and immunohistochemistry (IHC). IHC was performed on retinas from mice injected with the viral vector to quantify the hit rate and specificity of the virus to RGCs in the GCL. Additionally, RGC cell density was quantified in eyes that received intravitreal injection and compared to the fellow eye, and age matched-non-injected control mice to observe whether viral transduction had a negative impact on the retina or led to a reduced RGC count. For detailed protocols on techniques used within this chapter, see Chapter 2 Materials and Methods.

3.3. Results

3.3.1. In Vivo Characterization of GCaMP6s in Wildtype and Transgenic Mice

C57Bl/6 mice that received intravitreal injection of the AAV2-CAG-GCaMP6s viral vector had notable fluorescence with *in vivo* CSLO imaging 1-week post injection (Figure 3.1A). Cell density, quantified from *in vivo* fluorescence images, showed an increase from 150 (57) cells/mm^2 at 1-week post-injection, to 384 (43) cells/mm^2 at the final 8-week timepoint. There was a significant increase in cell density over the first 5 weeks ($p< 0.05$) but stabilized thereafter (Figure 3.1B). Fluorescence was primarily expressed in somas and RGC axons, although there was expression detectable in some dendrites (Figure 3.2).

Seven (64%) of the 11 Thy1-GCaMP6s transgenic mice showed fluorescent cells with *in vivo* CSLO. Labelling appeared dim, sparse, and inconsistent among animals (Figure 3.3), with a mean cell density of 145 (45) cells/mm^2. Thy1-GCaMP6s mice had significantly fewer cells visible *in vivo* than AAV-injected mice at the 8-week imaging timepoint ($p< 0.001$; Figure 3.4).

Ganglion cell complex (GCC) thickness was segmented from peripapillary OCT circle scans (Figures 3.5A and 3.5B). Baseline thickness was 79.8 (4.9) μm and following 8-weeks of AAV transduction was 80.3 (5.1) μm. There were no significant changes in GCC thickness detected between weeks, or between baseline and the 8-week timepoint ($p= 0.94$; Figure 3.5C).

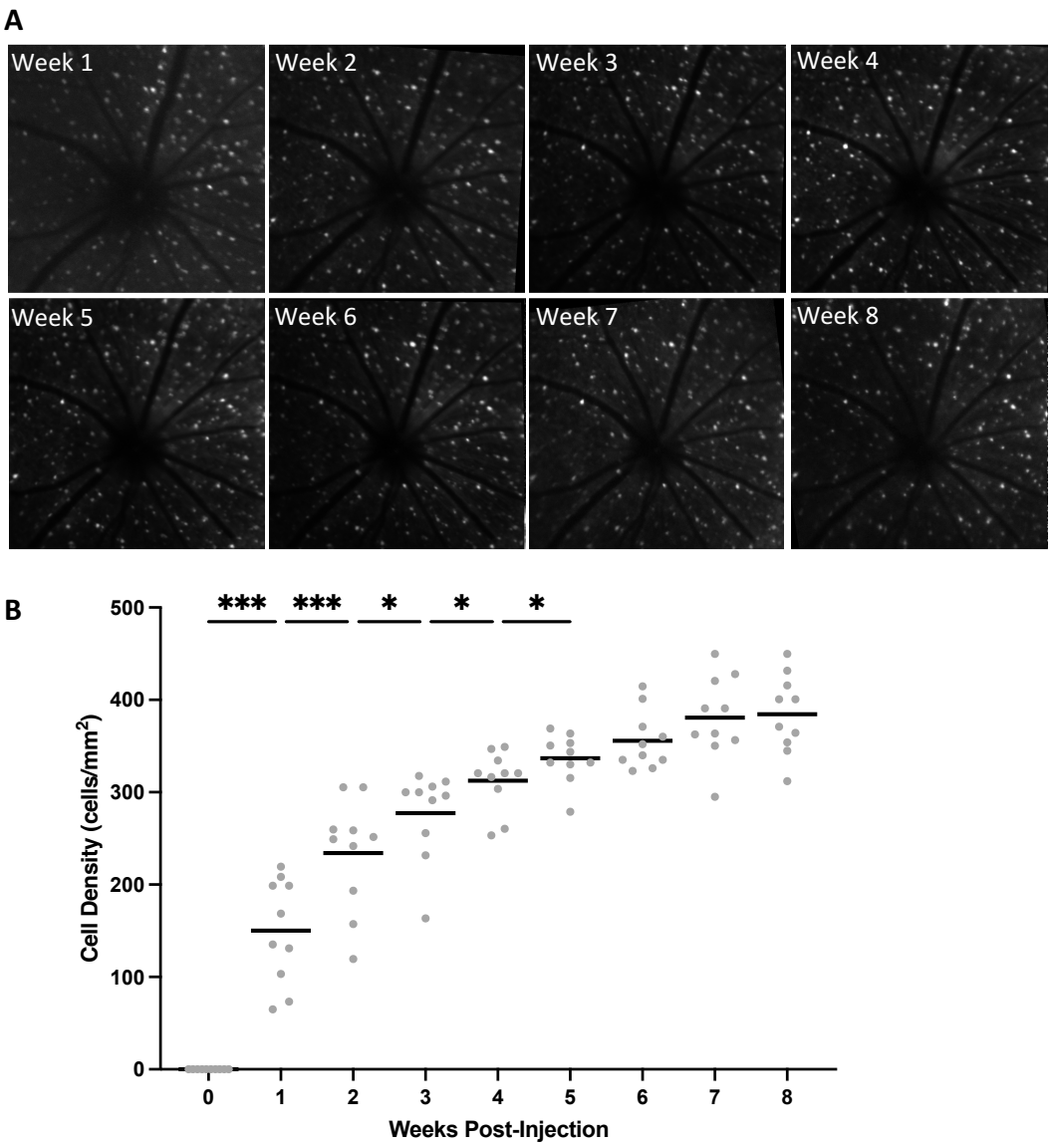

Figure 3.1. *In vivo* viral transduction following intravitreal injection of AAV2-CAG-GCaMP6s. A) Representative images acquired in the same mouse over 8-weeks following intravitreal injection of AAV2-CAG-GCaMP6s. B) Repeated measures one-way ANOVA with Tukey's multiple comparisons found significance over 5-weeks following intravitreal injection. n= 10; * = $p< 0.05$; *** = $p< 0.001$.

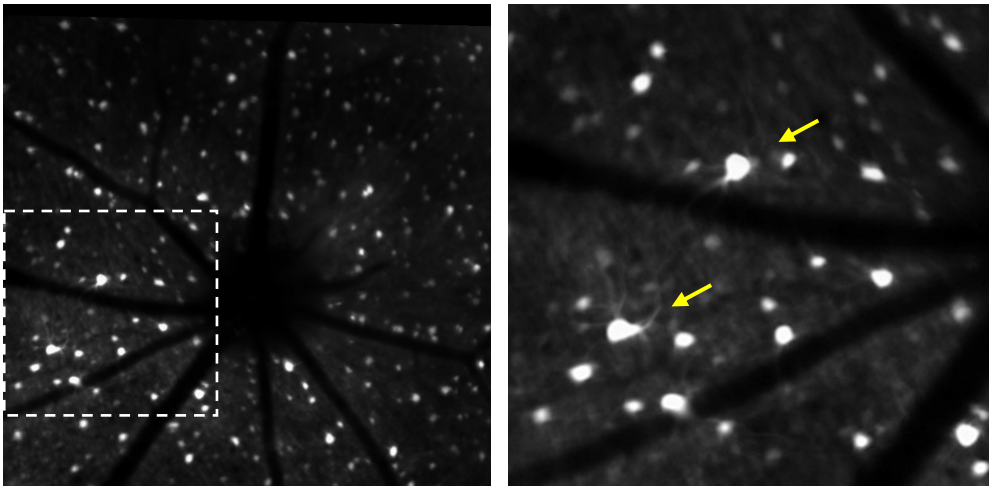

Figure 3.2. Dendrite visualization of GCaMP6s positive cells. *In vivo* fluorescence images from a mouse injected with AAV2-CAG-GCaMP6s shows GCaMP expression in both somas and dendrites. Right image demonstrates the selected region at higher magnification.

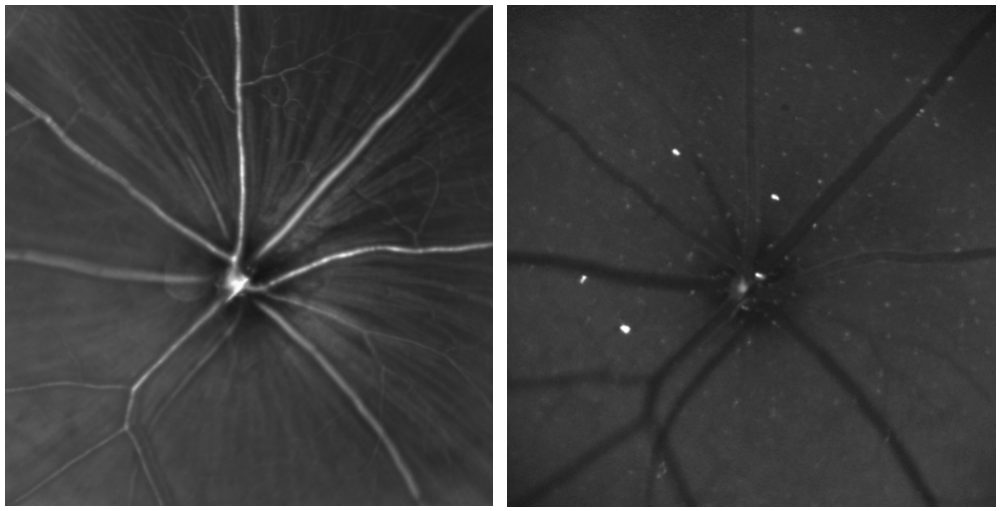

Figure 3.3. *In vivo* CSLO images of a Thy1-GCaMP6s transgenic mouse. Representative IR image (left) and fluorescence image acquired from the same Thy1-GCaMP6s mouse with 488nm light (right).

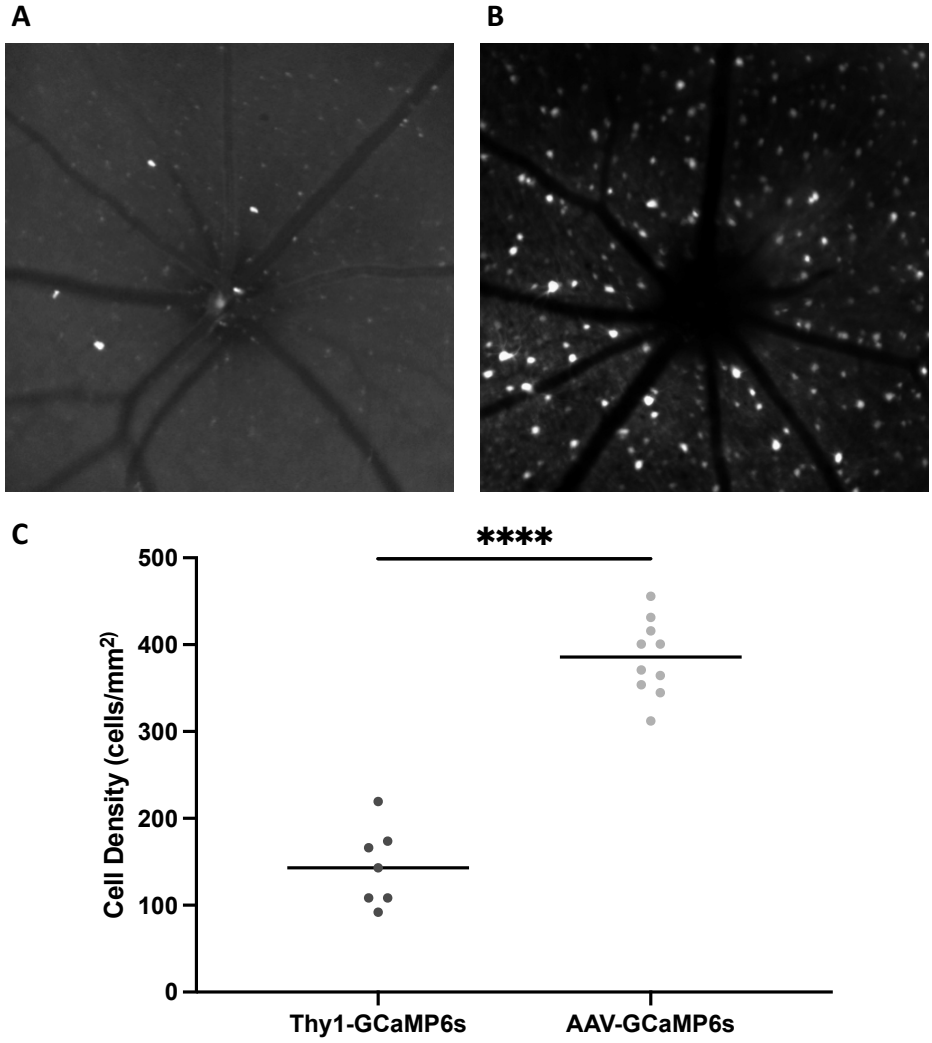

Figure 3.4. Comparison of *in vivo* GCaMP expression in AAV-CAG-GCaMP6s injected mice and Thy1-GCaMP6s transgenic mice. Representative images comparing *in vivo* fluorescence in a A) Thy1-GCaMP6s transgenic mouse and B) AAV2-CAG-GCaMP6s injected mouse 8-weeks post-intravitreal injection. C) Quantification of cellular fluorescence *in vivo* in transgenic vs AAV injected mice, respectively. Unpaired t-test confirmed a significant difference between groups (**** = p< 0.0001); n= 7 Thy1-GCaMP6s, and n= 10 AAV2-CAG-GCaMP6s.

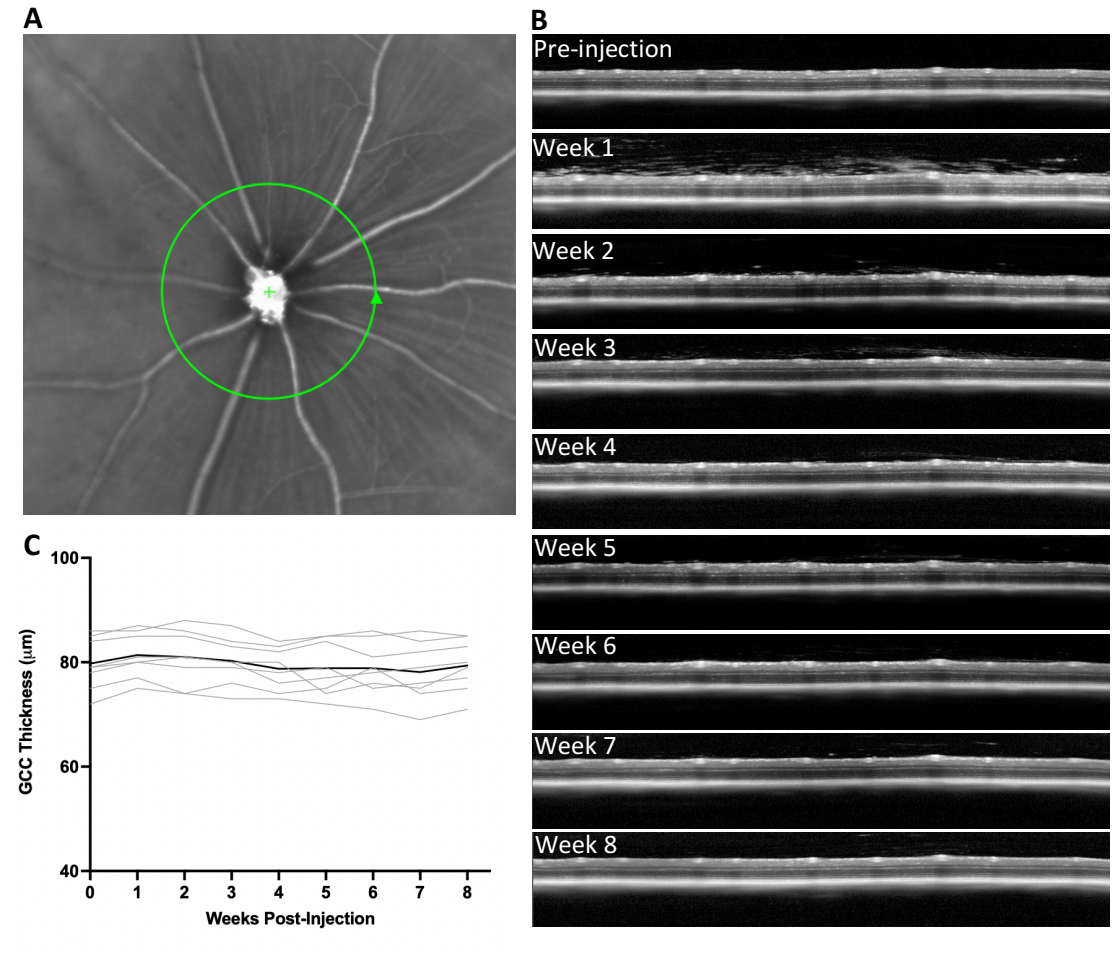

Figure 3.5. Longitudinal OCT scans of the left eye of a mouse following intravitreal injection of AAV2-CAG-GCaMP6s. A) *In vivo* infrared image of a mouse retina with the location of the OCT peripapillary circle scan. B) OCT peripapillary circle scans acquired in a representative mouse weekly over the 8-week time course post-AAV injection. C) Quantification of GCC thickness, as segmented from the ILM to the outer boarder of the IPL. Repeated measures one-way ANOVA with Tukey's multiple comparisons confirmed no significant changes in GCC thickness (p= 0.94); n= 10.

3.3.2. Comparison of AAV2-CAG-GCaMP6s and Thy1-GCaMP6s Function Using Calcium Imaging

KA-evoked depolarizations generated Ca^{2+} transients, which were measured as changes in GCaMP6s fluorescence ($\Delta F/F_0$). Fluorescence returned to baseline levels following KA washout (Figure 3.6A). In both the virus injected group and Thy1-GCaMP6s group, the transients produced were consistent over the four KA treatments, and there were no significant differences found in the average transient amplitude across KA treatments in either group ($p= 0.93$ and $p= 0.29$ in AAV2-CAG-GCaMP6s and Thy1-GCaMP6s, respectively; Figure 3.6B). AAV-transduced GCaMP6s produced significantly larger Ca^{2+} transients to the same concentration of KA compared to the transgenic mice ($p< 0.001$; Figure 3.6B).

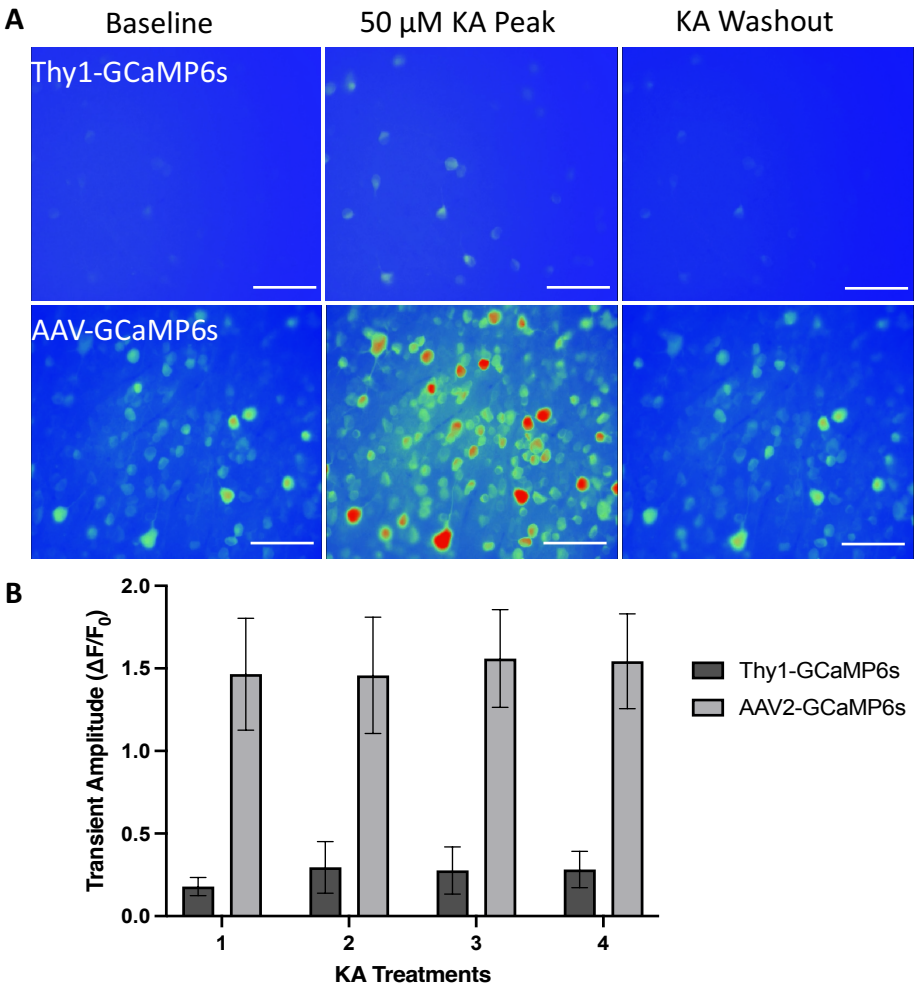

Figure 3.6. Intact-isolated retina Ca^{2+} imaging experiments in Thy1-GCaMP6s transgenic mice and AAV2-CAG-GCaMP6s injected mice. A) Pseudocoloured images from representative Ca^{2+} imaging experiments performed in retinas form a Thy1-GCaMP6s transgenic mouse (top) and a wildtype mouse injected with AAV2-CAG-GCaMP6s (bottom). Images (left to right) show baseline fluorescence, the fluorescence peak following stimulation with 50 µM KA, and following KA washout. Scale bars = 50 µM. B) Mean data show transient amplitudes across 4 KA treatments for both groups. Data reported as mean, with error bars indicating SD. Unpaired t-test confirmed significant difference between groups ($p< 0.0001$); n= 7 retinas from Thy1-GCaMP6s mice, and n= 10 retinas from AAV2-CAG-GCaMP6s mice.

3.3.3. Hit Rate and Specificity of AAV2-CAG-GCaMP6s to Retinal Cells Within the GCL

Immunohistochemistry performed in retinas from virus injected mice showed GCaMP6s labelling was widespread across the retina. Figure 3.7 shows a representative whole mounted retina labelled for RBPMS, ChAT, and GFP (to enhance AAV-transduced GCaMP). The number of RBPMS-positive, ChAT-positive, and GFP-positive cells from the virus-injected mice were quantified and both hit rate (proportion of RGCs labelled by the virus), and specificity were calculated. The average density of RBPMS-positive cells was 3278 (352) cells/mm^2, of ChAT-positive cells was 1147 (345) cells/mm^2 and of GFP-positive cells was 1007 (318) cells/mm^2 (Figure 3.8A).

Colocalization analysis was performed to determine the hit rate and specificity of the virus to retinal cells within the GCL. Of the total RBPMS-positive cells, 27% (5%) were GFP-positive. Of the GCaMP expressing cells (GFP-positive), 74% (6%) colocalized with RBPMS, 12% (3%) with ChAT, and 14% (5%) with cells did not colocalize with RBPMS or ChAT (Figure 3.8B).

The RBPMS-positive cell densities quantified from virus injected eyes, fellow-eyes, and eyes from non-injected mice were not significantly different from each other with average densities of 3278 (352) cells/mm^2, 3102 (299) cells/mm^2, and 3149 (401) cells/mm^2 in each group, respectively ($p= 0.66$; Figure 3.9).

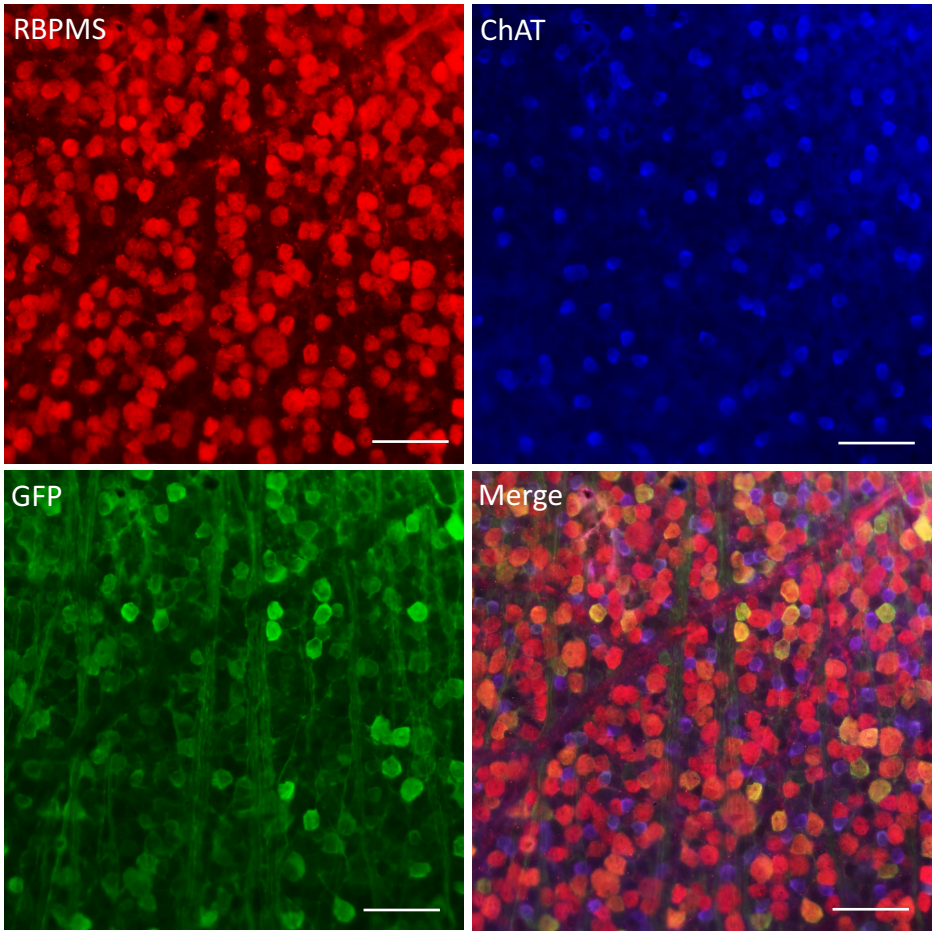

Figure 3.7. Immunohistochemical staining of retinal neurons in the GCL from the retina from a mouse injected with AAV2-CAG-GCaMP6s. Images show RBPMS labelling of RGCs, ChAT labelling of cholinergic amacrine cells, GFP labelling used to amplify the GCaMP fluorescence, and a panel showing the merged channels. Scale bars = 50µm.

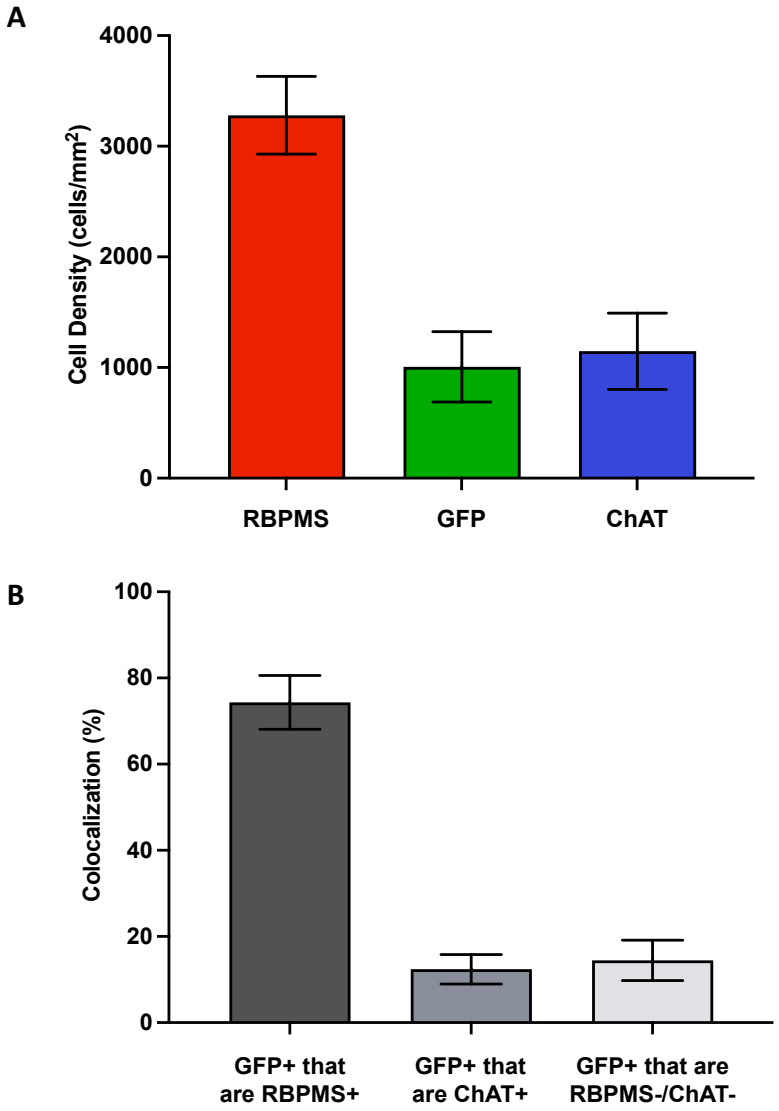

Figure 3.8. Cellular quantification and specificity of the AAV2-CAG-GCaMP6s viral vector to retinal cells within the GCL. A) Figure showing the average cell density of RBPMS-positive cells, GFP-positive cells (GCaMP-positive cells) and ChAT-positive cells labelled by IHC. B) Specificity of the viral vector to retinal cells within the GCL. GFP-positive cells that are RBPMS-positive indicate the specificity of the viral vector to RBPMS-positive RGCs. Figure also shows the specificity of the viral vector to ChAT-positive cells, and to RBPMS-negative/ChAT-negative cells. Data reported as mean (SD); n= 10.

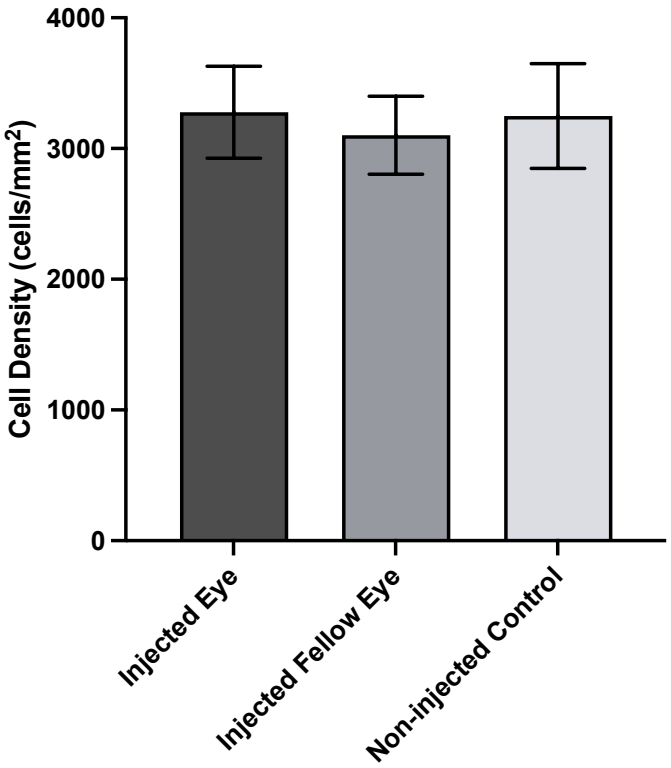

Figure 3.9. RBPMS quantification between retinas that received intravitreal injection and non-injected retinas. Figure shows average RBPMS-positive cellular density across 3 groups, AAV2-GCaMP6s injected mice, the fellow eye of an injected mouse, and a non-injected control mouse. One-way ANOVA with Tukey's multiple comparisons determined no significant difference between groups (p= 0.66). Data reported as mean (SD); n= 10 injected eye, n= 10 injected fellow eye, and n= 6 non-injected control eyes.

3.4. Summary of Findings

Findings from this initial characterization study examined the use of AAV to deliver the exogenous functional fluorescent marker, GCaMP6s, to neurons in the inner retina and compared this with a commercially available transgenic mouse line. Key findings from this chapter include:

1. The exogenous delivery of GCaMP6s via the AAV2-CAG-GCaMP6s viral vector provided robust labelling with *in vivo* CSLO in contrast to the Thy1-GCaMP6s transgenic mice which showed dim, spare and inconsistent labelling
2. The GCaMP6s expressed in both the transgenic and AAV-transduced wildtype mice yielded consistent functional responses, however, the latter produced larger Ca^{2+} transients to the same concentration of KA
3. AAV injection and transduction of GCaMP6s primarily labels RBPMS-positive cells, and to a smaller extent, displaced amacrine cells within the GCL. Moreover, it does not appear to have any negative impacts on structure, as indicated by GCC thickness and RBPMS-positive cell densities

CHAPTER 4. EFFECTS OF ACUTE AND CHRONIC INJURY ON RGC FUNCTION IN ADULT MICE

4.1. Chapter Objectives

The utilization of functional fluorescent proteins like GCaMP to detect changes in cell function following models of optic nerve damage has been reported both *in situ* following ONT (Blandford et al., 2017) and more recently, *in vivo* with visible light following induction of OH using silicone oil (Li et al., 2022). We sought to utilize the recently developed hydrogel model of EG to study the effects of elevated IOP on *in vivo* and histological measures of RGC loss, and functional loss using Ca^{2+} imaging. The chapter specific objectives were:

i) Characterize the IOP profile over 8-weeks following induction of EG, and subsequent effects of IOP on various *in vivo* structural markers of RGC survival, specifically *in vivo* cell density and GCC thickness

ii) Examine the responses of GCaMP6s in eyes of mice with ONT and EG compared to control mice

iii) Quantify RBPMS-positive cell densities following ONT and EG and evaluate the relationship between IOP and cell loss

4.2. Experimental Design

In this study, we sought to quantify both structural and functional loss in adult mice following 3-days of ONT, 4-weeks of EG, and 8-weeks of EG. In the EG groups, IOP

measurements, *in vivo* fluorescence images and peripapillary OCT circle scans were acquired weekly over 4-, and 8-weeks.

Functional Ca^{2+} imaging experiments were first performed in intact-isolated retinas from mice following 3-days of ONT (n= 6) to determine if the GCaMP produced by viral transduction could be used to visualize and evaluate early functional changes. Following these initial experiments, we performed functional experiments in mice following 4-, and 8-weeks EG (n= 10 and 13 respectively). For both ONT and EG groups, the injury was induced following 8-weeks of initial viral transduction. Quantification of RBPMS-positive cells was performed for each group to evaluate and compare cell loss in these models. Detailed protocols for both ONT and EG are described in Chapter 2 Materials and Methods.

4.3. Results

4.3.1. Characterization of Intraocular Pressure and In Vivo Analyses Following Experimental Glaucoma

The IOP was increased from baseline when measured at 1-week post-injection and remained elevated over the experimental time course. The mean IOP at baseline was 10.1 (0.6) mmHg and over 8-weeks was 19.1 (1.8) mmHg (Figure 4.1). The average IOP elevation relative to baseline in adult EG mice over 8-weeks was 9.7 (2.0) mmHg.

In vivo fluorescence imaging was performed at the final 3-day timepoint for the ONT group, and weekly over the EG time course. *In vivo* fluorescence images following 3-days of ONT demonstrated a visible decrease in fluorescently labelled cells (Figure

4.2). Following EG induction, the optical media remained sufficiently clear for follow-up images to be obtained weekly (Figure 4.3A). Quantification of fluorescent, GCaMP6s expressing, cells was conducted for each weekly *in vivo* fluorescence image throughout the EG time course. The GCaMP6s cell density was 356 (37) cells/mm^2 at baseline (8-weeks following initial AAV injection) and decreased 12% to 313 (33) cells/mm^2 at 4 weeks, and 18% to 290 (36) cells/mm^2 at 8-weeks post-EG (Figure 4.3B).

In parallel to the EG experimental group, an additional group of mice were imaged weekly with *in vivo* CSLO over 8-weeks but did not have EG-induction. The control group was used to mimic the protocol being used in the EG groups, and to determine if the loss observed in the EG groups was significant from the weekly imaging sessions. When *in vivo* cell densities from control and EG mice were compared, significant differences began at 5-weeks post-EG induction and continued for the remainder of the time course ($p< 0.001$, $p< 0.001$, $p< 0.001$, $p= 0.005$, at weeks 5, 6, 7, and 8, respectively; Figure 4.3C).

In addition to fluorescence imaging, OCT imaging was performed to quantify changes in GCC thickness (Figure 4.4A and Figure 4.4B). The average GCC thickness at baseline, and following 8 weeks of viral transduction was 83.2μm (3.6) μm. The GCC thickness was decreased to 78.2 $\pm$ 4.3 μm and 72.4 (3.1) μm following 4-, and 8-weeks of EG, respectively. When this was compared to control mice, there was a 5% decrease at 4-weeks, and 12% at 8-weeks post-EG which were both found to be significant ($p= 0.045$ and $p< 0.001$, respectively; Figure 4.4C).

To determine the relationship between IOP and measures of *in vivo* structural change, correlation analyses were performed between IOP and *in vivo* cell density (Figure 4.5A) and IOP and GCC thickness at 8-weeks post-EG (Figure 4.5B). For both analyses, the Pearson correlation coefficients were negative, at -0.39 ($p= 0.19$), and -0.59 ($p= 0.015$), for *in vivo* cell density and GCC thickness, respectively.

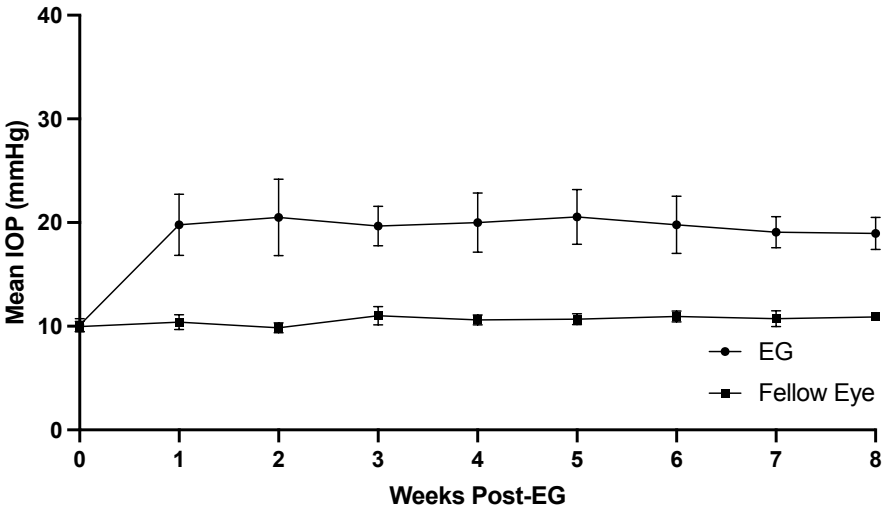

Figure 4.1. Intraocular pressure in adult EG mice. The average IOP in both the experimental and control eyes over 8-weeks of EG. Error bars represent standard deviation; n= 13.

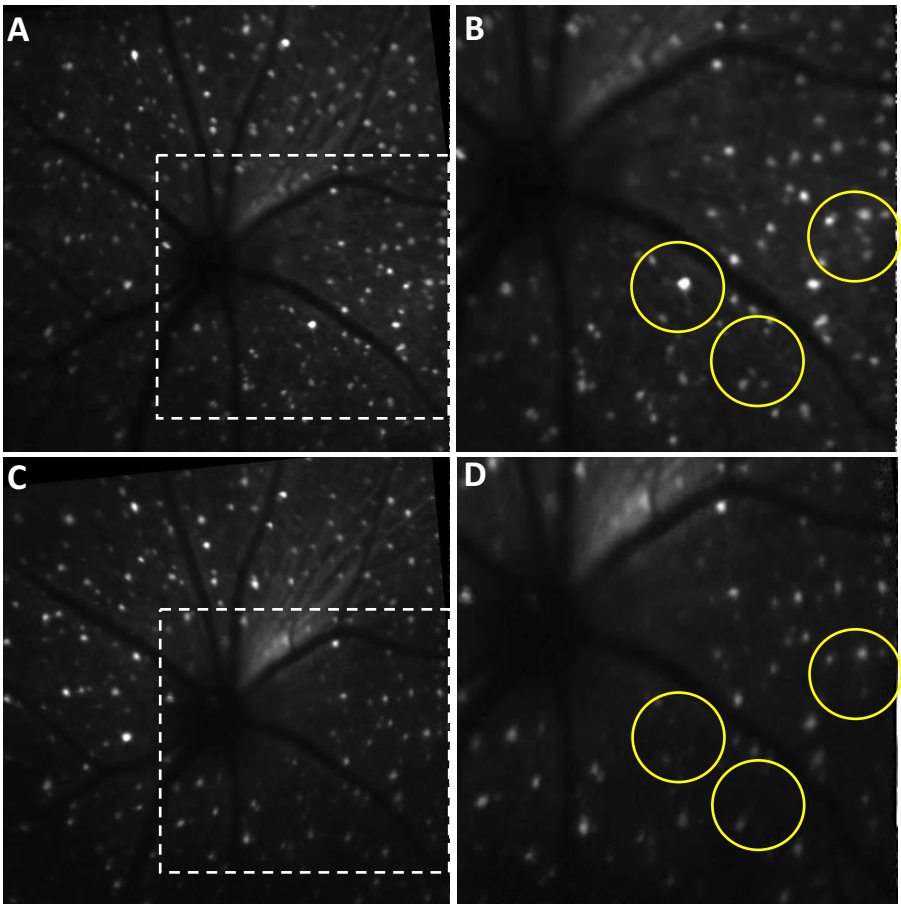

Figure 4.2. *In vivo* fluorescence imaging following ONT. *In vivo* fluorescence images from the same mouse at baseline, and following 3-days of ONT. A-B) 8-weeks following initial intravitreal injection of AAV2-CAG-GCaMP6s, and C-D) 3-days following ONT. Panels B and D demonstrate selected regions at higher magnification, with circles indicating regions of decreased cellular fluorescence.

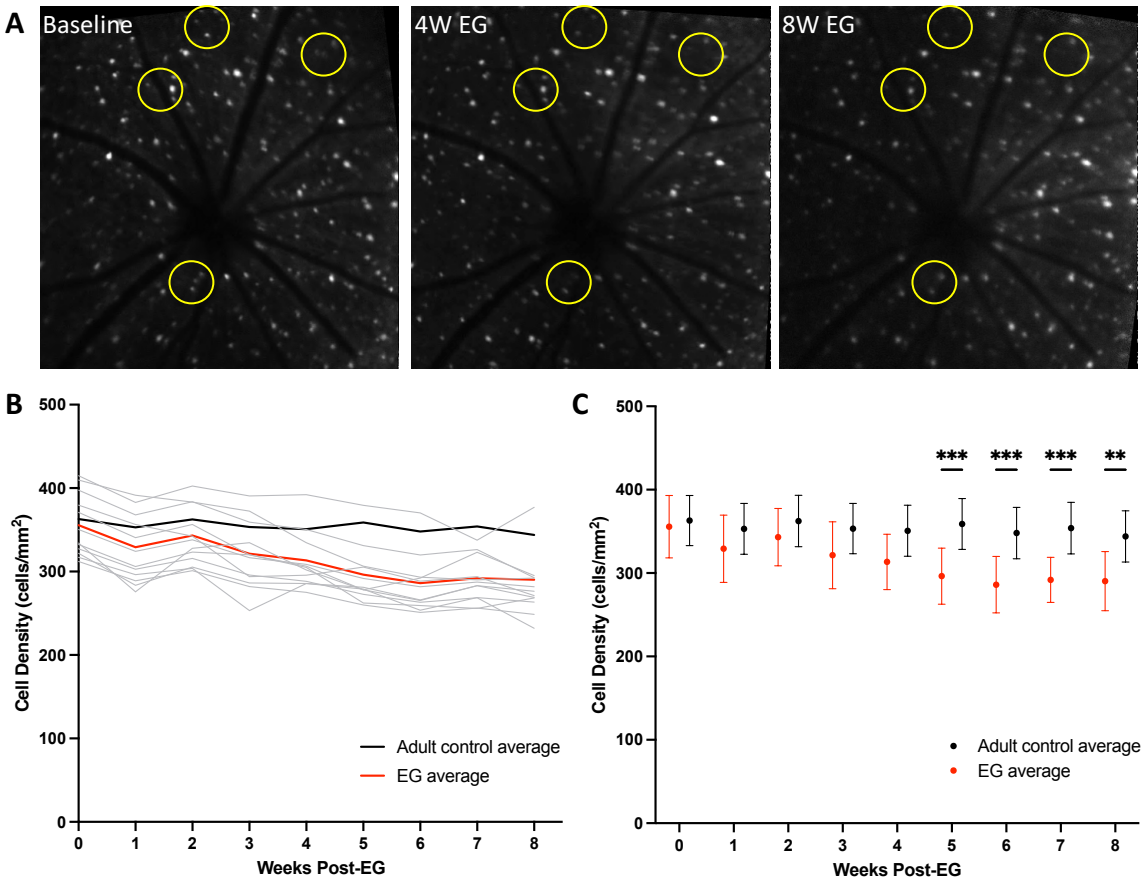

Figure 4.3. *In vivo* fluorescence imaging in adult EG. A) *In vivo* fluorescence images from a representative mouse that received EG showing cell density at baseline, 4-weeks post-EG, and 8-weeks post-EG. Yellow circles indicate regions of decreased cellular fluorescence. B) Quantification of *in vivo* cellular density over 8 weeks. Light grey lines indicate individual mice, the black line represents the average cell density in the control group, and the red line represents the average in the EG group. C) Two-way ANOVA shows significant differences between control groups and EG group cell densities beginning at 5-weeks until the final 8-week timepoint. Error bars represent standard deviation. ** = p< 0.01; *** = p< 0.001; n= 8 adult control, and n= 13 EG.

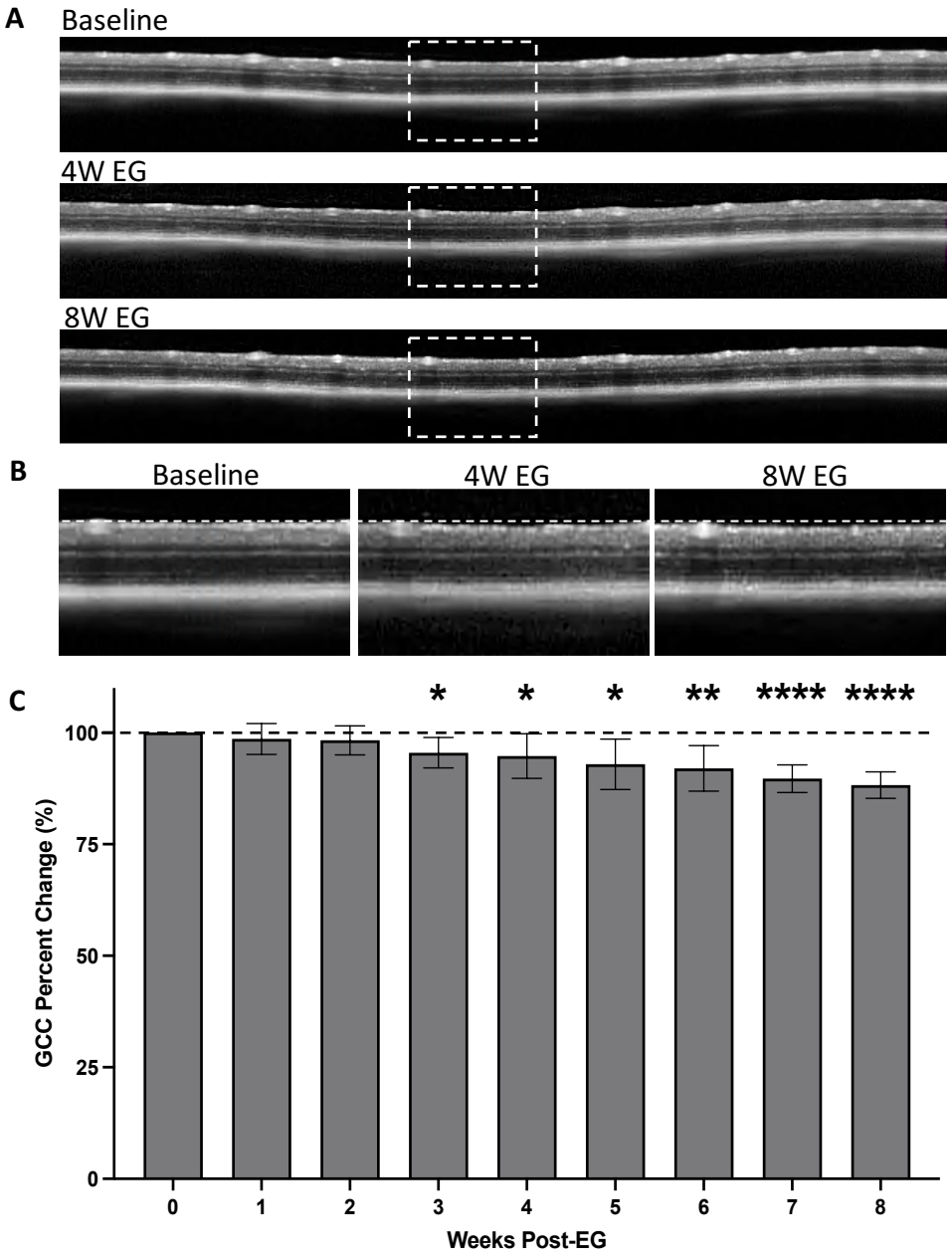

Figure 4.4. OCT peripapillary circle scans and GCC quantification following EG. A) Peripapillary OCT circle scans from an adult mouse that received EG at baseline, 4-weeks-EG, and 8-weeks-EG. B) Magnified regions of the OCT scans show decreased GCC thickness (segmented from the ILM to the outer boarder of the IPL). C) Quantification of the average decrease in GCC thickness over 8-weeks of EG. Error bars represent standard deviation. One-way repeated measures ANOVA with Tukey's multiple comparisons shows significant loss starting at 3 weeks-EG. * = $p < 0.05$; ** = $p < 0.01$; **** = $p < 0.0001$; n= 13.

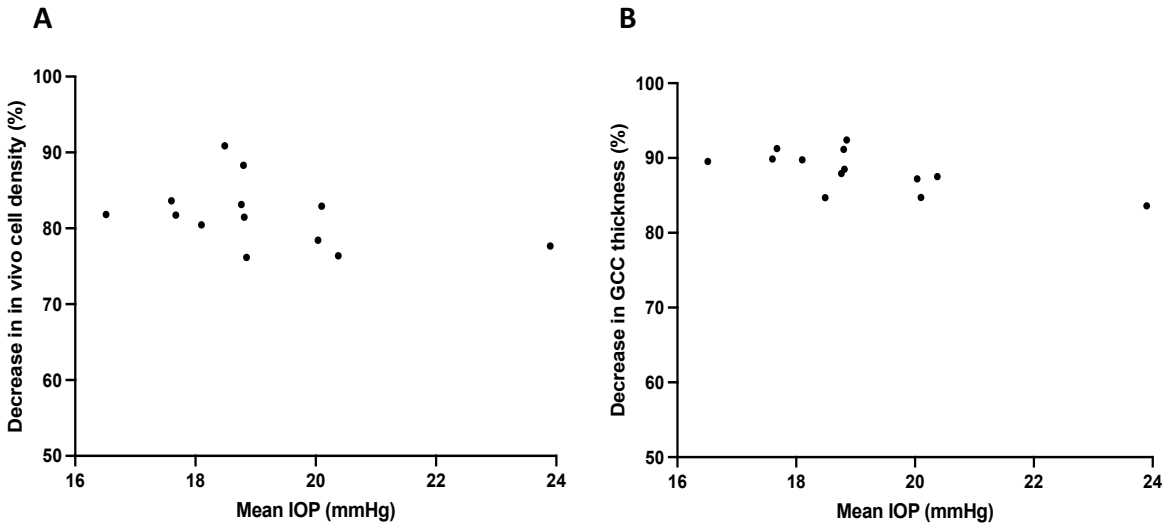

Figure 4.5. Correlation plots showing relationship between IOP, *in vivo* cellular density and GCC thickness in adult EG. Correlation plots showing relationship between mean IOP and A) the decrease in *in vivo* cell density quantified over 8-weeks post-EG, and B) the decrease in GCC thickness. Each data point represents one animal. Correlation analyses found Pearson correlation coefficients of -0.39 and -0.59 at 4, and 8-weeks of EG, respectively; n= 13.

4.3.2. Comparison of Functional Loss Following Optic Nerve Transection and Experimental Glaucoma

Functional Ca^{2+} imaging experiments were first performed on intact-isolated retinas from mice following 3-days of ONT. The GCaMP produced consistent transients over 4 KA treatments that returned to baseline following KA washout (Figure 4.6). The average transient amplitudes were not significantly different across the 4 KA treatments ($p= 0.79$). The ONT group was decreased 33% compared to controls ($p< 0.001$).

Ca^{+} imaging experiments were then performed on intact-isolated retinas from mice following 4-, or 8-weeks of EG (Figure 4.7). In both 4-week and 8-week EG groups, GCaMP produced consistent transients that were not significantly different from each other across the 4 KA treatments ($p= 0.81$ and $p= 0.86$, for 4-week and 8-week EG respectively). When compared to controls, there was a 17% decrease at 4-weeks EG and 37% at 8-weeks EG ($p= 0.003$ and $p< 0.001$, respectively; Figure 4.8). Interestingly, when the 4-week and 8-week EG groups were compared to ONT, ONT was significantly lower than the 4-week EG group ($p= 0.033$), but not significantly different from the 8-week EG group ($p= 0.76$).

Finally, correlation analyses performed between IOP and transient amplitude following 4-weeks and 8-weeks of EG (Figure 4.9) found r values of -0.53 ($p= 0.11$) and -0.62 ($p< 0.05$).

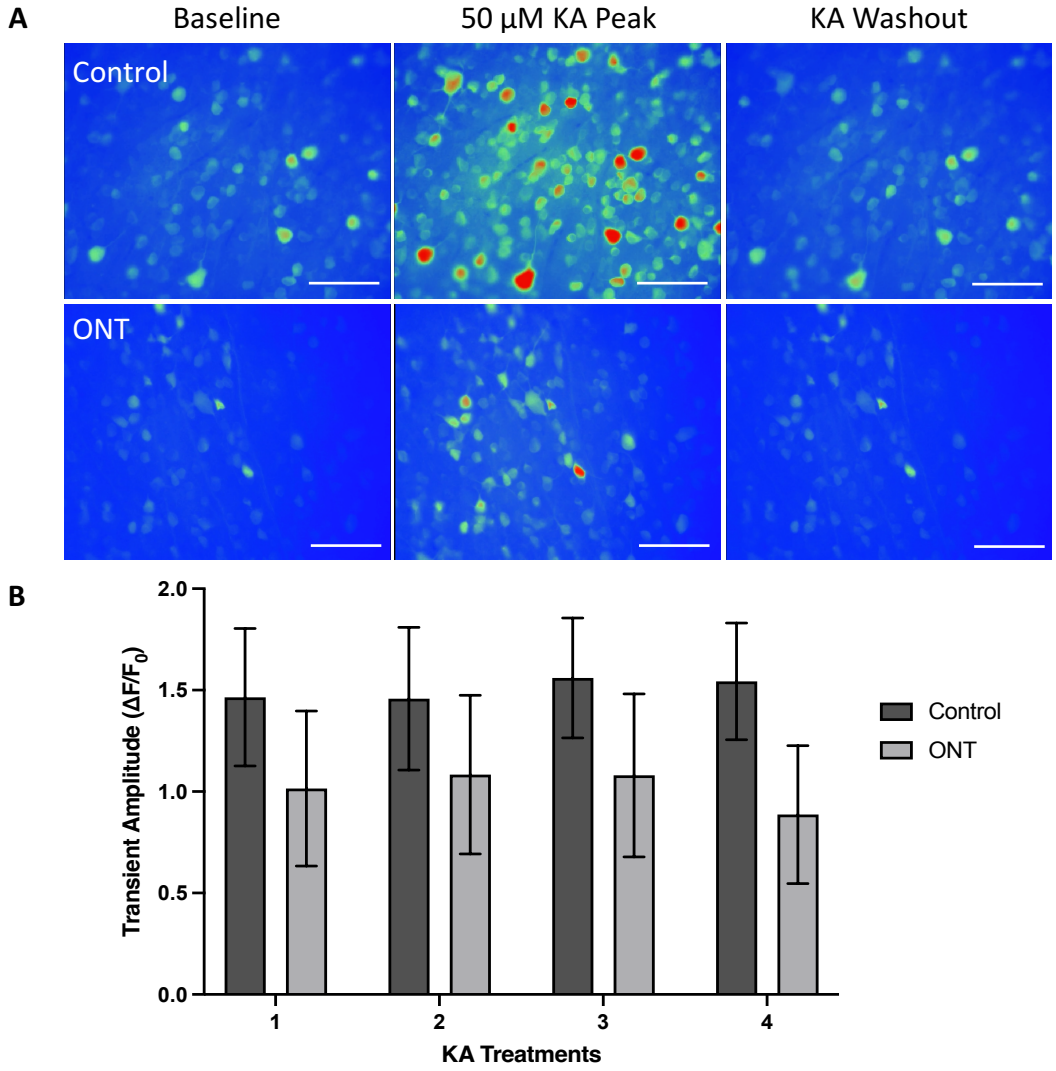

Figure 4.6. Ca^{2+} imaging experiments following ONT. A) Pseudocoloured images from Ca^{2+} imaging experiments in controls, and following 3-days of ONT, show (left-right) baseline fluorescence, the 50µM KA induced peak fluorescence, and following KA washout where cells returned to baseline fluorescence. Scale bars = 50 µm. B) Mean data showing transient amplitudes across 4 KA treatments for control and ONT groups. Data reported as mean, with error bars indicating standard deviation; n= 10 retinas from control mice, and n= 6 retinas from mice that had 3-days ONT.

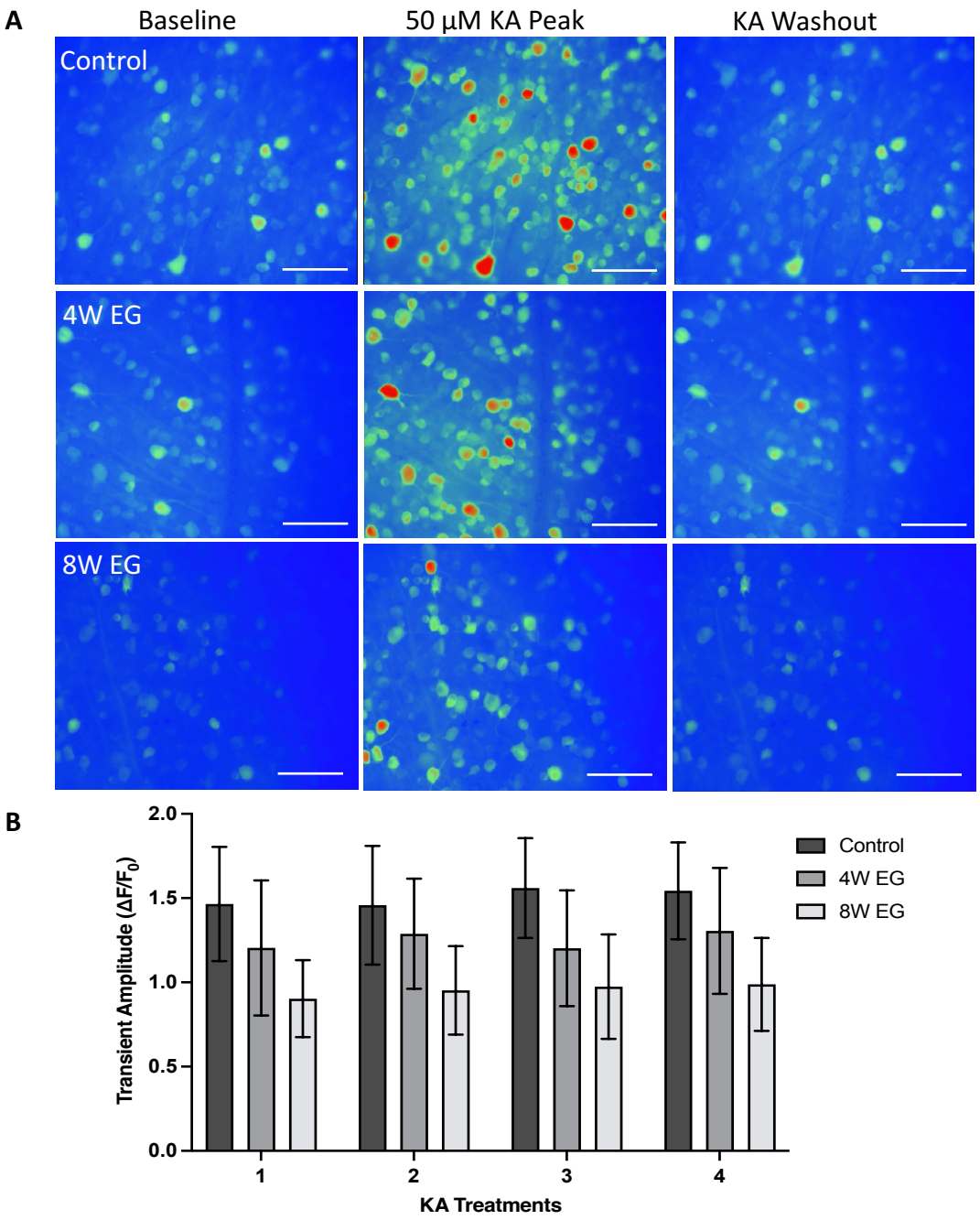

Figure 4.7. Ca^{2+} imaging experiments following EG in adult mice. A) Pseudocoloured images from Ca^{2+} imaging experiments in controls, and following 4-, and 8-weeks of EG, show (left-right) baseline fluorescence, the 50µM KA induced peak fluorescence, and following KA washout where cells returned to baseline fluorescence. Scale bars = 50 µm. B) Mean data showing transient amplitudes across 4 KA treatments for control and EG groups. Data reported as mean, with error bars indicating standard deviation; n= 10 retinas from controls, n= 10 retinas from 4W EG, and n= 13 retinas from 8W EG.

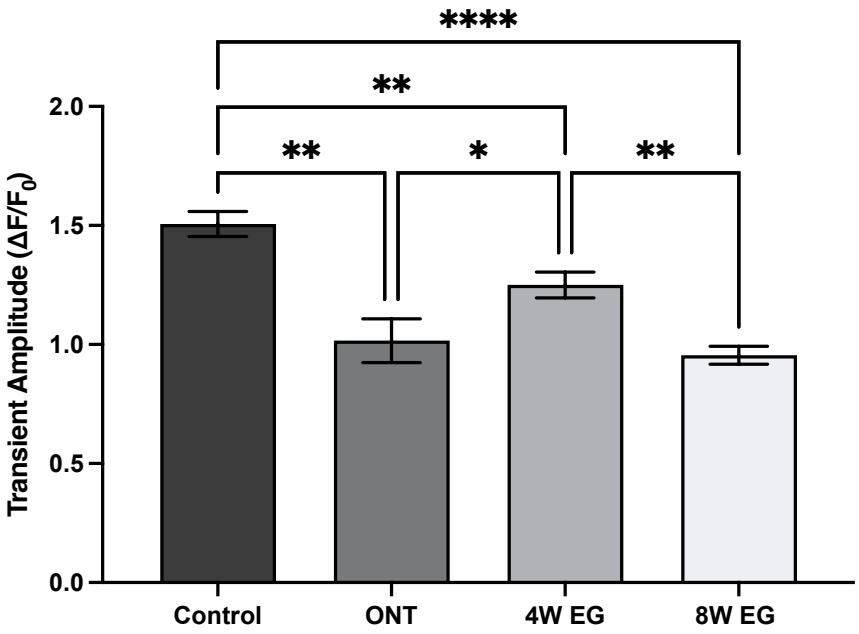

Figure 4.8. Comparison of transient amplitudes in ONT and EG in adult mice. Figure showing average transient amplitudes for control, and each experimental group. One-way ANOVA with Dunnett's multiple comparison shows significance between all groups except for ONT and 8-week EG which showed a non-significant relationship. * = p< 0.05; ** = p< 0.01; **** = p< 0.0001; n= 10 controls, n=6 ONT; n= 10 4W EG, and n= 13 8W EG.

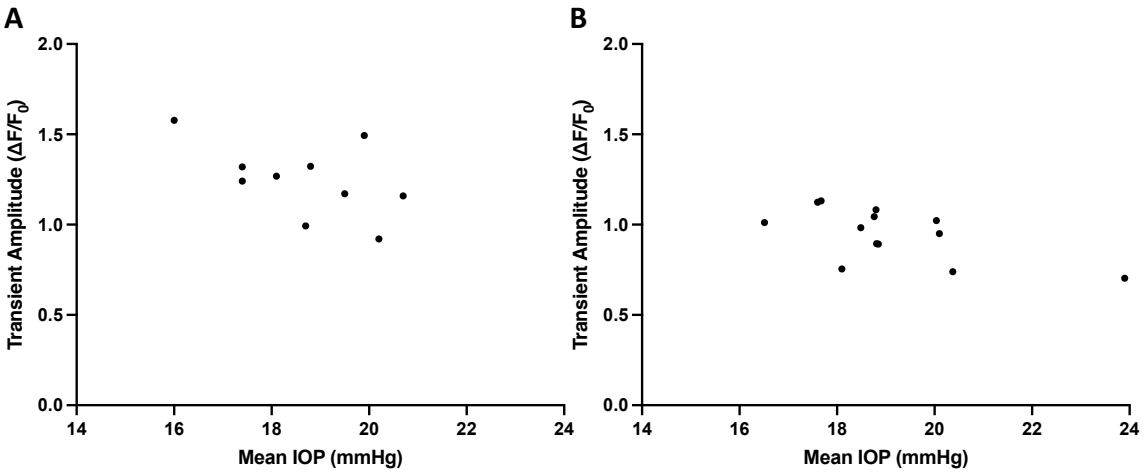

Figure 4.9. Correlation plots showing relationship between IOP and transient amplitudes in adult mice. Graphs (left to right) show correlation plots between IOP and the average transient amplitudes in mice following A) 4-, and B) 8-weeks of EG, respectively. Each data point represents one animal at their corresponding IOP. Correlation analyses found Pearson correlation coefficients of -0.53 and -0.62 at 4, and 8-weeks of EG, respectively. n= 10 retinas from 4W EG, and n= 13 retinas from 8W EG.

4.3.3. Immunohistochemical Analyses

RBPMS-positive cell quantification was performed in wholemounted retinas from each group (3-days ONT, 4-week EG, and 8-week EG; and representative micrographs are shown in Figure 4.10). After ONT, the RBPMS-positive cell densities were reduced to 2613 (274) cells/mm^2 in the experimental eyes, in comparison to 3225 (291) cells/mm^2 in fellow eyes. In the 4-week EG group, 2658 (152) cells/mm^2 in the experimental eyes vs 3114 (109) cells/mm^2 fellow eyes, and in the 8-week EG group 2471 (163) cells/mm^2 in the experimental eyes vs 3223 (140) cells/mm^2 in the fellow eyes. These values corresponded to a loss of 19%, 15%, and 23% in ONT, 4W EG and 8W EG groups, respectively. When compared to control eyes, the RBPMS-positive cell density was significantly reduced in all groups ($p< 0.0001$). Correlation analysis between IOP and RBPMS quantification at 4- and 8-weeks of EG (Figure 4.11A and 4.11B) showed negative correlations of -0.45 ($p= 0.19$) and -0.68 ($p= 0.011$), respectively.

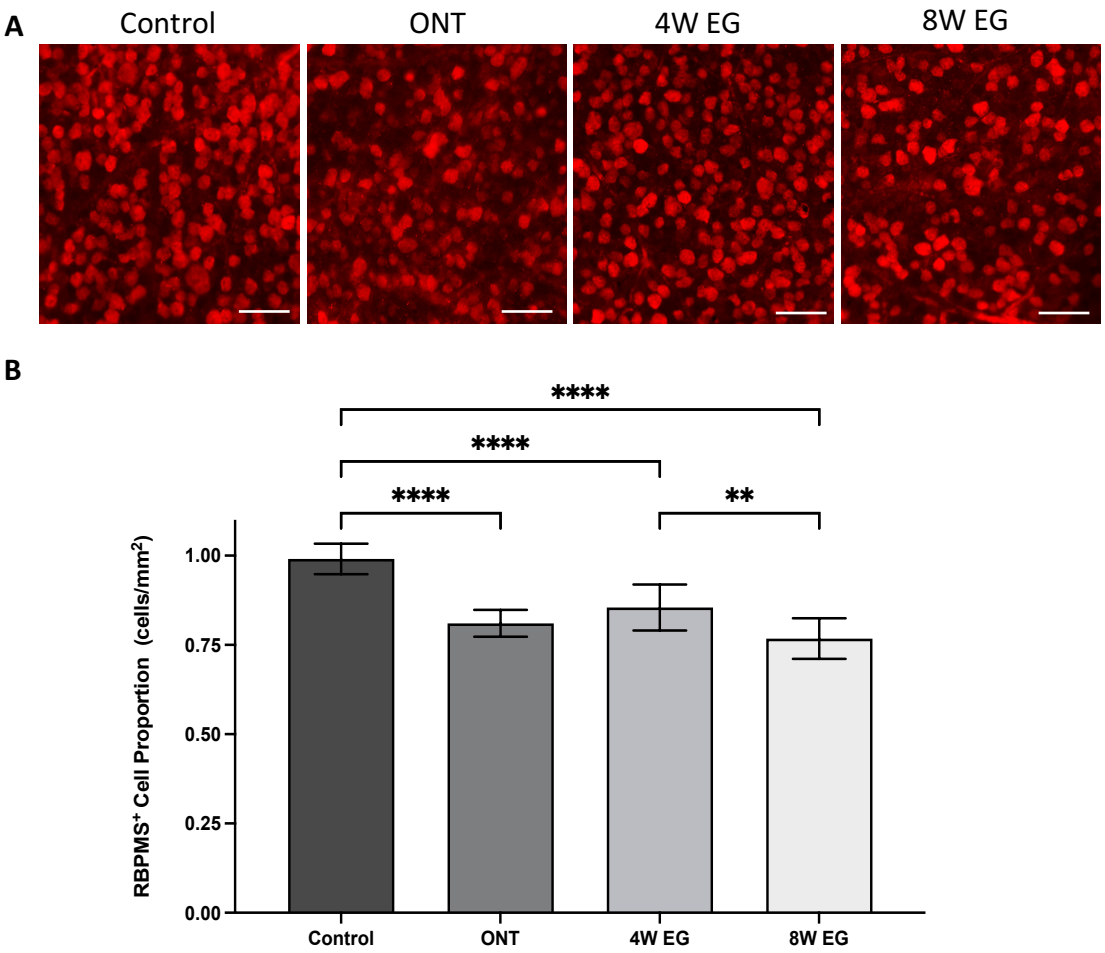

Figure 4.10. Immunohistochemistry following ONT and EG. A) Panels show immunohistochemical staining (left to right) of RBPMS, GFP, ChAT, and a merge panel for retinas from control mice, 3-days of ONT, 4-, and 8-weeks of EG. B) RBPMS-positive cell densities were quantified for both right and left eyes, and histogram shows the proportions for each group. A one-way ANOVA with Dunnett's multiple comparison determined significance between all groups except for between 3-day ONT and 8-week EG which was non-significant. ** = p< 0.01; *** = p< 0.001; **** = p< 0.0001; n= 10 controls, n=6 ONT; n= 10 4W EG, and n= 13 8W EG.

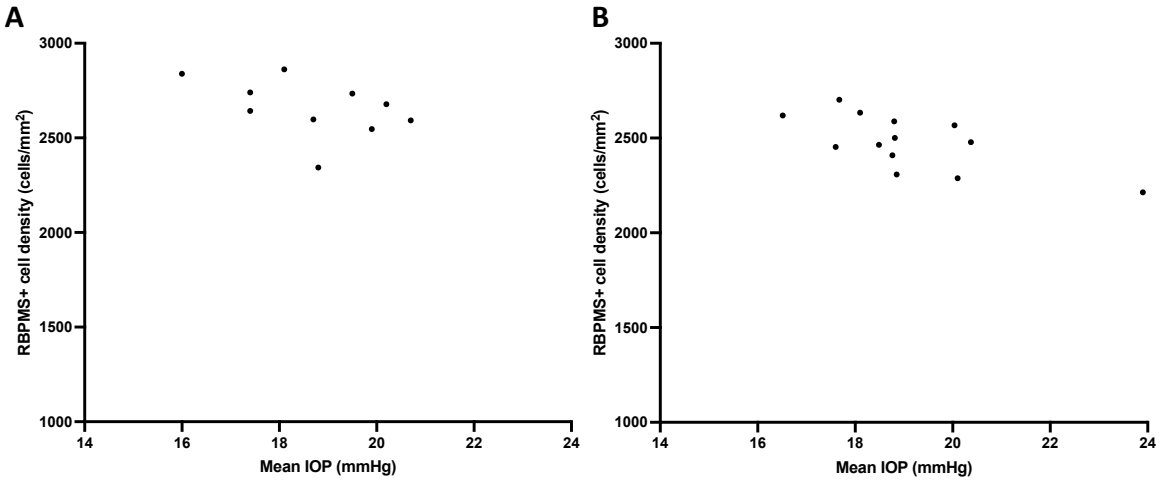

Figure 4.11. Correlation plots showing relationship between IOP and RBPMS immunohistochemical quantification in adult EG. Figures show correlation relationship between IOP and RBPMS-positive cell density following A) 4-weeks, and B) 8-weeks of EG (left to right, respectively). Each data point represents one animal. Correlation analysis found Pearson correlation coefficients of -0.45 and -0.68 at 4-, and 8-weeks of EG, respectively; n= 10 4W EG, and n= 13 8W EG.

4.3. Summary of Findings

The results of this chapter describe the use of AAV2-CAG-GCaMP6s as a tool for monitoring parameters of structural loss with both *in vivo* and histological measures, and functional loss with intact-isolated retinal preparations, following optic nerve injury. Key findings from this chapter include:

1. *In vivo* CSLO/OCT imaging demonstrated decreases of both fluorescent cell density and GCC thickness at 4-weeks post-EG, 8-weeks post EG
2. Compared to controls, significant decreases in transient amplitude were measured with Ca^{2+} imaging as early as 3-days following ONT and following 4- and 8-weeks of EG. Interestingly, 3-day ONT and 8-week EG groups were not significantly different from each other
3. All experimental groups reported significant loss of RBPMS-positive RGCs and, in the EG groups, showed negative correlations with IOP

CHAPTER 5. EFFECTS OF AGE AND EXPERIMENTAL GLAUCOMA ON RGC FUNCTION

5.1. Chapter Objectives

This chapter sought to answer fundamental questions about viral longevity and RGC function in aged mice and sought to examine the effect of age and EG by inducing EG in mice approximately 2 years of age, or 1.5 years post-viral injection. The chapter specific objectives were:

1. Characterize the AAV2-CAG-GCaMP6s viral expression in mice aged with the virus compared to mice injected with the viral vector at 18-months of age with *in vivo* CSLO and OCT imaging
2. Evaluate cell function using Ca^{2+} imaging in mice aged with the virus compared to mice injected with the viral vector at 18-months of age
3. Examine the effects of both age and EG on RGC structure and function with *in vivo* imaging, Ca^{2+} imaging, and immunohistochemistry

5.2. Experimental Design

In this study, we used two groups of mice that aimed to address age and AAV2-CAG-GCaMP6s injection: the *aged* group (n=8) and the *old* group (n= 5 for *in vivo* analyses and 10 for Ca^{2+} imaging and IHC). In the aged group, a subset of mice had an intravitreal injection of the AAV2-CAG-GCaMP6s vector at 3 months of age. These mice were imaged with *in vivo* CSLO and OCT imaging weekly over the initial 8-weeks, like the adult control group, and then were imaged every 6-months until 18-months following a

single viral injection. The aged group was used to determine the persistence of the GCaMP expression in the inner retina. In the *old* group, mice were injected with the viral vector at 18-months of age and were imaged weekly over 8-weeks to with *in vivo* CSLO and OCT imaging to monitor viral transduction and GCC thickness. Following the final *in vivo* imaging timepoint in both groups, mice were euthanized, and retinas were dissected and prepared for Ca^{2+} imaging and immunohistochemistry.

Finally, a subset of mice that received viral injection at 3-months of age and were aged with the virus to 18-months post-injection, were divided into two EG groups. EG was induced following the 18-month *in vivo* imaging timepoint. After induction of EG, mice were monitored over 4-weeks (n= 10) or 8-weeks (n= 8) with weekly *in vivo* imaging and IOP measurements. Following the final *in vivo* imaging and IOP timepoint, mice were euthanized, and retinas were dissected and prepared for Ca^{2+} imaging and immunohistochemistry.

5.3. Results

5.3.1. In Vivo Quantification of Viral Labelling and Inner Retinal Thickness in Aged and Old Mice

Mice within the aged group showed similar trends to previously reported groups over the initial 8-weeks post-AAV injection, with *in vivo* cell density increasing over the initial 5-weeks and plateauing to 8-weeks (Figure 5.1A). The aged group mice were subsequently imaged at 6-, 12-, and 18-months post-injection and showed a gradual decrease in cell labelling (Figure 5.1B). When analyzed, the change in cell density

between 2-months and 6-months, 6-months and 12-months, and 12-months and 18-months were all non-significant (p= 0.87, p= 0.51, and p= 0.70, respectively), however, there was a significant decrease between 2-months and 12-months, and 2-months and 18-months (p= 0.042 and p= 0.004, respectively).

In the old group, cell fluorescence was quantified from *in vivo* fluorescence images over 8-weeks following AAV injection (Figure 5.2A). Labeling was visible in all mice 1-week post-injection. Cell density was quantified from *in vivo* fluorescence images and showed an increase from 177 (26) cells/mm^2 at 1-week post-injection, to 405 (43) cells/mm^2 at the final 8-week timepoint, with significant increases in cell density occurring over the first 4-weeks (Figure 5.2B). Similar to *in vivo* labelling in adult mice, GCaMP6s fluorescence was primarily expressed in somas and RGC axons, although there was expression detectable in some dendrites (Figure 5.3). *In vivo* cell density at 8-weeks post-injection was compared to the aged mice 18-month timepoint and the latter had significantly fewer cells with average densities of 405 (34) cells/mm^2 and 348 (54) cells/mm^2, respectively (p=0.042). Moreover, *in vivo* cell densities were compared between old mice and adult mice 8-weeks post-injection (average density of 384 (43) cells/mm^2), and there was no significant difference between them (p= 0.34).

In vivo OCT imaging was performed at the same timepoints over 18-months of the aged-group and GCC thickness measurements were quantified. GCC thickness measurements decrease over 18-months from 81.9 (1.8) μm at baseline, to 76.8 (1.9) μm at 18-months post-intravitreal injection (Figure 5.4) The decrease in thickness was significant starting at 6-months post AAV-injection (p= 0.014) and continued over 18-

months ($p < 0.001$, baseline vs 18-months). When GCC thickness was compared between aged mice at the 18-month post-injection timepoint to aged control mice, they were not-significantly different ($p = 0.11$). GCC thickness was also quantified over 8-weeks following AAV-injection.

GCC thickness measurements performed following AAV2-CAG-GCaMP6s injection in old mice showed a non-significant increase in average GCC thickness at 3-weeks post-injection ($p = 0.17$) and a significant increase at 4-weeks post-injection ($p = 0.049$). However, the GCC thickness returned to baseline levels and there was no significant difference between baseline and 8-weeks post injection ($p = 0.96$; Figure 5.5).

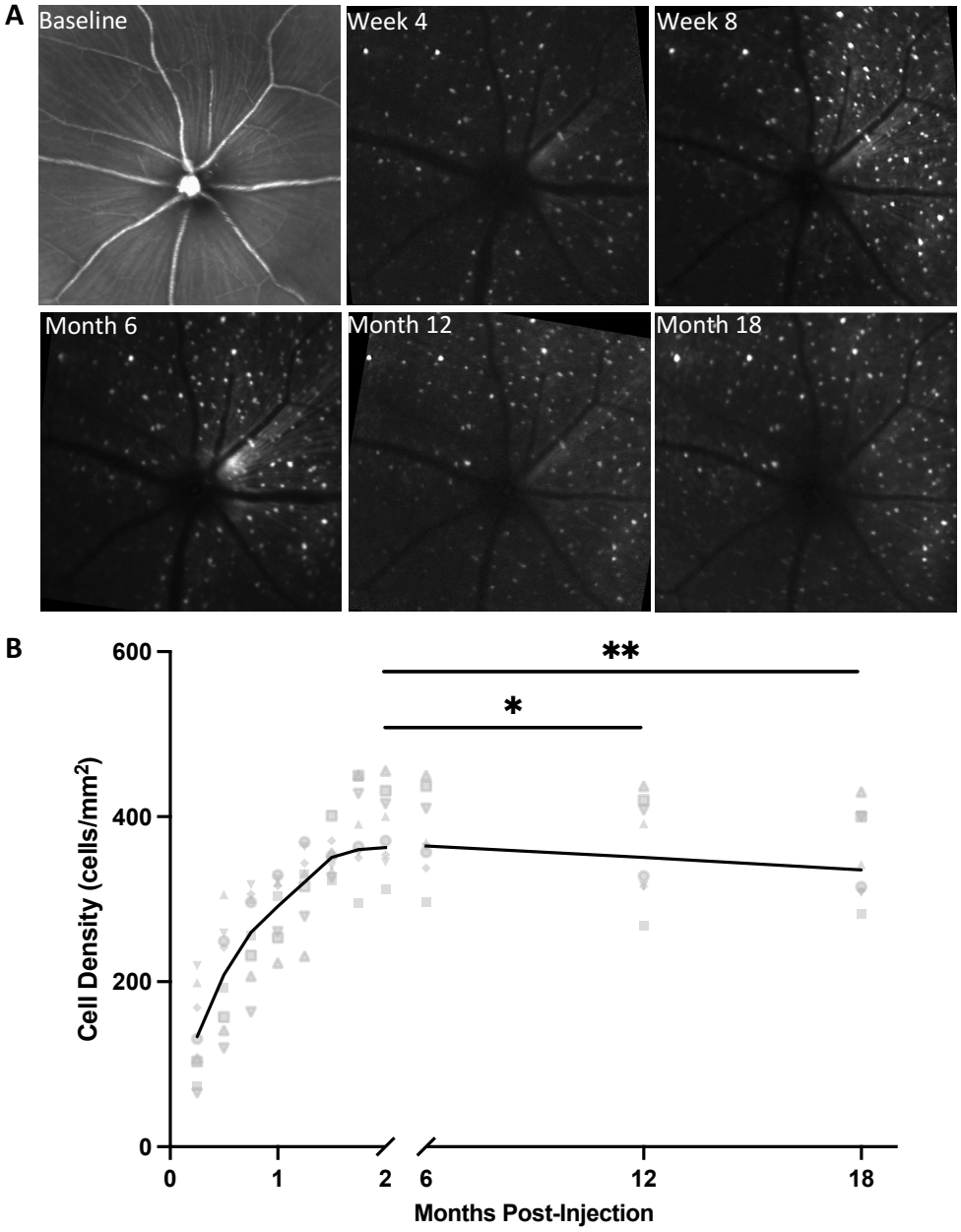

Figure 5.1. Persistence of AAV2-CAG-GCaMP expression over 18-months. A) *In vivo* fluorescence images of a representative mouse injected with the virus at 3-months of age and aged to 18-months post-injection. B) Quantification of *in vivo* cellular density over 18-months post injection shows an increase in cellular labelling which plateaus over the initial 2 months, then a gradual and significant decrease between 2-months and 12-month, and 2-months and 18-months post-injection with RM one-way ANOVA with Tukey's multiple comparisons. * = $p < 0.05$; ** = $p < 0.01$; n= 8.

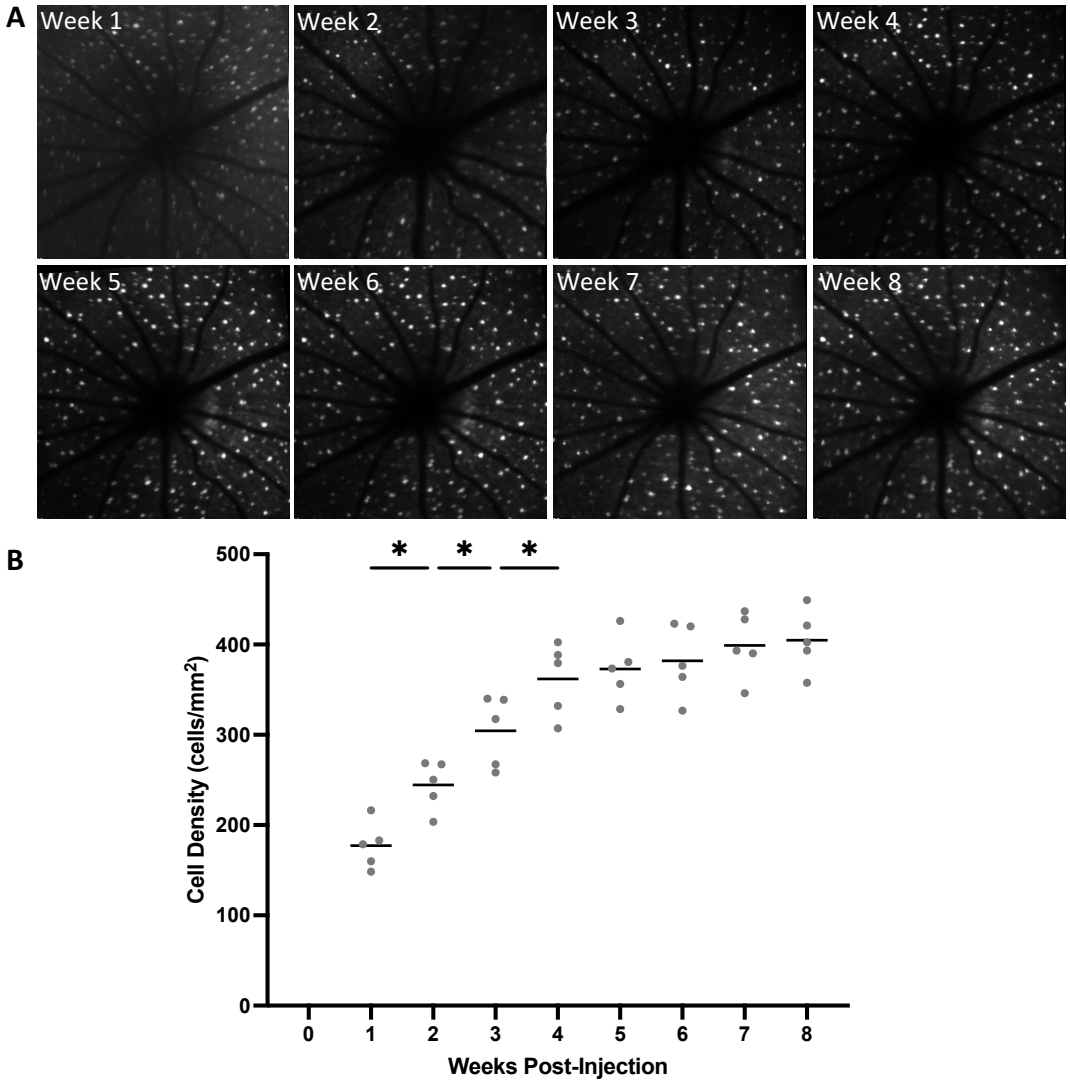

Figure 5.2. *In vivo* viral transduction in old mice. A) Representative images acquired in an old mouse over 8-weeks following intravitreal injection of AAV2-CAG-GCaMP6s. B) Quantification of cellular labelling over the 8-weeks. RM one-way ANOVA with Tukey's multiple comparisons found significance over 4-weeks following intravitreal injection. * = p< 0.05; n= 5.

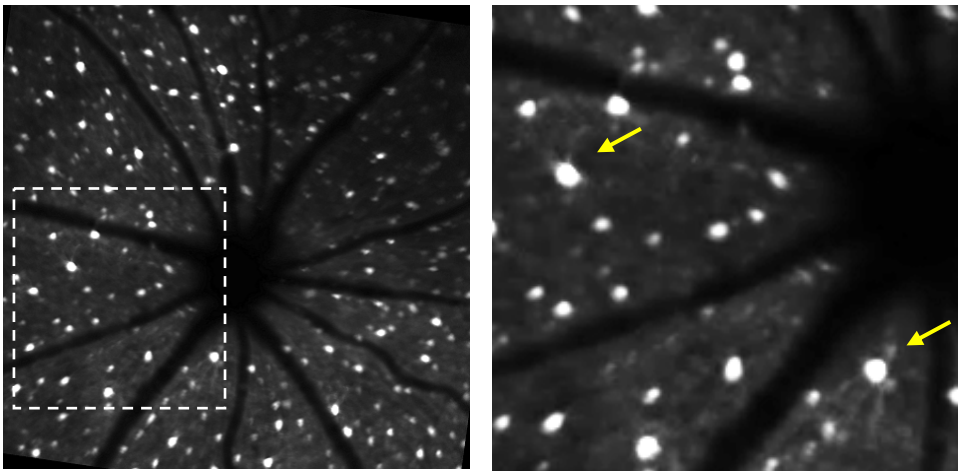

Figure 5.3. Dendrite visualization of GCaMP6s positive cells in an old mouse. *In vivo* fluorescence images from an old mouse injected with AAV2-CAG-GCaMP6s shows GCaMP expression in both somas and dendrites. Right image demonstrates the selected region at higher magnification.

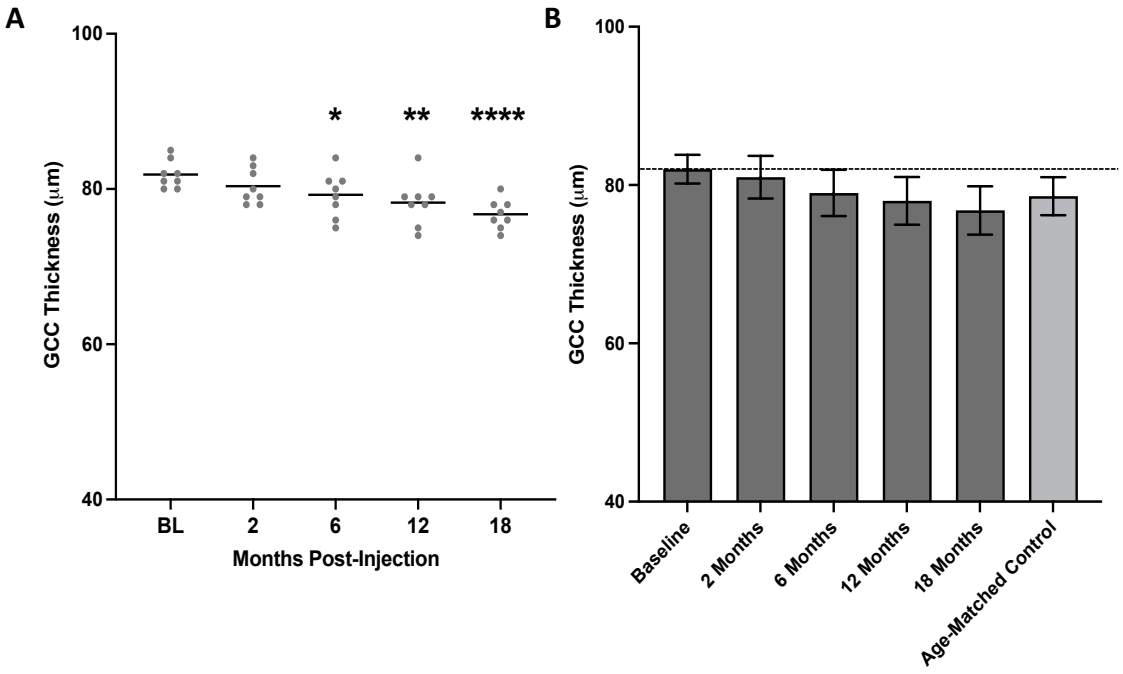

Figure 5.4. GCC thickness over 18-months of viral transduction. A) Average GCC thickness quantified from *in vivo* peripapillary OCT circle scans in mice aged with the virus until 18-months post-intravitreal injection. RM one-way ANOVA with Tukey's multiple comparisons found significant decreases in GCC thickness over 18 months. * = p< 0.05; ** = p< 0.01; **** = p< 0.0001. B) When compared to the average GCC thickness in age-matched controls, 18-month-old mice that had not received an intravitreal injection, an unpaired t-test found no significant difference (p= 0.10); n= 8 aged mice, and n= 5 age-matched controls.

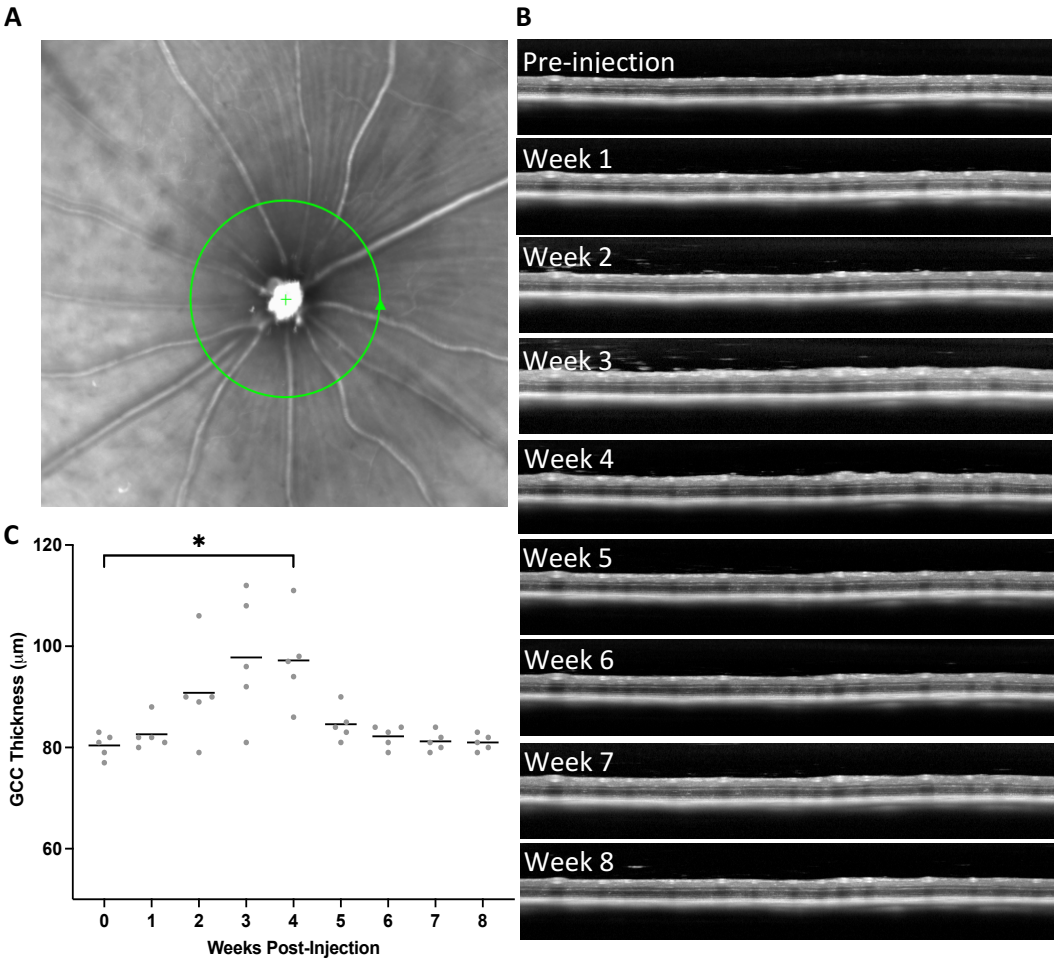

Figure 5.5. Longitudinal OCT scans of the left eye of an old mouse following intravitreal injection of AAV2-CAG-GCaMP6s. A) *In vivo* infrared image of the retina of an 18-month-old mouse with the location of the OCT peripapillary circle scan. B) OCT peripapillary circle scans acquired in a representative mouse weekly over the 8-week time course post-AAV injection. C) Quantification of GCC thickness, as segmented from the ILM to the outer boarder of the IPL. Repeated measures one-way ANOVA with Tukey's multiple comparisons found a significant increase in GCC thickness at 4-weeks post-injection (* = $p < 0.05$) but confirmed no significant changes in GCC thickness between other timepoints, or between baseline and 8-weeks post-injection ($p = 0.96$); $n = 5$.

5.3.2. Functional Characterization of Aged and Old Mice with Ca^{2+} Imaging

Functional Ca^{2+} imaging experiments were performed on intact-isolated retinas from both the aged and old groups (Figure 5.6A). Ca^{2+} imaging experiments from both aged and old groups showed that cells could return to baseline following each KA treatment, and the responses observed were consistent. Intragroup analyses showed no significant differences across the 4 KA treatments in either aged, or old groups ($p= 0.67$ and $p= 0.72$; Figure 5.6B). When average transient responses were compared between adult mice, aged mice, and old mice there were significant differences between adult and aged, and adult and old ($p= 0.004$ and $p= 0.024$), but no significance between aged and old groups ($p= 0.93$; Figure 5.7).

5.3.3. Immunohistochemical Characterization of Viral Transduction in Aged and Old Mice

Cell density quantification and colocalization analyses were performed in both aged and old mice to determine if there were differences in RBPMS-positive, or GCaMP-positive cell densities (Figure 5.8 and Figure 5.9). In the aged group, the average density of RBPMS-positive cells was 2533 (396) cells/mm^2, of ChAT-positive cells was 900 (209) cells/mm^2 and of GFP-positive cells was 727 (194) cells/mm^2. In the old group, the average density of RBPMS-positive cells was 2638 (315) cells/mm^2, of ChAT-positive cells was 896 (116) cells/mm^2 and of GFP-positive cells was 1131 (123) cells/mm^2 (Figure 5.10A).

Colocalization analysis was performed in both the aged and old group to determine the hit rate and specificity of the virus to retinal cells within the GCL. Of the

total RBPMS-positive cells, 20% (6%), and 31% (6%) were GFP-positive in the aged and old groups, respectively. Of the GCaMP-positive cells (GFP-positive) in the aged group, 70% (10%) colocalized with RBPMS, 15% (5%) with ChAT, and 15% (8%) with RBPMS/ChAT-negative cells. In the old group, 71% (8%) colocalized with RBPMS, 12% (4%) with ChAT, and 17% (9%) did not colocalize with RBPMS or ChAT (Figure 5.10B).

The cell density, hit rate and specificity data in the adult and aged groups were also compared to those of adult mice (see Chapter 3 for detailed results from adult mice). Compared to adults, there were significant decreases in both aged and old RBPMS densities ($p< 0.0001$ and $p< 0.001$, respectively). ChAT-positive cell densities were also decreased in both aged and old groups compared to adults, although it was non-significant ($p= 0.66$ and $p= 0.65$, respectively). The GFP-positive cell density in the aged group was decreased from adults, although non-significant ($p= 0.25$). Interestingly, the GFP-positive cell density was similar between the old group and in adults. Because of the differences in RBPMS-positive, and GFP-positive cells across groups, there were different observed hit rates across groups, with a hit rate of 27%, 20%, and 31%, in adult mice, aged mice, and old mice, respectively. The specificity of the virus to RBPMS-positive, ChAT-positive, and RBPMS-negative/ChAT-negative cells was not-significantly different across adult, aged, and old groups.

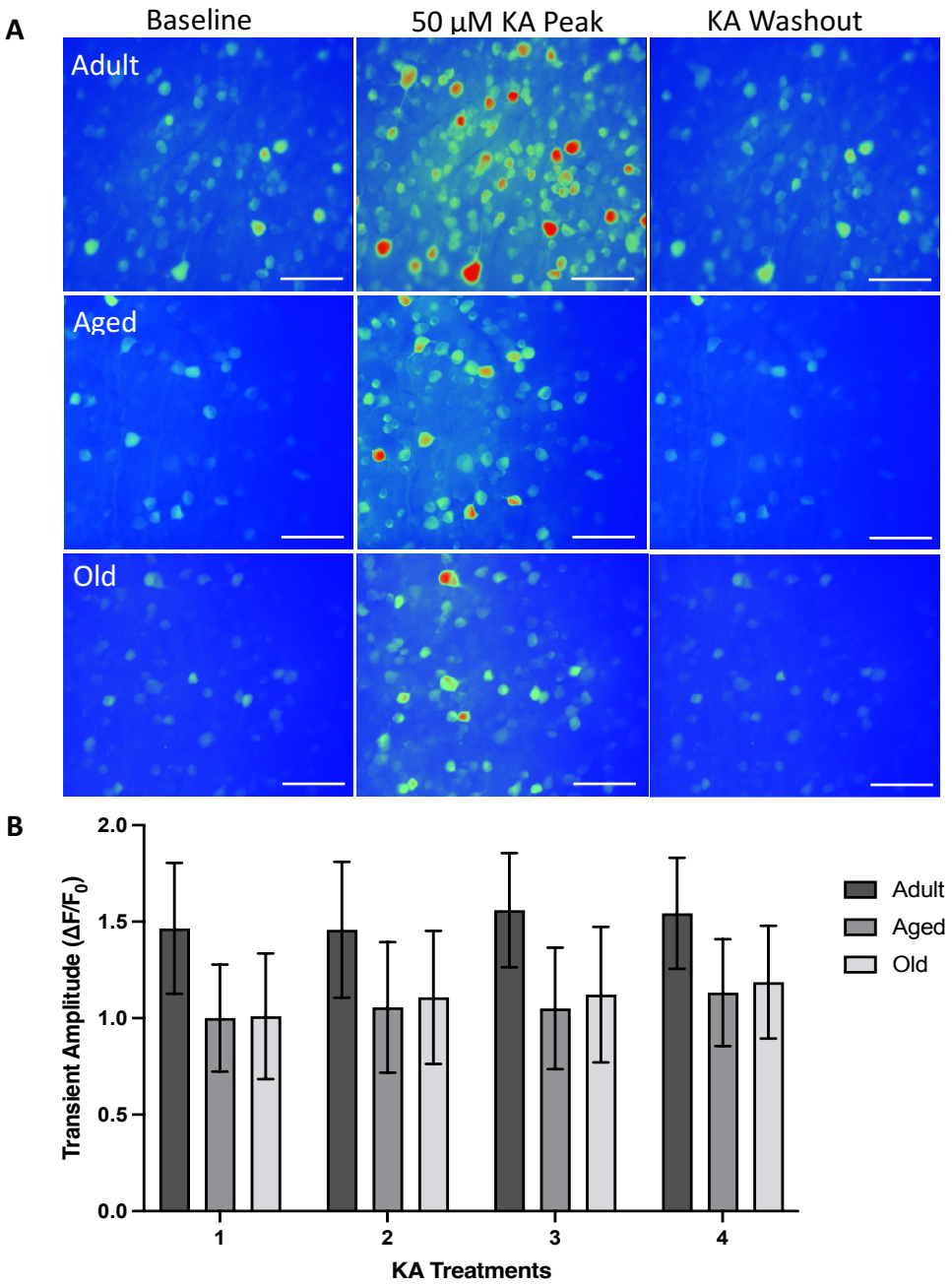

Figure 5.6. Calcium imaging experiments in aged and old mice. A) Pseudocoloured images from Ca^{2+} imaging experiments from an adult control mouse, from a mouse injected with the viral vector at 3-months and aged with the virus until 18-months post-injection, and in an old mouse injected with the virus at 18-months post-injection. Images show (left-right) baseline fluorescence, the 50µM KA induced peak fluorescence, and following KA washout where cells returned to baseline fluorescence. Scale bars = 50 µm. B) Mean data showing transient amplitudes across 4 KA treatments for adult, aged, and old groups. Data reported as mean, with error bars indicating standard deviation; n= 10 adult controls, n= 8 aged, and n= 10 old.

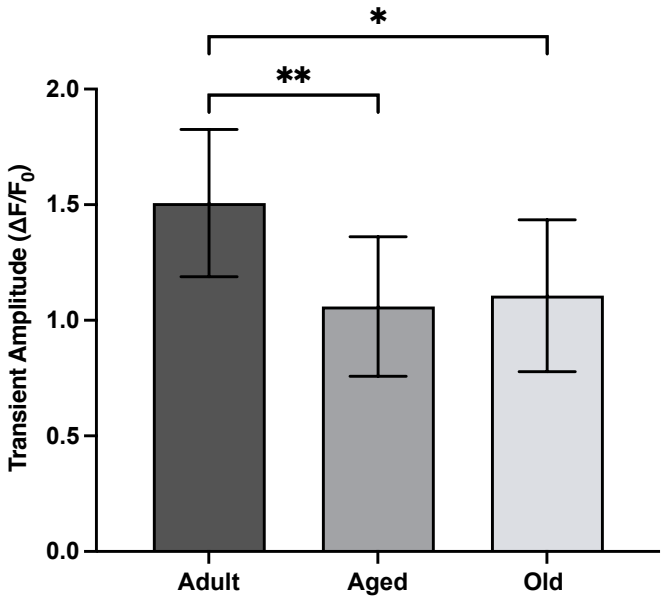

Figure 5.7. Comparison of transient amplitudes in aged and old mice to adults. Figure showing the average transient amplitude in adult control mice, and aged and old groups. One-way ANOVA with Dunnett's multiple comparisons shows significant decreases between adult control mice and aged mice (p=0.004, and adult control mice and old mice (p= 0.024). Results also find no significant difference between aged and old groups (p= 0.93). * = p< 0.05; ** = p< 0.01; n= 10 adult controls, n= 8 aged, and n= 10 old.

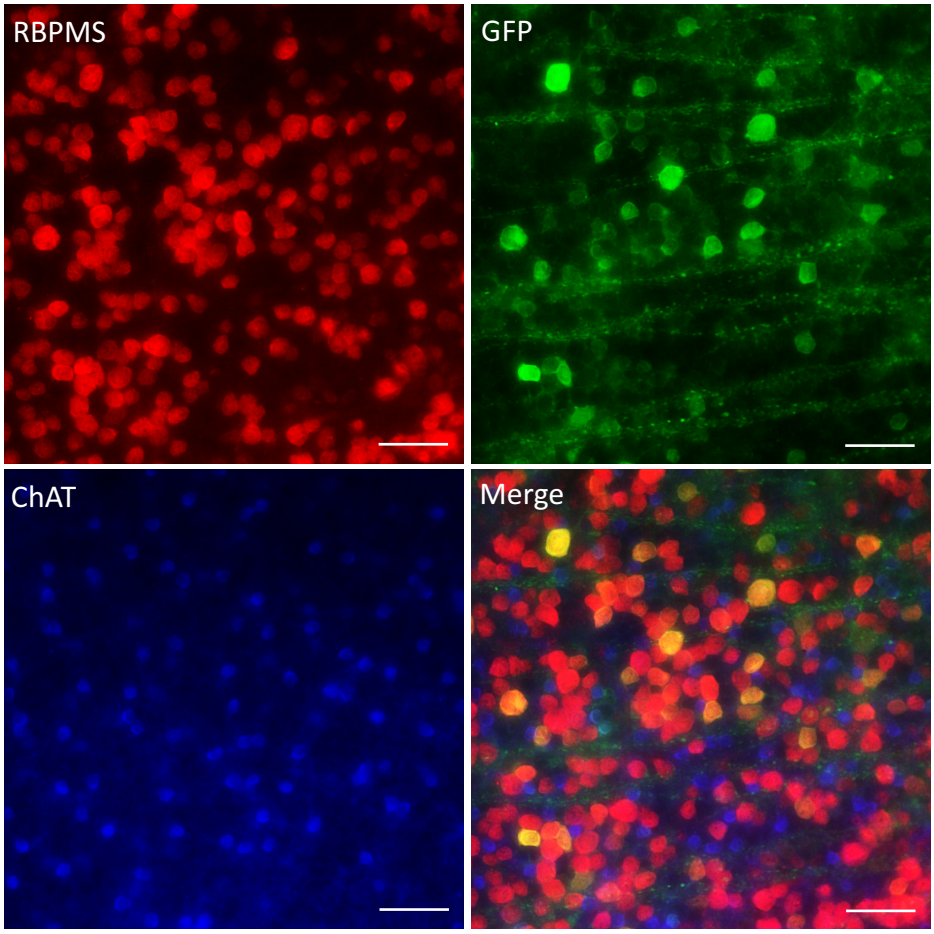

Figure 5.8. Immunohistochemical staining of retinal neurons in the GCL from the retina from a mouse injected with AAV2-CAG-GCaMP6s at 3-months of age and aged with the virus to 18-months post injection. Images show RBPMS labelling of RGCs, ChAT labelling of cholinergic amacrine cells, GFP labelling used to amplify the GCaMP fluorescence, and a panel showing the merged channels. Scale bars = 50µm.

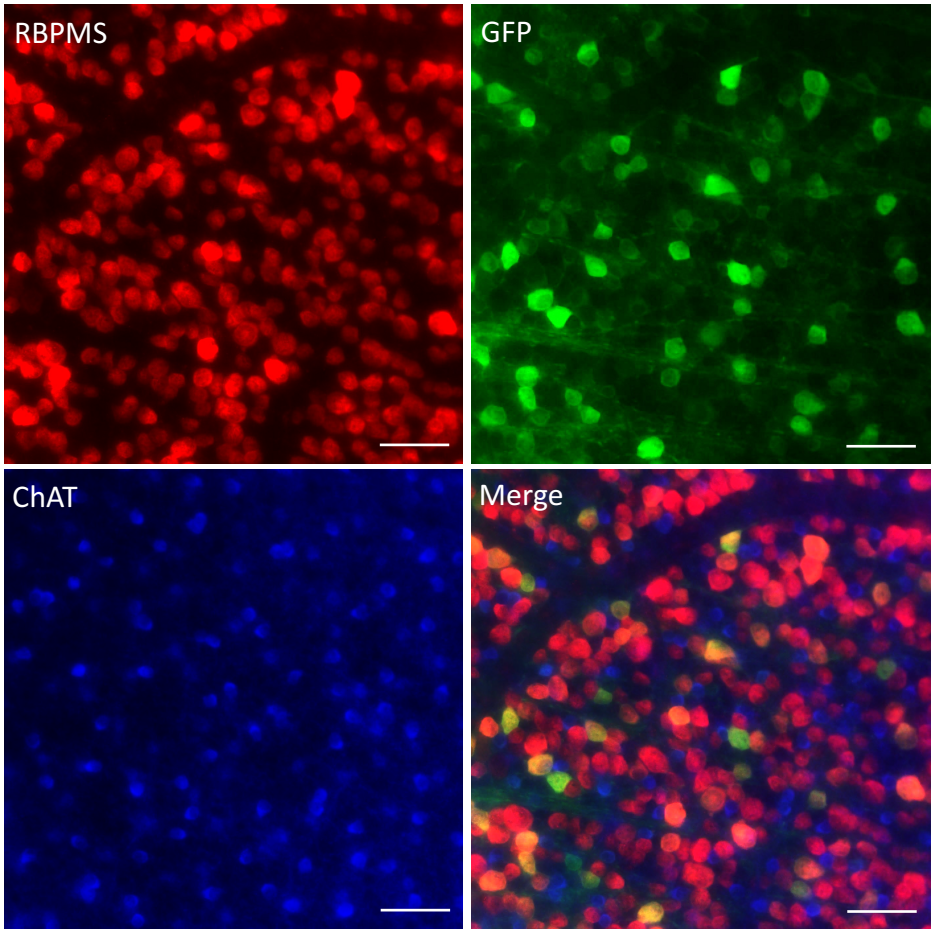

Figure 5.9. Immunohistochemical staining of retinal neurons in the GCL from the retina from an old mouse injected with AAV2-CAG-GCaMP6s at 18-months of age. Images show RBPMS labelling of RGCs, ChAT labelling of cholinergic amacrine cells, GFP labelling used to amplify the GCaMP fluorescence, and a panel showing the merged channels. Scale bars = 50µm.

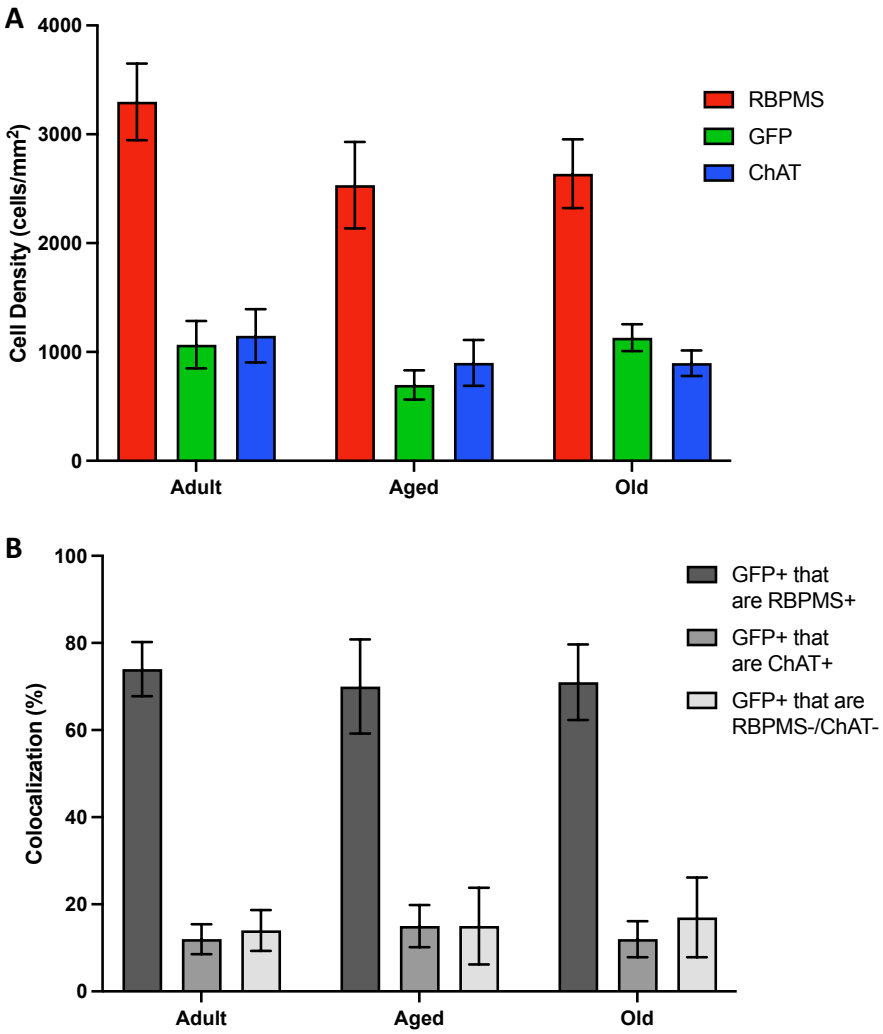

Figure 5.10. Comparison of cellular density and specificity of the AAV2-CAG-GCaMP6s viral vector to retinal cells within the GCL in mice aged with the virus and mice injected with the virus when 18-months of age. A) Figure showing the average cell density of both GFP-positive cells (GCaMP-positive cells) labeled by intravitreal injection, RBPMS-positive cells labelled by immunohistochemistry, and cholinergic amacrine cells (ChAT-positive cells) in both the aged and old groups. B) Figure showing the specificity of the viral vector to RBPMS-positive cells, ChAT-positive cells, and to RBPMS-negative/ChAT-negative cells in the three different groups of mice. Error bars represent standard deviation. n= 10 adult, n= 8 aged, n= 10 old.

5.3.4. In Vivo Analyses of Effects of Experimental Glaucoma and Age

Following the 18-month post-AAV-injection *in vivo* imaging timepoint, a subset of aged mice received EG. The IOP was increased from baseline when measured at 1-week post-injection and remained elevated over the experimental time course. The mean IOP at baseline was 10.9 $\pm$ 0.6 mmHg and over 8-weeks was 22.2 (4.1) mmHg (Figure 5.11). The average IOP elevation relative to baseline in aged EG mice over 8-weeks was 11.3 (4.3). There was a small but significant difference in baseline IOP measurements between adult EG mice and aged EG mice, with baseline IOPs of 10.1 (0.6) and 10.9 (0.6) mmHg, respectively (p=0.008). Although there was a difference in baseline pressures, the two groups had similar degrees of IOP increase relative to their baseline (p= 0.32).

In vivo fluorescence CSLO images were acquired weekly over the EG timepoints in aged mice, and cell densities were quantified (Figure 5.12). The GCaMP6s cell density was 350 (53) cells/mm^2 at baseline (18-months following initial AAV injection) and decreased 17% to 290 (44) cells/mm^2 at 4 weeks, and 28% to 250 (38) cells/mm^2 at 8-weeks post-EG (Figure 5.13A). This was compared with *in vivo* cell densities from adult EG mice weekly, over 8-weeks, and there was a significant difference between the groups beginning at 4-weeks following EG-induction (Figure 5.13B).

GCC thickness was quantified over the duration of the EG time course in aged EG mice (Figure 5.14A, Figure 5.14B), and there was a decrease of 7% (1%) at 4-weeks, and 16% (5%) at 8-weeks of EG (Figure 5.14C). The GCC thickness percent change was compared between adult EG and aged EG mice, and although there was a small

difference (5% (5%) at 4-weeks and 12% (3%) at 8-weeks, respectively in adult EG) between the adult and aged EG groups, there were no significant differences detected at any timepoints (Figure 5.15).

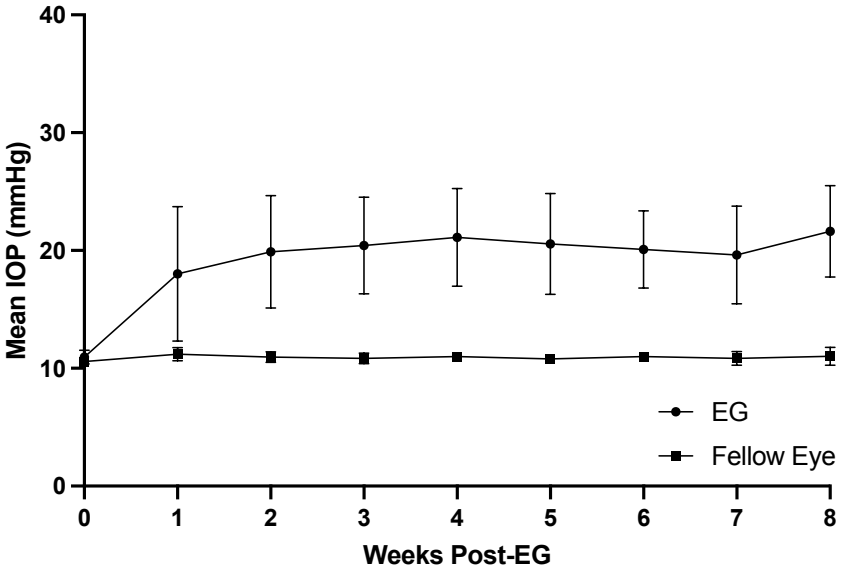

Figure 5.11. Intraocular pressure in aged EG mice. The average IOP in both the experimental and control eyes over 8-weeks of EG. Error bars represent standard deviation. n= 8.

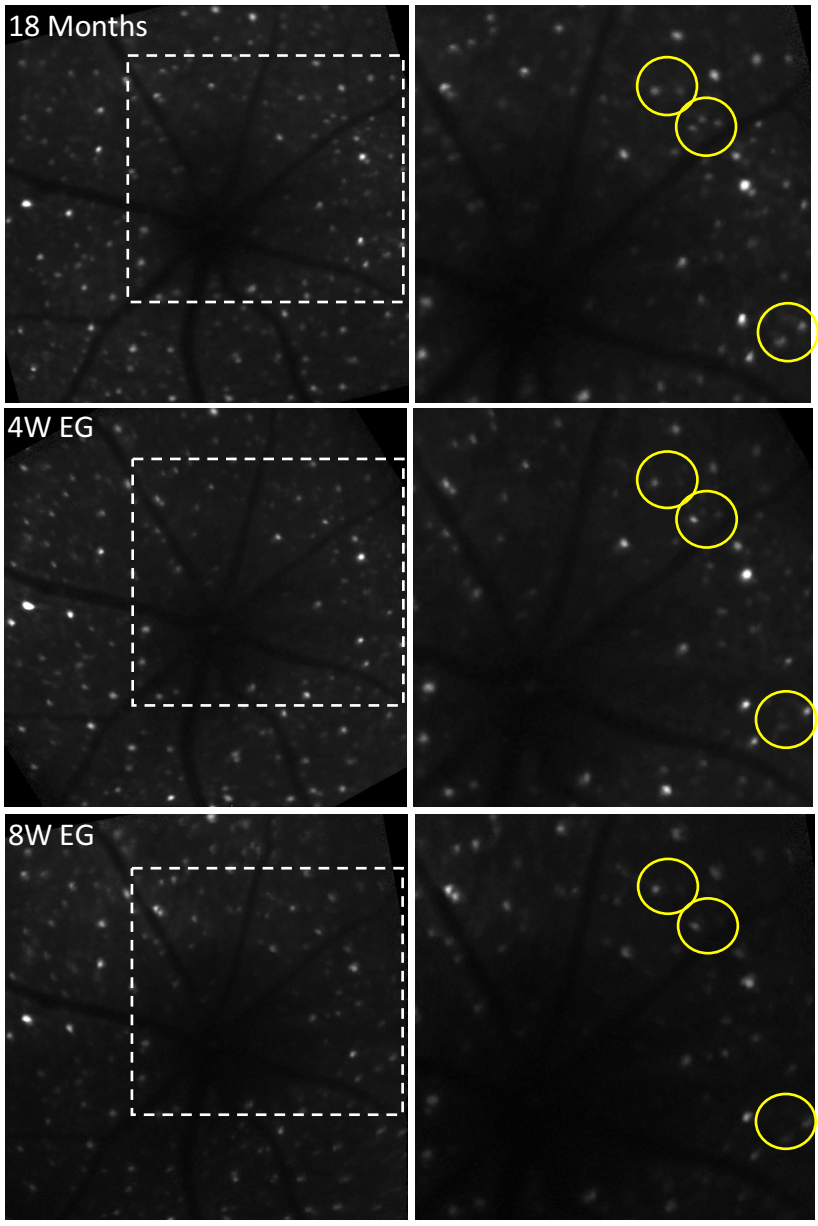

Figure 5.12. *In vivo* fluorescence imaging in aged EG. *In vivo* fluorescence images from a representative aged mouse that received EG at baseline (the 18-month post-AAV injection timepoint), 4-weeks post-EG, and 8-weeks post-EG. Images to the right show a region with increased magnification. Yellow circles indicate decreased cellular fluorescence.

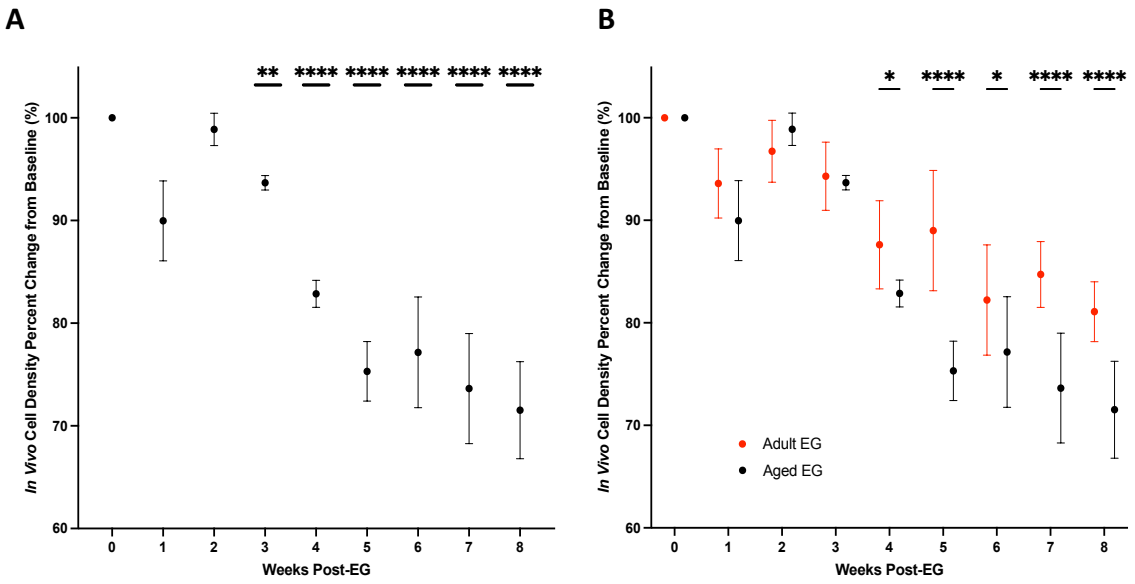

Figure 5.13. *In vivo* cellular density following aged EG. A) Quantification of *in vivo* density over 8-week expressed as a percent change from baseline. RM one-way ANOVA found significant started at 3-weeks post-EG induction. B) Two-way ANOVA shows significant differences between adult and aged EG groups over the experimental time courses beginning at 4-weeks. * = p< 0.05; ** = p< 0.01; **** = p< 0.0001; n= 13 adult EG, and n= 8 aged EG.

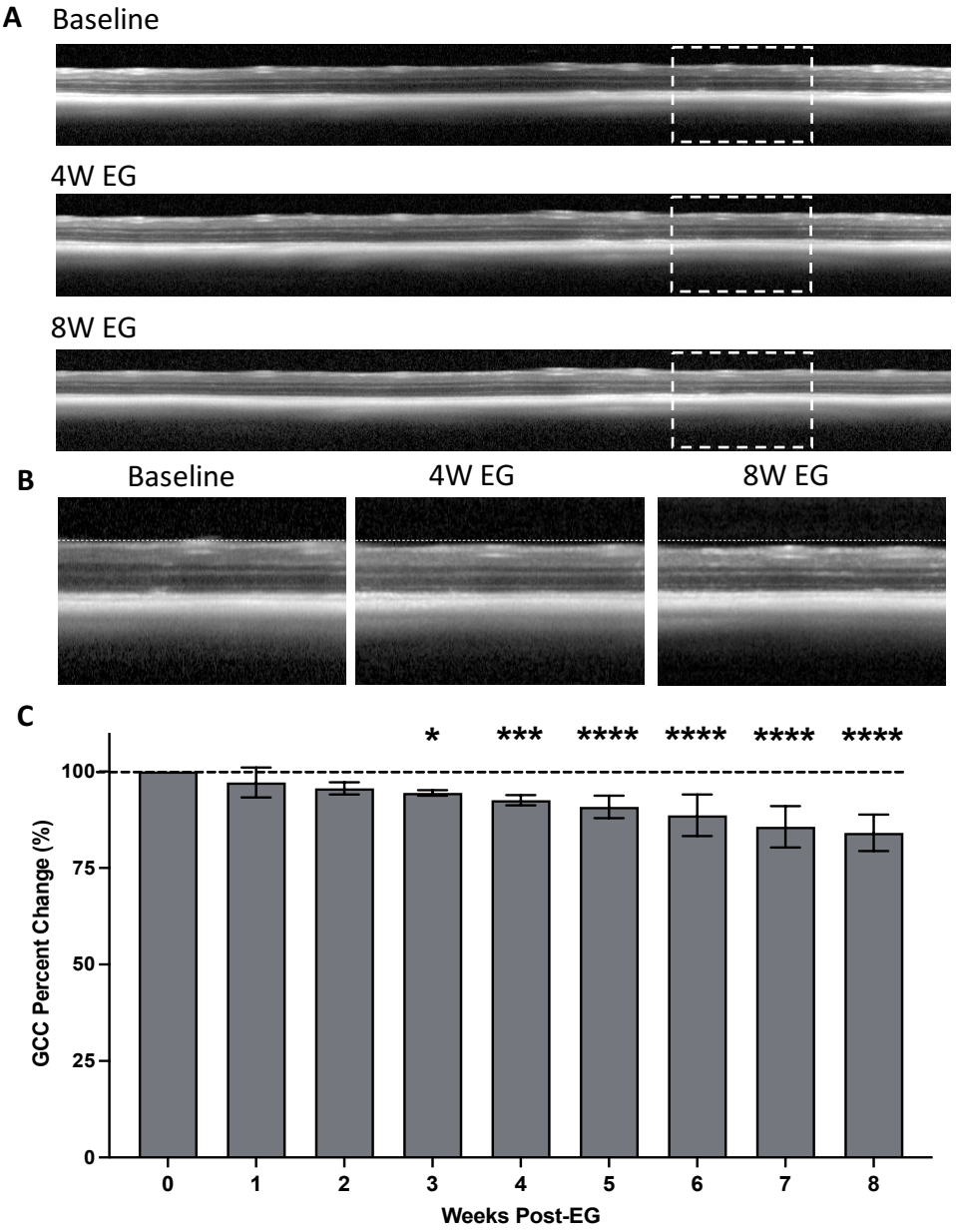

Figure 5.14. OCT peripapillary circle scans and GCC quantification in aged EG. A) Peripapillary OCT circle scans from a mouse that received EG at baseline, 4-weeks post-EG, and 8-weeks post-EG. B) Magnified regions of the OCT scans showing decreased GCC thickness (segmented from the ILM to the outer boarder of the IPL). C) Quantification of the average decrease in GCC thickness over 8-weeks of EG. Error bars represent standard deviation. One-way repeated measures ANOVA with Tukey's multiple comparisons shows significant loss beginning at 3-weeks post-EG induction. * = $p < 0.05$; *** = $p < 0.001$; **** = $p < 0.0001$; n= 8.

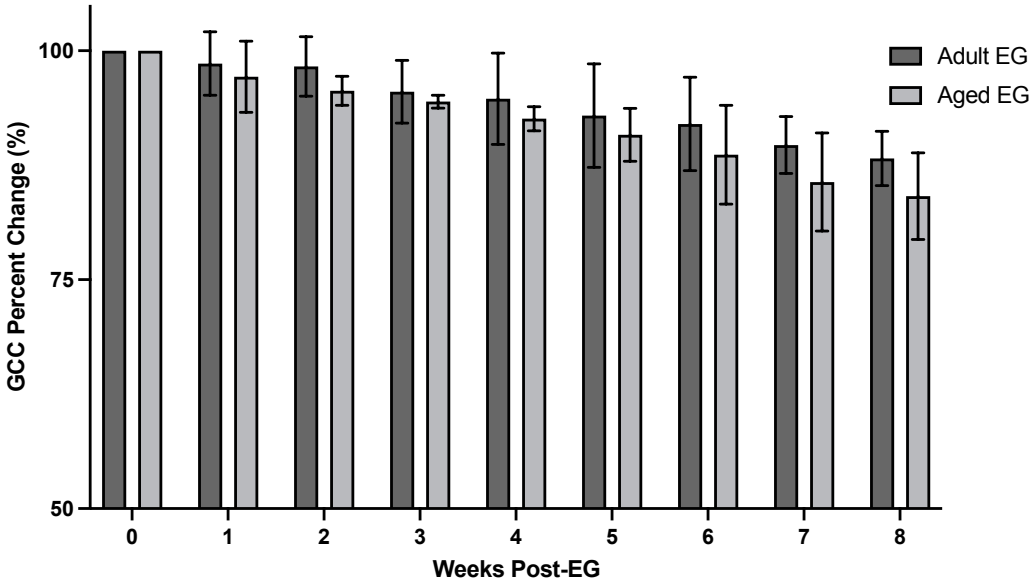

Figure 5.15. Comparison of and GCC thickness in adult and aged EG. Figure showing average GCC percent change from baseline weekly, over 8-weeks of EG in adult and aged EG. Two-way ANOVA found no significance between any of the timepoints. n= 13 adult EG, n= 8 aged EG.

5.3.5. Functional Characterization in Aged Experimental Glaucoma Mice

Ca^{2+} imaging experiments were performed on 4-week and 8-week aged EG mice (Figure 5.16A). In both 4-week and 8- week EG groups, GCaMP produced consistent transients that were not significantly different from each other across the 4 KA treatments ($p= 0.29$ and $p= 0.74$, for 4-week and 8-week EG respectively; Figure 5.16B). When compared to aged controls, the 4-week EG group was significantly decreased 36% and 8-week EG group was significantly decreased 65% ($p= 0.002$ and $p< 0.001$, respectively; Figure 5.17). Correlation analyses performed between IOP and transient amplitude following 4-weeks and 8-weeks of EG (Figure 5.18) found r values of -0.53 ($p= 0.11$) and -0.71 ($p= 0.05$).

The aged EG group was also compared to adult EG groups (Figure 5.19A). Although the two groups had no difference in degree of IOP increase, they had significantly different average transient amplitudes. There were significant differences between the transient amplitudes of the adult 4-week EG group, and aged 4-week EG groups, and between the adult 8-week EG, and aged 8-week EG group ($p< 0.001$, and $p< 0.001$, respectively; Figure 5.19B). Interestingly there was no significant difference found between the transient amplitudes of the aged control mice, and the adult mice that had 8-weeks of EG ($p= 0.25$).

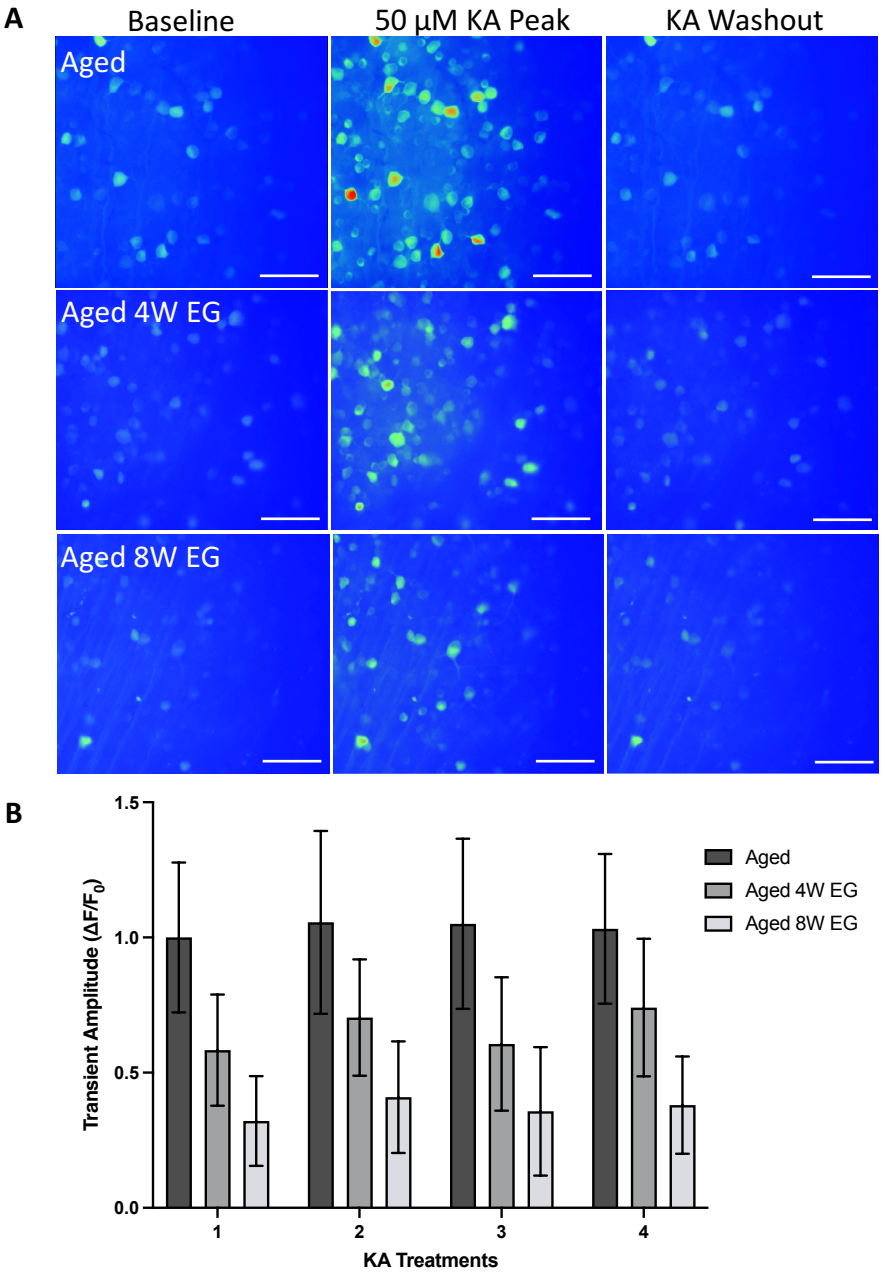

Figure 5.16. Ca^{2+} imaging experiments following EG in aged mice. A) Pseudocoloured images from calcium imaging experiments in aged controls, and following 4-, and 8-weeks of EG, show (left-right) baseline fluorescence, the 50µM KA induced peak fluorescence, and following KA washout where cells returned to baseline fluorescence. Scale bars = 50 µm. B) Mean data showing transient amplitudes across 4 KA treatments for control and EG groups. Data reported as mean, with error bars indicating standard deviation; n= 8 aged, n= 10 aged 4W EG, and n= 8 aged 8W EG.

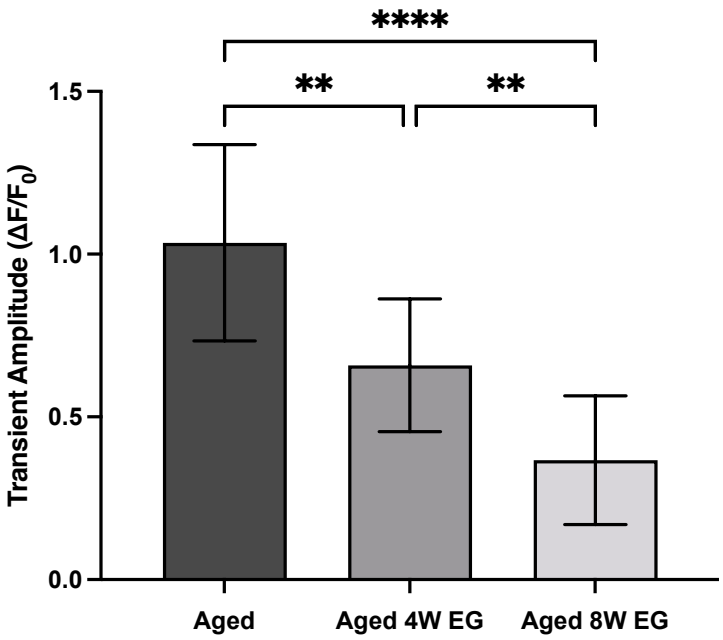

Figure 5.17. Comparison of transient amplitudes across EG groups. Figure showing average transient amplitudes for control, and following 4-, and 8-weeks EG. One-way ANOVA with Dunnett's multiple comparison shows significance between all groups. ** = p< 0.01; **** = p< 0.0001; n= 8 aged, n= 10 aged 4W EG, and n= 8 aged 8W EG.

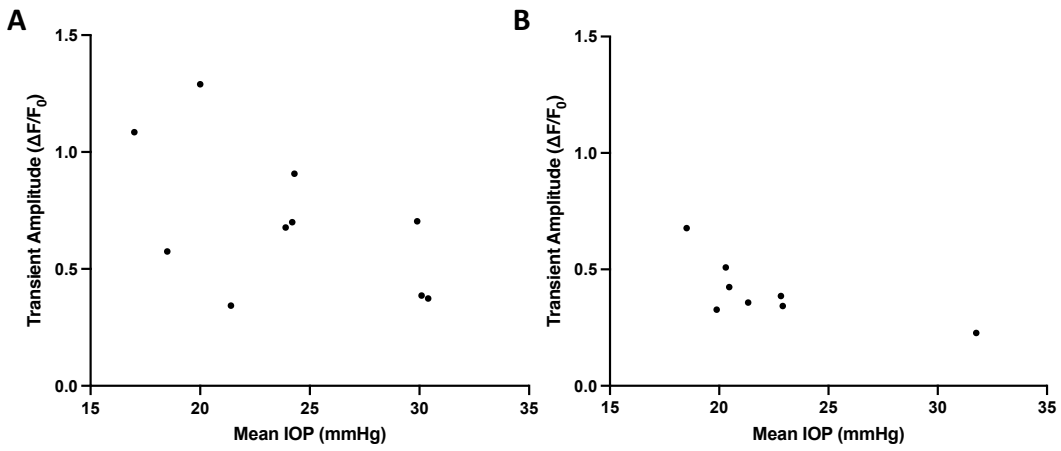

Figure 5.18. Correlation plots showing relationship between IOP and transient amplitudes in aged EG. Graphs (left to right) show correlation plots between IOP and the average transient amplitudes in mice following A) 4-, and B) 8-weeks of EG, respectively. Each data point represents one animal at their corresponding IOP. Correlation analyses found Pearson correlation coefficients of -0.53 and -0.71 at 4-, and 8-weeks of EG, respectively. n= 10 4W EG; n= 8 8W EG.

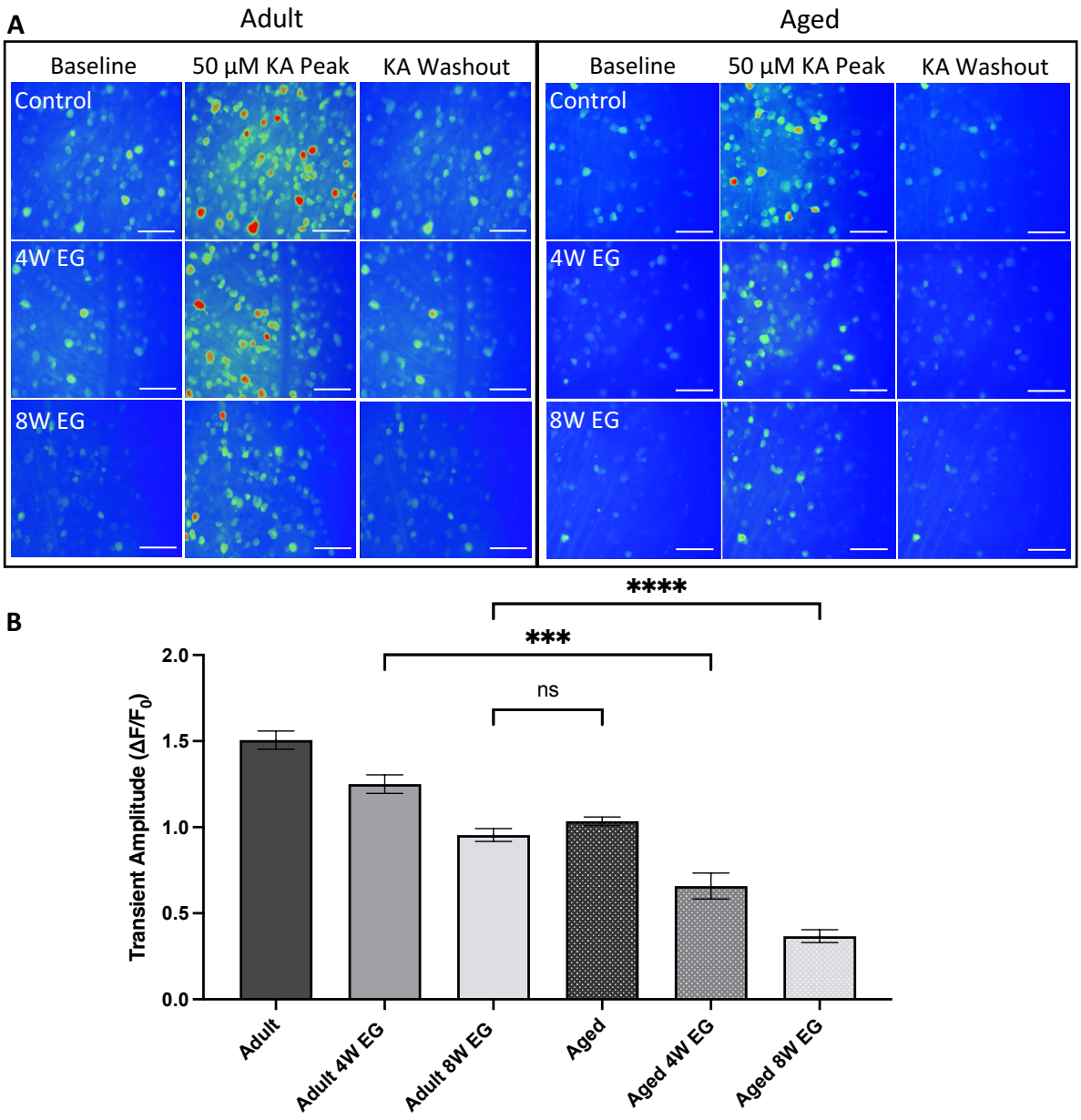

Figure 5.19. Comparison of transient amplitudes between adult and aged EG groups. Figure showing average transient amplitudes for control, 4-, and 8-week of EG in adults, and aged groups. Two-way ANOVA with Tukey's multiple comparisons shows significance between 4-week adult EG and 4-week aged EG ($p < 0.001$), and 8-week adult EG and 8-week aged EG ($p < 0.001$). Interestingly, the difference between 8-week adult EG and aged control showed a non-significant relationship ($p = 0.25$). *** = $p < 0.001$; **** = $p < 0.0001$. n= 10 adult, n= 10 adult 4W EG, n= 13 adult 8W EG, n= 8 aged, n=10 aged 4W EG, and n= 8 aged 8W EG.

5.3.6. Immunohistochemical Analyses Following Experimental Glaucoma in Aged Mice

RBPMS-positive cell quantification was performed in wholemounted retinas from the aged 4-week 8-week EG mice. Representative micrographs are shown in Figure 5.20A. In the 4-week EG group, 2147 (188) cells/mm^2 in experimental vs 2778 (361) cells/mm^2 fellow-eyes, and in the 8-week EG group 1787 (210) cells/mm^2 in the experimental vs 2692 (322) cells/mm^2 in the fellow eyes (Figure 5.20B). These values corresponded to a loss of 23%, and 34% in 4-week EG and 8-week EG groups, respectively. When compared to aged control eyes, the RBPMS-positive cell density was significantly reduced in both groups ($p< 0.001$). Correlation analysis between IOP and RBPMS quantification at 4- and 8-weeks of EG (Figure 5.21A, Figure 5.21B) showed negative correlations of -0.68 ($p= 0.09$) and -0.67 ($p= 0.10$), respectively.

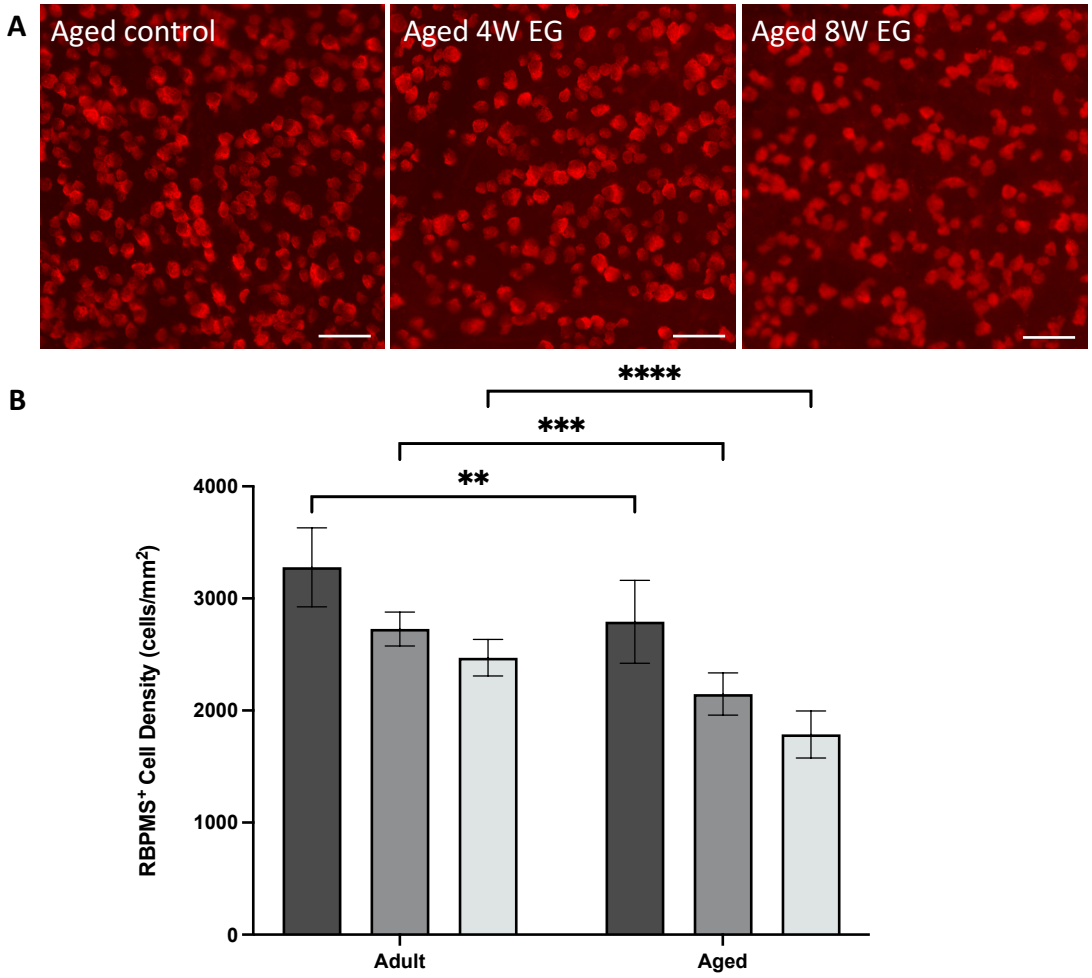

Figure 5.20. Immunohistochemistry following aged EG. A) Panels show RBPMS immunohistochemical staining (left to right) of retinas from aged control mice, 4-, and 8-weeks of EG. B) RBPMS-positive cell densities were quantified for both 4-week, and 8-week EG groups. Histogram shows comparison of RBPMS-positive counts between adult EG and aged EG. A two-way ANOVA with Tukey's multiple comparison test determined significance between groups. ** = p< 0.01; *** = p< 0.001; **** = p< 0.0001. n= 10 adult, n= 10 adult 4W EG, n= 13 adult 8W EG, n= 8 aged, n=7 aged 4W EG, and n= 7 aged 8W EG.

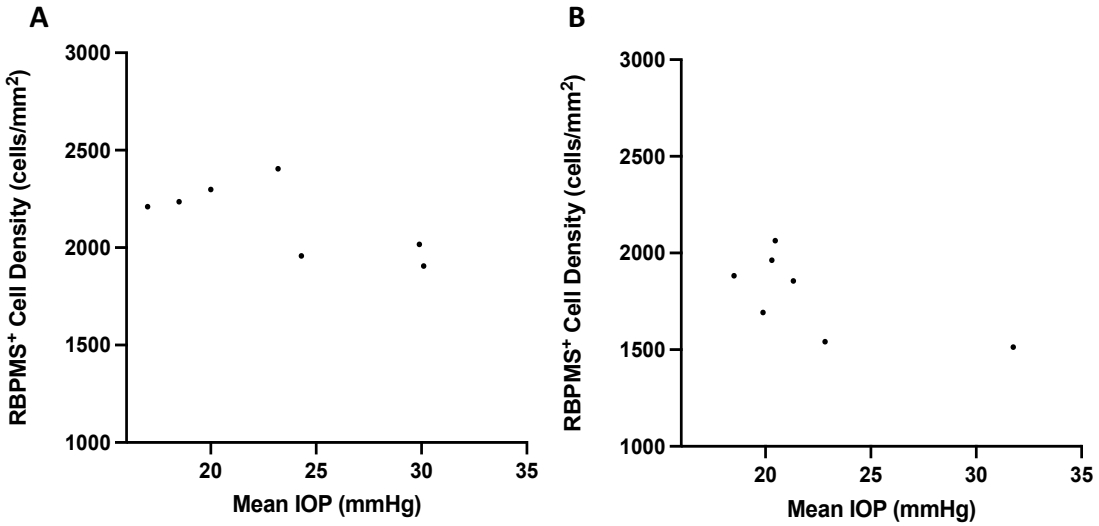

Figure 5.21. Correlation plots showing relationship between IOP and RBPMS immunohistochemical quantification in aged EG. Figures show correlation relationship between IOP and RBPMS-positive cell density following A) 4-weeks, and B) 8-weeks of EG (left to right, respectively). Each data point represents one animal. Correlation analysis found Pearson correlation coefficients of -0.68 (p= 0.09) and -0.67 (p= 0.10) at 4-, and 8-weeks of EG, respectively. n= 7 aged 4W EG, and n= 7 aged 8W EG.

5.4. Summary of Findings

The results of this chapter describe the use of AAV2-CAG-GCaMP6s as a tool for monitoring both structural and functional loss of inner retinal cells in aged conditions and elaborated on the effects of both age and EG on cell function. Key findings from this chapter include:

1. The viral labelling persists to 18-months post-single viral-injection. Viral labelling remains visible with *in vivo* imaging, and the GCaMP remains functional in response to KA in Ca^{2+} imaging experiments. Interestingly, there was no difference in functional responses between mice aged with the virus, and old mice injected with the virus
2. In mice aged with the virus, there are fewer GCaMP-positive cells when quantified with immunohistochemistry than in old mice injected with the virus at 18-months of age. This, in combination with significantly fewer RBPMS-positive cells in aged, and old mice, resulted in a higher hit rate of the virus in old mice
3. Adult and aged EG mice had the same degree of IOP elevation, yet aged EG mice experienced greater functional loss than adult mice (approximately doubled). Aged EG mice also had more structural changes, quantified with *in vivo* fluorescence imaging and immunohistochemistry

CHAPTER 6. DISCUSSION

6.1. Summary of Major Findings

The work presented in this thesis characterized the AAV2-CAG-GCaMP6s viral vector as a tool to study both structural and functional loss in RGCs. We began by describing AAV2-CAG-GCaMP6s in adult wild type mice, where we characterized *in vivo* transduction, functional properties, and specificity of the virus to RGCs within the GCL. We found a significant increase in viral transduction with *in vivo* CSLO imaging over 5-weeks following intravitreal injection, after which the degree of labelling plateaued. Functional responses to 50 μM KA generated significantly larger transient responses in wild type mice injected with the viral vector when compared to commercially available Thy1-GCaMP6s transgenic mice. Finally, colocalization studies using immunohistochemistry showed the virus primarily labeled RGCs, and to a smaller extent ChAT-positive amacrine cells, and RBPMS-negative/ChAT-negative cells, which potentially represent other classes of displaced amacrine cells within the GCL.

In chapter 4, we utilized GCaMP6s produced through viral transduction to monitor structural and functional loss following ON damage in adult mice. *In vivo* CSLO and OCT data demonstrated significant decreases in *in vivo* cell densities and GCC thickness over the EG-time course. Functional Ca^{2+} imaging experiments performed in retinas from mice that had 3-days of ONT, 4-weeks of EG, or 8-weeks of EG showed that all groups had significantly decreased transient amplitudes when compared to adult

controls. Interestingly, the average transient amplitude in the 3-day ONT group was not significantly different from the 8-week EG group.

In chapter 5, we first explored the effects of age on RGC function. We characterized the persistence of GCaMP expression following a single-viral injection. In the aged group, there was a gradual and significant decrease of *in vivo* cell density over 18-months. GCC thickness also decreased significantly over 18-months but when compared to age-matched controls, GCC thickness was not significantly different. In the old group, *in vivo* cell density increased significantly over 4-weeks post-injection before stabilizing and showed similar levels of transduction as in adult mice. Functional comparisons between aged and old groups showed no significant difference, although they were both significantly decreased compared to adult control mice.

The effects of both age and EG on RGC structure and function were also described in chapter 5. We found larger proportional decreases in *in vivo* fluorescence and GCC thickness measurements in aged EG mice when compared to adult EG mice over 8-weeks. Functional loss approximately doubled at 4-, and 8-weeks of EG in aged mice compared to adult mice. Finally, RBPMS-positive cell density showed significantly more cell loss following 4-, and 8-weeks of EG in aged mice compared to adults.

6.2. AAV as a Tool to Express Structural and Functional Markers

Intravitreal injections are a commonly used clinical technique that have been adapted for use in experimental research to deliver therapeutics, neuroprotective agents, or structural and functional markers for diagnostic purposes to the retina. When

using viral vectors to deliver agents to the inner retina, viral transduction rate into retinal cells is an important consideration. Originally, we chose to monitor transduction over five weeks based on previously published work from our laboratory which demonstrated a significant increase in fluorescently labelled cells until 4-weeks following intravitreal injection of AAV2-CAG-GFP (Smith & Chauhan, 2018). Additional publications have suggested that optimal transduction can be achieved between two- and eight-weeks post-injection (Bar-Noam et al., 2016; Borghuis et al., 2011; Cheong et al., 2018; Weitz et al., 2013). Our data showed a significant progressive increase in cell density with *in vivo* imaging weekly over five-weeks using the AAV2-CAG-GCaMP6s viral vector, so we extended the time course to 8-weeks post-intravitreal injection to ensure the labelling reached a plateau. The plateau was critical as we sought to quantify loss *in vivo* following EG, and additional transduction following EG induction could lead to an underestimate of *in vivo* RGC loss.

Functional studies examining GCaMP delivered by AAV vectors have been performed both *in situ* with pulse stimulation through an electrode (Borghuis et al., 2011; Weitz et al., 2013) and *in vivo* using CSLO imaging (Li et al., 2022), or two-photon (2P) imaging with optical stimuli (Bar-Noam et al., 2016; Cheong et al., 2018; Qin et al., 2020). Red-shifted GECIs such as jRGECO1a are also used to monitor cellular function in the retina (Chen et al., 2013; Cheong et al., 2018). At the time this thesis work was initiated, GCaMP6s was primarily being used in the field because it had increased dynamic range in comparison to other GCaMP variants such as GCaMP3. However, there have been improvements in GCaMP kinetics, with GCaMP7 (Dana et al., 2019) and

GCaMP8 (Zhang et al., 2023), which are now being used to study functional activity of RGCs. GCaMP8 is described as having improved kinetics and a larger dynamic range without compromising sensitivity or brightness (Zhang et al., 2023).

The viral serotype and promotor are important determinants of cellular hit rate and specificity. The AAV2 serotype was chosen for this thesis work because it has been shown in animal models to effectively label inner retinal neurons using intravitreal injection techniques (Cheong et al., 2018; Harvey et al., 2002; Martin et al., 2002; Smith & Chauhan, 2018), is being utilized in clinical trials (Bainbridge et al., 2008, 2015; Cukras et al., 2018), and was previously used in our laboratory to transduce RGCs with structural markers (Smith & Chauhan, 2018).

In this thesis, we used the ubiquitous promotor, CAG. Although potentially less specific to RGCs, ubiquitous promotors allow high levels of expression and transduction into retinal cells and are smaller in size (Grieger & Samulski, 2005; Hanlon et al., 2017), compared to cell specific promotors which tend to be larger in size and less suitable for viral delivery. For example, Thy1 is a promotor highly specific to RGCs, however its size prevents its use in AAV vectors due to the packaging capacity of the virial vector itself (Hanlon et al., 2017). A study published recently by Nieuwenhuis and colleagues used AAV2 to compare five promoters and their corresponding transduction characteristics (Nieuwenhuis et al., 2023). They found CAG and SYN promotors had the strongest transgene expression in the retina, ON, and brains of adult mice, in comparison to CBA, CMV and PGK, which all showed more moderate expression (Nieuwenhuis et al., 2023). Our results with IHC found a hit rate of 27% of AAV2-CAG-GCaMP6s to RBPMS-positive

cells. Moreover, we found a 74% specificity to RGCs within the GCL, which is comparable to other work published by Smith and Chauhan (Smith & Chauhan, 2018).

Small gene promotors derived from human DNA, such as DCX, have also been developed in attempts to achieve higher specificity in inner retinal cells as there is evidence that DCX is expressed in RGCs, amacrine and bipolar cells (Sánchez-Farías & Candal, 2015). When the DCX promotor was used in an AAV2 viral vector, there was a higher specificity to RGCs than the ubiquitous promotor CAG (de Leeuw et al., 2014; Smith & Chauhan, 2018). For our work, we could have used an RGC-specific promotor instead of the ubiquitous promotor CAG, however, hit rate must be considered. For example, DCX and SYN which are both more specific to RGCs, can lead to lower, and higher hit rates, respectively, than what we observed with the CAG promotor. Depending on the research question and type of study, a promotor that provides high cell-type specificity, or one that labels larger proportions of cells may be more favourable. However, for the purposes of our research and the goal of performing functional analysis on individual RGCs in both intact isolated retina and *in vivo*, a hit rate of 25-30% is advantageous.

We also evaluated the specificity of the viral vector to displaced amacrine cells within the GCL. Our results showed a 12% specificity with ChAT-positive cells, and 14% with RBPMS-negative/ChAT-negative cells. The RBPMS-negative/ChAT-negative cells within the GCL could represent either RBPMS-negative RGCs or displaced amacrine cells. Kwong and colleagues found a nearly complete colocalization between RBPMS and FG, suggesting RBPMS is a highly reliable marker for RGCs (Kwong et al., 2010, 2011;

Rodriguez et al., 2014), therefore, it is not probable that RBPMS-negative RGCs are making up a large proportion of the RBPMS-negative/ChAT-negative cell population we observed. Displaced amacrine cells can make up to approximately 60% of neurons within the GCL in mice (Jeon et al., 1998), with the majority expressing ChAT or GABA, and to a much smaller extent, glycine or glutamate (Atan, 2018; Haverkamp & Wässle, 2000; Jeon et al., 1998; Müller et al., 2007). It is likely that some of the virus-labelled cells in our results that are RBPMS-negative/ChAT-negative are other classes of displaced amacrine cells, which could be further examined with immunohistochemical labels for these cells.

6.3 Effects of Experimental Glaucoma on Structural and Functional Loss

6.3.1. In Vivo Analyses Following Experimental Glaucoma in Adult Mice

Rodent and NHP models of glaucoma have led to better understanding of mechanisms of structural and functional loss. The hydrogel model of EG used in this thesis has previously been used to induce EG over 4-weeks, where the IOP remained elevated over the entirety of experimental time course (Chan et al., 2019; Di Pierdomenico et al., 2022). The results presented in chapters 4 and 5 show that the IOP remains elevated, without the need for repeat injections over 8-weeks following EG-induction. Moreover, with this model, the ocular media remains clear and serial *in vivo* imaging of the retina could be performed.

While significant structural loss was detected through *in vivo* fluorescence and OCT imaging, we report less cell loss compared to that reported by Chan and colleagues

(2019). In the present study, we found a 12% loss of *in vivo* cell density, whereas Chan and colleagues reported 63% *in vivo* cell loss 4-weeks post-EG (Chan et al., 2019), although the reported IOP elevations were similar in both their study and ours. The differences in *in vivo* cell loss observed could be related to the labeling method used in the two studies. The mice we used were injected with AAV2-CAG-GCaMP6s and had a hit rate of 27% to RGCs, whereas they used Thy1-YFP-G transgenic mice which drive YFP expression in 96% of RGCs in the mouse retina (Chan et al., 2019; Leung et al., 2008). The difference observed between their *in vivo* counts and ours could in part be to downregulation of the Thy1 promotor which is known to occur following induction of EG (Huang et al., 2006). An alternative consideration is that perhaps there is preferential labelling by the viral vector to more resilient types of RGCs such as ON RGCs or ipRGCs (El-Danaf & Huberman, 2015; Li et al., 2006) which have been shown to be more resistant to IOP elevation. To our knowledge there have not been any reports of selective viral transduction in the literature to date. Interestingly, the RBPMS-positive cell densities reported in our study showed 15% loss at 4-weeks EG, and Chan and colleagues reported 20% loss (Chan et al., 2019). They reported a large difference between their *in vivo* and histological cell counts. The *in vivo* loss we detected using the AAV2-CAG-GCaMP6s viral vector is closer to our histological counts, indicating viral transduction perhaps provides a more representative measure of cell loss occurring in EG in this model.

Currently OCT thickness measurements are used in the clinic to monitor and measure glaucoma progression and estimate RGC loss. However, work performed in

NHPs by Fortune and colleagues demonstrates that in a model of EG, there is significant variation, with approximately a two-fold difference in axonal counts at a given OCT thickness measurement (Fortune et al., 2015). Moreover, animals with comparable axonal counts, could have a two-fold difference in OCT thickness (Fortune et al., 2015). The differences between axonal counts and OCT thickness measurements could be due to inter-individual variability, or the effects of non-neuronal tissue within the RNFL in NHPs and humans that influences the thickness measurements. Using the hydrogel model, we found 5% and 12% decreases in GCC thickness at 4-, and 8-weeks of EG, respectively, which is comparable to previously reported data in mice at 4-weeks (Di Pierdomenico et al., 2022). When GCC thickness measurements were compared to histological RBPMS-positive cell counts, the cell counts showed significantly more loss than what was detected using OCT. Taken together, observations from clinical and experimental research, such as the work presented in this thesis, indicate that although OCT is a useful, non-invasive technique for monitoring changes in retinal thickness, it may not be adequately sensitive to detect changes occurring to RGCs when compared to other measures such as RGC function (Bar-Noam et al., 2016; Blandford et al., 2019).

6.3.2. Functional Analyses Following Optic Nerve Transection and Experimental Glaucoma in Adult Mice

The present study showed significant functional loss at 3-days following ONT in intact-isolated retinal preparations. Functional loss at 3-days post-ONT using Ca^{2+} imaging has been shown previously in Thy1-GCaMP3 transgenic mice (Blandford et al.,

2019), with further loss of function at 5-, and 7- days post-ONT. Blandford and colleagues (2019) noted that especially at 5-, and 7-days post-ONT, GCaMP-positive cells were still visible with intact-isolated Ca^{2+} imaging, although they did not produce functional responses, indicating functional loss may precede structural loss (Blandford et al., 2019). It is possible we would have found similar results in our ONT group; however, we did not study timepoints beyond 3-days post-ONT. Other studies which used ERG to evaluate functional loss following ONC in mice found reductions in the positive scotopic threshold response and photopic negative response (pSTR and PhNR, respectively; measures of inner retinal function) as early as 3-days post-ONC (Liu et al., 2014). At the 3-day post ONC timepoint, there was no significant cell loss observed with histology (Liu et al., 2014), providing more evidence that functional loss may precede structural loss. Functional evaluation of the retina using ERG has also been performed at longer timepoints following ONT in both mice (Alarcón-Martínez et al., 2010; Smith et al., 2014) and rats (Alarcón-Martínez et al., 2009; Bui & Fortune, 2004). In rats, results have indicated 24% and 41% reductions in pSTR and nSTR amplitudes, respectively, compared to fellow eyes 1-week post ONT (Bui & Fortune, 2004). Other groups have shown similar results of 40% and 60% reduction in nSTR components at 2-, and 4-weeks post-ONT (Alarcón-Martínez et al., 2009). Similar findings are reported in mice, where there are substantial decreases in both RGC function and structure over 2-weeks post ONT, of 40% and 82%, respectively (Alarcón-Martínez et al., 2010).

Interestingly, following 9-weeks post-ONT (Bui & Fortune, 2004) and 12-weeks post-ONT, (Alarcón-Martínez et al., 2010), there are residual STR responses, despite

there being very few surviving RGCs. Although there may be some resilient RGCs contributing to this response, it is more likely amacrine cells are generating these responses (Alarcón-Martínez et al., 2009; Bui & Fortune, 2004; Sieving, 1991), as they are not heavily affected by ONT (Carter et al., 1987). Thus, it is possible that amacrine cells may be contributing to the functional responses observed in Ca^{2+} imaging following ONT in the present study. However, specificity studies indicated that only a small portion of virus labelled cells were presumptive amacrine cells, thus we chose to include all GCaMP expressing cells in the analysis. We considered performing size exclusion criteria on our experiments, however, there is an overlap between the soma size of large amacrine cells and small RGCs (Jeon et al., 1998). Overall, any amacrine cells included in the analysis potentially contributed to an underestimation of the significant functional loss demonstrated after ONT.

Significant functional loss of 17% and 37% was found following 4-and 8-weeks of EG, respectively, when compared to adult controls. To our knowledge, Ca^{2+} imaging using intact-isolated retina preparations has not been used previously to study functional loss following EG. Previous studies using the hydrogel model examined functional changes with ERG, where Chan and colleagues (2019) reported a significant decrease in the pSTR in the hydrogel-injected eye compared to fellow eyes at 4-weeks post-EG. However, there was no significant differences in a-wave, and b-wave-amplitudes (indicative of photoreceptor function), and histology confirmed no damage to the outer retina (Chan et al., 2019). These findings contrast what has been found in models of acute IOP elevation (Bui et al., 2005; Hartsock et al., 2016; Kim et al., 2013;

Kong et al., 2009) and hypertonic saline injection into episcleral veins (Fortune et al., 2004), where there are decreases in a-wave and b-wave amplitudes with ERG. Although we did not measure outer retinal structure or function, there were no observable changes to outer retinal thickness with OCT imaging.

Interestingly, we observed comparable loss of function between 3-days of ONT, and 8-weeks of EG in adult mice, although these are two different models of RGC death. Proteomics and transcriptomics have shown similarities in early gene expression following ONC and EG, as both models involve RGC axonal injury and retrograde signalling to the soma. However, there are also dissimilarities and differential gene expression because of the nature, and timing of the two types of injury (Stowell et al., 2011; Wang et al., 2021; Yang et al., 2007). The similarities in functional loss we observed between the 3-day ONT, and 8-week adult EG group, could be explained by some of the overlap in gene expression at the early timepoint we analyzed, specifically in the ONT group.

6.3.3. Immunohistochemical Analyses Following Optic Nerve Transection and Experimental Glaucoma in Adult Mice

Our results showed 15% and 23% loss of RGCs with RBPMS-immunohistochemistry at 4-weeks, and 8-weeks of EG, respectively, which is comparable to what has been published previously using the hydrogel model (Chan et al., 2019; Di Pierdomenico et al., 2022). In comparison to other inducible EG models, like the microbead model, where 5%-40% RGC loss is reported over 3-8 weeks (Cone et

al., 2010; Ito et al., 2016; Samsel et al., 2011; Sappington et al., 2010), our results fall within this range. Based on our data and what has been previously reported, it possible that the hydrogel model may produce more sustained elevations in IOP, and more consistent levels of RGC structural and functional loss. In contrast, some models such as laser photocoagulation, hypertonic saline injection, or intracameral injection of microbeads, show more fluctuations in IOP due to the need for repeat procedures to maintain IOP elevation, which likely contributes to variations in the amount of RGC loss.

6.4. Senescence and Experimental Glaucoma

6.4.1. Comparison of Viral Transduction in Aged and Old Mice

We found persistence in viral expression with both *in vivo* imaging, and immunohistochemistry over 18-months post-single viral injection. Although there have been reports of AAV transgene expression persisting longer than 100 days in inner retinal cells (Smith & Chauhan, 2018), and 6-12 months in muscle (Kessler et al., 1996; Xiao et al., 1996), to our knowledge, the persistence of GCaMP expression and determining its functionally viability at these later timepoints has not been documented in the literature to date.

We found a decrease in GCaMP-positive cells quantified with *in vivo* CSLO imaging and immunohistochemistry over 18-months post-injection when compared to adult mice. We also found a significant loss of RBPMS-positive cells, and a non-significant loss of ChAT-positive cells in mice aged with the virus compared to adult controls. RBPMS-positive and ChAT-positive cell counts were not significantly different

in mice aged with the virus when compared to old control mice, indicating these are most likely age-related results, and not occurring as a result of the viral injection. Age-related loss of RGCs has been documented previously in C57Bl/6 mice, where there can be a loss of up to 50% by 18-months of age (Danias et al., 2003), as well as age-related decreases in ChAT-positive cells in the GCL (Samuel et al., 2011). Interestingly, in addition to an age-related decrease in both RBPMS-positive cells, and GCaMP-positive cells separately, we also found a decrease in the proportion of RBPMS-positive cells that are GCaMP-positive, indicating that GCaMP is potentially being cleared from cells over time.

Our findings agree with a study published by Polinski and colleagues that quantified GFP-positive cells following AAV-GFP injection into the mesencephalon and nigrostriatal system in the brains of adult and aged rats (Polinski et al., 2016). There were no significant differences in GFP-positive cell densities quantified in adult and aged mice, however, they did find significantly lower GFP protein levels in aged rats when compared to adult rats using Western blot. Their data indicate that age-related decreases in transgene expression may not be detected using total counts (Polinski et al., 2016). Therefore, it is possible that by performing cell counts, we may not be appreciating the differences in transgene expression between groups, as cell counts provide a binary measure of expression and protein quantification methods would provide more sensitive analysis. It is important to note that our findings contrast with other literature which showed age-related reductions in AAV expression in brains of adult and aged rats when quantified with immunohistochemical quantification (Polinski

et al., 2015; Wu et al., 2004). Taken together, these studies emphasize the need for more research to better understand how transgene expression is impacted by age in both brain and retina.

We had hypothesized that the viral hit rate in old mice would be a comparable to, or potentially less than what we observed in adult mice depending on the effectiveness of viral transduction into aged cells within the retina. Although we found an age-related decrease in RBPMS-positive cells in old mice compared to adult control mice with IHC, the *in vivo* cell density was not-significantly different following 8-weeks of transduction in old mice than in adult control mice. Moreover, the number of GCaMP-positive cells in old mice transduced with the virus was not significantly different than in adult mice when quantified with IHC. Because of the age-related decrease in RGCs and the virus exhibiting similar transduction in old and adult mice, it led to a higher hit rate in the old mice.

The specificity of the virus to RBPMS-positive cells, and ChAT-positive cells was comparable between adult control mice, mice aged with the virus, and old mice groups, indicating it is the hit rate that may vary with age, and not the overall specificity. To our knowledge, this has not been compared in the literature to date. Understanding how viral characteristics may change over time, and the impact cellular degeneration has on viral expression is important if AAV technology is going to continue to be used to monitor functional loss in disease.

There was no significant difference between the average transient amplitudes in the aged and old group, although they were both significantly decreased from adult

control mice, indicating age-related decreases in cell function can be seen using AAV2-CAG-GCaMP6s irrespective of the timing of intravitreal injection. Age related functional changes to the outer retina in mice have been reported previously using ERG, where there is decreased A and B wave amplitudes with aged mice when compared to adult mice (Ferdous et al., 2021; Gresh et al., 2003; Li et al., 2001; Park et al., 2023; Williams & Jacobs, 2007).

Age-related research in rodents has mainly focused on loss of outer retinal function, with less emphasis on inner retinal function. One paper by Charng and colleagues did find a loss of inner retinal function (decreased nSTR and pSTR) with ERG (Charng et al., 2011). Age-related loss of visual acuity measured with visual field testing in humans suggests an age-related decrease in sensitivity with increasing age (Haas et al., 1986; Jaffe et al., 1986; Spry & Johnson, 2001). Research into effects of normal aging in inner retina, and specifically RGC function is critical for parsing out effects of normal aging from disease in age-related diseases like glaucoma.

Moreover, our results showed the decrease in cell function observed in aged control mice was not statistically different than adult mice that had 8-weeks of EG. Although there has been inner retinal functional loss detected in both adult EG (Bui et al., 2005; Chan et al., 2019; Hartsock et al., 2016; Kong et al., 2009), and in aged controls (Charng et al., 2011), a direct comparison of RGC function between these two conditions has not been performed. The comparison between adult EG and aged controls groups contributes to the importance of using aged animals to study EG, as age-related loss of function occurs in the absence of disease models.

6.4.2. Effects of Elevated IOP and Age on RGC Function

Although IOP and age are the two most identified risk factors for both the progression and development of glaucoma, EG is primarily studied in adult mice. We found several baseline measurements prior to inducing EG that were statistically different between adult and aged mice. First, we found a small, but significantly higher baseline IOP in the aged mice compared to the adult mice prior to the induction of EG, which aligns with previous studies (David et al., 1987; Di Pierdomenico et al., 2022; Wong et al., 2009), but not with another study which found a significant decrease in IOP with age (Savinova et al., 2001). We also found a statistically thinner baseline GCC thickness in aged mice when compared to adult mice. Age-related thinning of the GCC compared to adult controls has been previously shown in mice (Di Pierdomenico et al., 2022). Similar findings in humans have shown age-related thinning of the RNFL (Chauhan et al., 2020; Deng et al., 2022).

Following EG induction, when IOP elevation was calculated as a change from baseline, there was no significant difference between aged and adult mice. Both adult and aged EG groups followed similar GCC thickness time courses, with the aged EG groups showing a larger, but non-significant decrease in GCC thickness over 4-, and 8-weeks compared to adult EG mice. These findings agree with previously reported work from our laboratory using this hydrogel model (Di Pierdomenico et al., 2021).

Despite the adult and aged EG groups having similar levels of IOP elevation, we found nearly a 2-fold difference in the amount of functional loss observed in at 4-weeks and 8-weeks post-EG in the aged group when compared to the adult EG group, with 17%

and 37% loss at 4-weeks in adult and aged EG, respectively. Corresponding figures at 8-weeks were 36% and 65%. Interestingly, when we considered all structural and functional parameters we analyzed, IOP elevation had the largest impact on cell function, which could represent early changes during RGC degeneration prior to irreversible cell loss.

To our knowledge, Ca^{2+} imaging experiments have not been performed following EG in adult and aged mice, however, there have been several groups that have compared functional results in adult and aged mice in following periods of elevated IOP using ERG. PhNRs show longer recovery times following acute IOP elevation in aged rats (Lim et al., 2014) and mice (Chrysostomou & Crowston, 2013; Lee et al., 2022), when compared to their adult counterparts. For example, during an experiment where IOP was elevated stepwise from 10 mmHg to 100 mmHg over the course of one-hour, there was recovery of b-wave amplitude measured with ERG within 2 hours following IOP elevation in adult rats (3 months of age) but was still attenuated more than 2 hours later in aged rats (14 months of age; (Lim et al., 2014). Similar findings in inner retina function showed, when IOP was raised 50 mmHg for 30 minutes in adult and aged mice, STRs and PhNRs showed recovery 7-days following IOP elevation in adult mice, but in 12-, and 18-month-old mice, full functional recovery was not observed until 4 weeks following the IOP elevation (Kong et al., 2012).

Our experiments did not find significant differences between GCC thickness in adult and aged EG mice, however, there were significant differences in RBPMS-positive cell quantification with immunohistochemistry. We found significantly lower RBPMS-

positive cell densities when we compared 4-weeks of EG in adults and aged mice, and similarly at 8-weeks of EG in adults and aged mice, which agrees with previously reported findings from our laboratory using the hydrogel model (Di Pierdomenico, et al., 2021). Age-related differences in cell loss following ONC have also been reported, where there was a 20% and 40% loss of RGCs 3-days post-ONC in adult and aged mice, respectively. Corresponding figures at 7-days post ONC were, 40% and 70% in adult and aged mice, respectively, when quantified with FG labelling (Ai et al., 2007; Blandford et al., 2019). Overall, findings suggest RGCs in aged mice are more susceptible to the same injury than adults.

Detecting early changes to RGCs prior to irreversible cell death is important for understanding neurodegenerative disease. Such early changes can be seen by studying cellular functional changes (Blandford et al., 2019), or changes to dendritic arbor structure (Henderson et al., 2021; Kalesnykas et al., 2012; Risner et al., 2018; Weber et al., 1998). In addition to age-related functional changes in aged EG, changes to dendritic structure have been studied and compared between adult and aged mice (Di Pierdomenico et al., 2021; Lee et al., 2022). Moreover, data from human retinas suggests that aging results in RGCs with smaller dendritic area, reduced branch points, and area under the curve following Sholl analyses in those aged 50 years or older compared to those under 30 years of age (Esquiva et al., 2017).

Di Pierdomenico and colleagues (2021) found that given the same IOP elevation, aged EG mice had greater loss of RGC dendritic complexity when compared to adult mice in Thy1-YFP line H mice, *in vivo* over 4-weeks of EG. Recently, Lee and colleagues

compared structural changes in ON-, and OFF-RGC dendritic arbors in adult and old mice following an acute elevated IOP. Their results showed a decrease in dendritic volume or complexity in ON-RGCs in both adult and old mice. OFF-RGC dendritic morphology became less complex in adult mice, but was unchanged in old mice (Lee et al., 2022). Future work that could correlate dendritic structural changes and functional analyses from the same cell, longitudinally, would provide valuable information about how cells change following IOP elevation.

The results of the aging studies performed in the current work highlight the importance of using aged animals to study age-related diseases like glaucoma. The need to use aged animals also extends to other CNS research where, apart from Alzheimer's disease research where aged rodents are used in 10% of total published literature, the use of aged animals in conditions such as stroke and Parkinson's disease, account for less than 5% of total studies (Sun et al., 2020). There are several factors that have contributed to the lack of aged animals used in research. Studies using adult mice are relatively less expensive, especially when the costs associated with purchasing aged mice, or generating aged mice are higher, and more time-consuming. Additionally, because young, or adult mice are readily available, larger sample sizes are easier to achieve without the need to consider the higher attrition rates present in aged animals. However, there is increasing evidence within the literature, in addition to that presented in this thesis, supporting the use of older mice to study EG, as the effects of IOP on cell structure and function can be significantly different.

6.5. Limitations and Future Directions

6.5.1. Experimental Glaucoma in Old Mice

To study effects of age and EG, we induced EG in mice aged with the virus. Inducing EG in aged mice allowed us to be able to study normal loss of cells over time, both RBPMS-positive, and GCaMP-positive. It is potentially the case that a better comparison could have been made if EG was induced following 8-weeks of viral transduction in old mice, to mimic the protocol that was used in the adult EG mice. Our data suggests that there is no difference in function between mice aged with the virus, and those mice injected with the virus when they were older, suggesting at least at baseline prior to EG induction, the cells are functionally similar. It would nonetheless be interesting to compare the aged EG data acquired in this thesis to an old EG group, where EG was induced following 8-weeks of viral transduction.

Another series of experiments which could be performed moving forward which would more closely represent a clinical scenario would be to inject mice with the viral vector shortly following induction of EG. Determining the success of viral transduction in mice that are experiencing elevated IOP related damage could be valuable if this tool is used for clinical diagnostics and to monitor disease progression. Similar work has been performed that showed successful transduction of RGCs with AAV viral vectors following ONC in mice (Nickells et al., 2017), therefore, it could also be hypothesized that there would not be impaired transduction in a model of EG. EG and intravitreal injection of the viral vector could be performed simultaneously, however, the level of inflammation would need to be closely monitored and considered when assessing damage.

6.5.2. GCaMP Protein Quantification

GCaMP protein levels quantified with Western blot were not performed in the present study. It is important to consider how GCaMP levels may change over time, specifically in mice injected with the virus and aged over long periods. AAV vectors are episomal and do not integrate into the host genome (Zincarelli et al., 2008), therefore, it is possible the amount of GCaMP protein may decrease over time. The amount of GCaMP6s protein within the cell may influence both baseline and peak fluorescence during Ca^{2+} imaging experiments because of the number of individual GCaMP proteins available to bind Ca^{2+} following chemical stimulation. For example, less GCaMP proteins within a cell could lead to artificially lower Ca^{2+} transients and an underestimation of function.

Future experiments could determine, when, following a single viral injection, a cell stops producing new GCaMP proteins and if there is gradual attrition of GCaMP proteins that occurs over time. In the aged group, our data suggests that along with a decrease in RBPMS-positive and GCaMP-positive cells, there is also a decrease in the proportion of RBPMS-positive cells that express GCaMP, indicating there may be a clearing of GCaMP proteins over time. If there is a gradual clearing of GCaMP proteins following AAV injection, it could influence timing of viral injections for aging and glaucoma research or represent a need to develop ways to perform repeat viral injections if long term AAV or transgene expression is required.

6.5.3. Functional Imaging

Ca^{2+} imaging performed in intact-isolated retinal preparations using chemical stimulation provides an adequate measure of the functional capacity of the cells expressing GCaMP and of the sensitivity of the GCaMP protein itself. However, chemical stimulation does not replicate functional responses under physiological conditions. Optical recordings in intact-isolated retinal preparations can be done, however, we did not have a microscope setup that would have permitted this evaluation. Performing optical stimulation in our intact-isolated retinal preparations would have required the addition of a light stimulus fed though the same submersion objective. Stimulation of this nature could be performed using either an ultraviolet (UV) stimulus, as mice have UV sensitive cone photoreceptors (Deegan & Jacobs, 1993; Jacobs et al., 1991), or 2P stimulation.

2P fluorescence imaging is an emerging tool in biological and biomedical research allowing high penetration depth into tissues, while minimizing phototoxicity compared to other imaging techniques such as confocal microscopy (Benninger & Piston, 2013). In single photon excitation, a photon of light is absorbed by a fluorophore, exciting it from its ground state to a higher energy excited state. Shortly after, the fluorophore returns to its ground state, emitting a photon of light (Wolf, 2013). In contrast, 2P excitation uses two photons of light, each photon with half the energy, but twice the wavelength, to excite the fluorescent reporter molecule with the same energy as single photon excitation (Benninger & Piston, 2013; Denk et al., 1995).

2P excitation ensures the excitation wavelength of fluorescent indicators such as GCaMP is outside of the spectral excitation wavelengths of the photoreceptors. For example, a wavelength of approximately 488 nm with single-photon excitation would directly excite both GCaMP and photoreceptors, therefore any increase in fluorescence detected could not be differentiated between direct stimulation of the GCaMP versus an increase in GCaMP fluorescence due to signal transduction from photoreceptors to RGCs. In contrast, with 2P excitation, the optimal excitation wavelength of GCaMP is decoupled from the photoreceptor excitation, using approximately 930 nm, and a visible light source.

Currently *in vivo* functional imaging using 2P excitation is being conducted to explore RGC function longitudinally with 2P imaging using GCaMP6s to successfully record *in vivo* functional Ca^{2+} transients using optical stimulation (Bar-Noam et al., 2016; Cheong et al., 2018; Qin et al., 2020). Future work in this area would extend the experiments we have performed using GCaMP to monitor functional loss in EG and in age to *in vivo* functional analysis using this 2P stimulation, as *in vivo* recordings could indicate a highly sensitive technique for monitoring RGC health prior to irreversible cell death in glaucoma.

6.5.4. Safety Studies and Markers of Retinal Health

GCC thickness measurements from segmented OCT images, along with cell densities quantified both *in vivo*, and from histological techniques were quantified as surrogate measures of RGC health. These measures, although informative, do not

provide sensitive information about the state of the RGC. For instance, segmented OCT images provide an estimate of RGC loss however, there are both neuronal, and non-neuronal tissues within the segmented layers. Additionally, IHC does not provide information on the functional status prior to tissue fixation, or where within the cell death pathway a cell would have been prior to tissue staining.

Additionally, as more studies are utilizing aged mice, it may be important to consider not only markers of cell health, but also the overall health of the animal. Aging is heterogeneous, because individuals age at varying rates, and there can be a large range in the health status of individuals with the same chronological age (Rockwood et al., 2000). The concept of frailty was introduced to consider the variability of aging or increased risk of adverse outcomes within people of the same age (Vaupel et al., 1979). Age, which is defined as a decline or deterioration of functional properties at the cellular or tissues level, differs slightly from that of frailty. Frailty is a closely related syndrome, that manifests as an age-related increased vulnerability to stressors, and decreased ability to maintain homeostasis (Fried et al., 2004). Frailty can be considered as deficit accumulation, where over someone's lifespan, they can be more or less likely to accumulate health deficits based on genetic predisposition, or environmental factors (Rockwood & Mitnitski, 2007). Similar patterns of deficit accumulation observed in humans have been seen in populations of C57Bl/6 mice, where both humans and mice show similar trends of increasing frailty index scores over their lifespans (Mitnitski et al., 2005; Rockwood et al., 2017). We did not perform frailty testing in our mice, however, we did observe behavioural differences across mice, with some continuing to be active,

while others appeared to have decrease locomotor activity, and a more hunched appearance. Future work could perform testing to assign frailty scores to the mice and correlate the scores with various structural and functional outcome measures following EG.

6.6. Conclusions

Elevated IOP and age are two important risk factors for glaucoma development and progression. The current clinical measures of RGC viability lack specificity and sensitivity to solely RGCs, and there is a need for a way to monitor not only RGC structure, but also their function over time. The ability to label RGCs using exogenous functional fluorescent markers and monitor their function following induction of EG is critical to understanding glaucoma pathology, and in developing tools to earlier diagnose functional loss. With increasing evidence suggesting functional loss may precede structural loss, the ability to detect cell dysfunction prior to irreversible cell death, could provide insights into effective therapeutic windows for treatments or neuroprotective strategies to prolong vision and quality of life.

Additionally, results from this thesis provide evidence to support using aged animals to study age-related diseases, like glaucoma. Given the aging population worldwide, it is critical to understand how age influences normal cell function, and susceptibility to disease. The differences between adult and aged animals should be considered when designing treatments and preclinical trails, so therapeutics can be

tailored for aging tissues and aging individuals, thereby increasing the likelihood of successful translation from animals to humans.

REFERENCES

Abbott, C. J., Choe, T. E., Burgoyne, C. F., Cull, G., Wang, L., & Fortune, B. (2014). Comparison of retinal nerve fiber layer thickness in vivo and axonal transport after chronic intraocular pressure elevation in young versus older rats. *PLoS ONE*, *9*(12).

Abdel-Majid, R. M., Archibald, M. L., Tremblay, F., & Baldridge, W. H. (2005). Tracer coupling of neurons in the rat retina inner nuclear layer labeled by Fluorogold. *Brain Research*, *1063*(2), 114–120.

Ai, L. W., Yuan, M., & Neufeld, A. H. (2007). Age-related changes in neuronal susceptibility to damage: Comparison of the retinal ganglion cells of young and old mice before and after optic nerve crush. *Annals of the New York Academy of Sciences*, *1097*, 64–66.

Alarcón-Martínez, L., Avilés-Trigueros, M., Galindo-Romero, C., Valiente-Soriano, J., Agudo-Barriuso, M., Villa, P. de la, Villegas-Pérez, M. P., & Vidal-Sanz, M. (2010). ERG changes in albino and pigmented mice after optic nerve transection. *Vision Research*, *50*(21), 2176–2187.

Alarcón-Martínez, L., de la Villa, P., Avilés-Trigueros, M., Blanco, R., Villegas-Pérez, M. P., & Vidal-Sanz, M. (2009). Short and long term axotomy-induced ERG changes in albino and pigmented rats. *Molecular Vision*, *15*, 2373–2383.

Allison, K., Patel, D., & Alabi, O. (2020). Epidemiology of Glaucoma: The Past, Present, and Predictions for the Future. *Cureus*.

Almasieh, M., & Levin, L. A. (2017). Neuroprotection in Glaucoma: Animal Models and Clinical Trials. *Annual Review of Vision Science*, *3*, 91–120.

Almasieh, M., Wilson, A. M., Morquette, B., Cueva Vargas, J. L., & Di Polo, A. (2012). The molecular basis of retinal ganglion cell death in glaucoma. *Progress in Retinal and Eye Research*, *31*(2), 152–181.

Amthor, F. R., Oyster, C. W., & Takahashi, E. S. (1984a). Morphology of on-off direction-selective ganglion cells in the rabbit retina. *Brain Research*, *298*(1), 187–190.

Andersen, J. K. (2004). Oxidative stress in neurodegeneration: Cause or consequence? *Nature Reviews Neuroscience*, *10*(7), S18.

Anderson, D. R. (1969). Ultrastructure of Human and Monkey Lamina Cribrosa and Optic Nerve Head. *Archives of Ophthalmology*, *82*(6), 800–814.

Anderson, D. R., Drance, S. M., & Schulzer, M. (1998). Comparison of glaucomatous progression between untreated patients with normal-tension glaucoma and patients with therapeutically reduced intraocular pressures. *American Journal of Ophthalmology*, *126*(4), 487–497.

Atan, D. (2018). Immunohistochemical phenotyping of mouse amacrine cell subtypes. *Methods in Molecular Biology*, *1753*, 237–248.

Babizhayev, M. A., & Bunin, A. Y. (1989). Lipid peroxidation in open-angle glaucoma. *Acta Ophthalmologica*, *67*(4), 371–377

Bachstetter, A. D., Xing, B., de Almeida, L., Dimayuga, E. R., Watterson, D. M., & Van Eldik, L. J. (2011). Microglial p38α MAPK is a key regulator of proinflammatory cytokine up-regulation induced by toll-like receptor (TLR) ligands or beta-amyloid (Aβ). *Journal of Neuroinflammation*, *8*.

Bainbridge, J. W. B., Mehat, M. S., Sundaram, V., Robbie, S. J., Barker, S. E., Ripamonti, C., Georgiadis, A., Mowat, F. M., Beattie, S. G., Gardner, P. J., Feathers, K. L., Luong, V. A., Yzer, S., Balaggan, K., Viswanathan, A., De Ravel, T. J. L., Casteels, I., Holder, G. E., Tyler, N., … Ali, R. R. (2015). Long-term effect of gene therapy on Leber's congenital amaurosis. *New England Journal of Medicine*, *372*(20), 1887–1897.

Bainbridge, J. W. B., Smith, A. J., Barker, S. S., Robbie, S., Henderson, R., Balaggan, K., Viswanathan, A., Holder, G. E., Stockman, A., Tyler, N., Petersen-Jones, S., Bhattacharya, S. S., Thrasher, A. J., Fitzke, F. W., Carter, B. J., Rubin, G. S., Moore, A. T., & Ali, R. R. (2008). Effect of gene therapy on visual function in Leber's congenital amaurosis. *New England Journal of Medicine*, *358*(21), 2231–2239.

Balakrishnan, B., & Jayandharan, G. (2014). Basic Biology of Adeno-Associated Virus (AAV) Vectors Used in Gene Therapy. *Current Gene Therapy*, *14*(2), 86–100.

Bar-Noam, A. S., Farah, N., & Shoham, S. (2016). Correction-free remotely scanned two-photon in vivo mouse retinal imaging. *Light: Science and Applications*, *5*(August 2015).

Bellezza, A. J., Rintalan, C. J., Thompson, H. W., Downs, J. C., Hart, R. T., & Burgoyne, C. F. (2003). Deformation of the lamina cribrosa and anterior scleral canal wall in early experimental glaucoma. *Investigative Ophthalmology and Visual Science*, *44*(2), 623–637.

Bennett, J., Ashtari, M., Wellman, J., Marshall, K. A., Cyckowski, L. L., Chung, D. C., McCague, S., Pierce, E. A., Chen, Y., Bennicelli, J. L., Zhu, X., Ying, G. S., Sun, J., Wright, J. F., Auricchio, A., Simonelli, F., Shindler, K. S., Mingozzi, F., High, K. A., & Maguire, A. M. (2012). Gene therapy: AAV2 gene therapy readministration in three adults with congenital blindness. *Science Translational Medicine*, *4*(120).

Bennett, J., Wellman, J., Marshall, K. A., McCague, S., Ashtari, M., DiStefano-Pappas, J., Elci, O. U., Chung, D. C., Sun, J., Wright, J. F., Cross, D. R., Aravand, P., Cyckowski, L. L., Bennicelli, J. L., Mingozzi, F., Auricchio, A., Pierce, E. A., Ruggiero, J., Leroy, B. P., … Maguire, A. M. (2016). Safety and durability of effect of contralateral-eye administration of AAV2 gene therapy in patients with childhood-onset blindness caused by RPE65 mutations: a follow-on phase 1 trial. *The Lancet*, *388*(10045), 661–672.

Benninger, R. K. P., & Piston, D. W. (2013). Two-photon excitation microscopy for unit 4.11 the study of living cells and tissues. *Current Protocols in Cell Biology*, *SUPPL.59*.

Bhat, R., Crowe, E. P., Bitto, A., Moh, M., Katsetos, C. D., Garcia, F. U., Johnson, F. B., Trojanowski, J. Q., Sell, C., & Torres, C. (2012). Astrocyte Senescence as a Component of Alzheimer's Disease. *PLoS ONE*, *7*(9).

Biermann, J., van Oterendorp, C., Stoykow, C., Volz, C., Jehle, T., Boehringer, D., & Lagrèze, W. A. (2012). Evaluation of intraocular pressure elevation in a modified laser-induced glaucoma rat model. *Experimental Eye Research*, *104*, 7–14.

Biswas, S., & Wan, K. H. (2019). Review of rodent hypertensive glaucoma models. *Acta Ophthalmologica*, *97*(3), e331–e340.

Bitto, A., Sell, C., Crowe, E., Lorenzini, A., Malaguti, M., Hrelia, S., & Torres, C. (2010). Stress-induced senescence in human and rodent astrocytes. *Experimental Cell Research*, *316*(17), 2961–2968.

Blandford, S. N., Hooper, M. L., Yabana, T., Chauhan, B. C., Baldridge, W. H., & Farrell, S. R. M. (2019). Retinal characterization of the thy1-GcaMP3 transgenic mouse line after optic nerve transection. *Investigative Ophthalmology and Visual Science*, *60*(1), 183–191.

Borghuis, B. G., Tian, L., Xu, Y., Nikonov, S. S., Vardi, N., Zemelman, B. V., & Looger, L. L. (2011). Imaging light responses of targeted neuron populations in the rodent retina. *Journal of Neuroscience*, *31*(8), 2855–2867.

Bouhenni, R. A., Dunmire, J., Sewell, A., & Edward, D. P. (2012). Animal models of glaucoma. *Journal of Biomedicine and Biotechnology*, *2012*.

Bringmann, A., Pannicke, T., Grosche, J., Francke, M., Wiedemann, P., Skatchkov, S. N., Osborne, N. N., & Reichenbach, A. (2006). Müller cells in the healthy and diseased retina. *Progress in Retinal and Eye Research*, *25*(4), 397–424.

Budenz, D. L., Anderson, D. R., Varma, R., Schuman, J., Cantor, L., Savell, J., Greenfield, D. S., Patella, V. M., Quigley, H. A., & Tielsch, J. (2007). Determinants of Normal Retinal Nerve Fiber Layer Thickness Measured by Stratus OCT. *Ophthalmology*, *114*(6), 1046–1052.

Bui, B. V., Edmunds, B., Cioffi, G. A., & Fortune, B. (2005). The gradient of retinal functional changes during acute intraocular pressure elevation. *Investigative Ophthalmology and Visual Science*, *46*(1), 202–213.

Bui, B. V., & Fortune, B. (2004). Ganglion cell contributions to the rat full-field electroretinogram. *Journal of Physiology*, *555*(1), 153–173.

Burgoyne, C. F. (2011). A biomechanical paradigm for axonal insult within the optic nerve head in aging and glaucoma. *Experimental Eye Research*, *93*(2), 120–132.

Burgoyne, C. F. (2015). The non-human primate experimental glaucoma model. *Experimental Eye Research*, *141*, 57–73.

Burgoyne, C. F., Downs, J. C., Bellezza, A. J., & Hart, R. T. (2004). Three-dimensional reconstruction of normal and early glaucoma monkey optic nerve head connective tissues. *Investigative Ophthalmology and Visual Science*, *45*(12), 4388–4399.

Bussel, I. I., Wollstein, G., & Schuman, J. S. (2014). OCT for glaucoma diagnosis, screening and detection of glaucoma progression. *British Journal of Ophthalmology*, *98*(SUPPL. 2).

Călin, E. F., (Patoni) Popescu, S. I., (Coman) Cernat, C. C., Patoni, C., Popescu, M.-N., & Mușat, O. (2021). Lipofuscin: a key compound in ophthalmic practice. *Romanian Journal of Ophthalmology*, *65*(2), 109–113.

Calkins, D. J. (2013). Age-related changes in the visual pathways: Blame it on the axon. *Investigative Ophthalmology and Visual Science*, *54*(14).

Campagno, K. E., Lu, W., Jassim, A. H., Albalawi, F., Cenaj, A., Tso, H.-Y., Clark, S. P., Sripinun, P., Gómez, N. M., & Mitchell, C. H. (2021). Rapid morphologic changes to microglial cells and upregulation of mixed microglial activation state markers induced by P2X7 receptor stimulation and increased intraocular pressure. *Journal of Neuroinflammation*, *18*(1), 217.

Campisi, J., & D'Adda Di Fagagna, F. (2007). Cellular senescence: When bad things happen to good cells. *Nature Reviews Molecular Cell Biology*, *8*(9), 729–740.

Caprioli, J. (2013a). Glaucoma: A disease of early cellular senescence. *Investigative Ophthalmology and Visual Science*, *54*(14).

Carter, D. A., Vidal-Sanz, M., & Aguayo, A. J. (1987). Long-term preservation of intrinsic retinal neurons after axotomy-induced death of retinal ganglion cells. *Soc Neurosci*, *13*, 1390.

Causin, P., Guidoboni, G., Harris, A., Prada, D., Sacco, R., & Terragni, S. (2014). A poroelastic model for the perfusion of the lamina cribrosa in the optic nerve head. *Mathematical Biosciences*, *257*, 33–41.

Cedrone, C., Culasso, F., Cesareo, M., Mancino, R., Ricci, F., Cupo, G., & Cerulli, L. (1999). Prevalence and incidence of age-related cataract in a population sample from Priverno, Italy. *Ophthalmic Epidemiology*, *6*(2), 95–103.

Cepurna, W. O., Kayton, R. J., Johnson, E. C., & Morrison, J. C. (2005). Age related optic nerve axonal loss in adult Brown Norway rats. *Experimental Eye Research*, *80*(6), 877–884.

Chan, K. C., Yu, Y., Ng, S. H., Mak, H. K., Yip, Y. W. Y., van der Merwe, Y., Ren, T., Yung, J. S. Y., Biswas, S., Cao, X., Chau, Y., & Leung, C. K. S. (2019). Intracameral injection of a chemically cross-linked hydrogel to study chronic neurodegeneration in glaucoma. *Acta Biomaterialia*, *94*, 219–231.

Chang, B., Smith, R. S., Hawes, N. L., Anderson, M. G., Zabaleta, A., Savinova, O., Roderick, T. H., Heckenlively, J. R., Davisson, M. T., & John, S. W. M. (1999). Interacting loci cause severe iris atrophy and glaucoma in DBA/2J mice. *Nature Genetics*, *21*(4), 405–409.

Charng, J., Nguyen, C. T. O., Bui, B. V., & Vingrys, A. J. (2011). Age-related retinal function changes in albino and pigmented rats. *Investigative Ophthalmology and Visual Science*, *52*(12), 8891–8899.

Chauhan, B. C. (1996). Confocal scanning laser tomography. *Canadian Journal of Ophthalmology*, *31*(3), 152–156.

Chauhan, B. C., LeVatte, T. L., Jollimore, C. A., Yu, P. K., Reitsamer, H. A., Kelly, M. E. M., Yu, D. Y., Tremblay, F., & Archibald, M. L. (2004). Model of Endothelin-1-Induced Chronic Optic Neuropathy in Rat. *Investigative Ophthalmology and Visual Science*, *45*(1), 144–152.

Chauhan, B. C., Pan, J., Archibald, M. L., LeVatte, T. L., Kelly, M. E. M., & Tremblay, F. (2002). Effect of intraocular pressure on optic disc topography, electroretinography, and axonal loss in a chronic pressure-induced rat model of optic nerve damage. *Investigative Ophthalmology and Visual Science*, *43*(9), 2969–2976.

Chauhan, B. C., Stevens, K. T., Levesque, J. M., Nuschke, A. C., Sharpe, G. P., O'Leary, N., Archibald, M. L., & Wang, X. (2012). Longitudinal in vivo imaging of retinal ganglion cells and retinal thickness changes following optic nerve injury in mice. *PLoS ONE*, *7*(6).

Chauhan, B. C., Vianna, J. R., Sharpe, G. P., Demirel, S., Girkin, C. A., Mardin, C. Y., Scheuerle, A. F., & Burgoyne, C. F. (2020). Differential Effects of Aging in the Macular Retinal Layers, Neuroretinal Rim, and Peripapillary Retinal Nerve Fiber Layer. *Ophthalmology*, *127*(2), 177–185.

Chen, H., & Weber, A. J. (2001). BDNF enhances retinal ganglion cell survival in cats with optic nerve damage. *Investigative Ophthalmology and Visual Science*, *42*(5), 966–974.

Chen, H., Wei, X., Cho, K. S., Chen, G., Sappington, R., Calkins, D. J., & Chen, D. F. (2011). Optic neuropathy due to microbead-induced elevated intraocular pressure in the mouse. *Investigative Ophthalmology and Visual Science*, *52*(1), 36–44.

Chen, L., Zhao, Y., & Zhang, H. (2017). Comparative anatomy of the trabecular meshwork, the optic nerve head and the inner retina in rodent and primate models used for glaucoma research. *Vision (Switzerland)*, *1*(1), 1–12.

Chen, T. W., Wardill, T. J., Sun, Y., Pulver, S. R., Renninger, S. L., Baohan, A., Schreiter, E. R., Kerr, R. A., Orger, M. B., Jayaraman, V., Looger, L. L., Svoboda, K., & Kim, D. S. (2013). Ultrasensitive fluorescent proteins for imaging neuronal activity. *Nature*, *499*(7458), 295–300.

Chen, Y., Qin, C., Huang, J., Tang, X., Liu, C., Huang, K., Xu, J., Guo, G., Tong, A., & Zhou, L. (2020). The role of astrocytes in oxidative stress of central nervous system: A mixed blessing. *Cell Proliferation*, *53*(3).

Cheong, S. K., Xiong, W., Strazzeri, J. M., Cepko, C. L., Williams, D. R., & Merigan, W. H. (2018). In vivo functional imaging of retinal neurons using red and green fluorescent calcium indicators. *Advances in Experimental Medicine and Biology*, *1074*, 135–144.

Chinta, S. J., Woods, G., Demaria, M., Rane, A., Zou, Y., McQuade, A., Rajagopalan, S., Limbad, C., Madden, D. T., Campisi, J., & Andersen, J. K. (2018). Cellular Senescence Is Induced by the Environmental Neurotoxin Paraquat and Contributes to Neuropathology Linked to Parkinson's Disease. *Cell Reports*, *22*(4), 930–940.

Chrysostomou, V., & Crowston, J. G. (2013). The photopic negative response of the mouse electroretinogram: Reduction by acute elevation of intraocular pressure. *Investigative Ophthalmology and Visual Science*, *54*(7), 4691–4697.

Colella, P., Ronzitti, G., & Mingozzi, F. (2018). Emerging Issues in AAV-Mediated In Vivo Gene Therapy. *Molecular Therapy - Methods and Clinical Development*, *8*, 87–104.

Coleman, A. L., Gordon, M. O., Beiser, J. A., & Kass, M. A. (2004). Baseline risk factors for the development of primary open-angle glaucoma in the Ocular Hypertension Treatment Study. *American Journal of Ophthalmology*, *138*(4), 684–685.

Coleman, A. L., & Miglior, S. (2008). Risk Factors for Glaucoma Onset and Progression. *Survey of Ophthalmology*, *53*(6 SUPPL.).

Cone, F. E., Gelman, S. E., Son, J. L., Pease, M. E., & Quigley, H. A. (2010). Differential susceptibility to experimental glaucoma among 3 mouse strains using bead and viscoelastic injection. *Experimental Eye Research*, *91*(3), 415–424.

Coppé, J. P., Desprez, P. Y., Krtolica, A., & Campisi, J. (2010). The senescence-associated secretory phenotype: The dark side of tumor suppression. *Annual Review of Pathology: Mechanisms of Disease*, *5*, 99–118.

Coppé, J. P., Patil, C. K., Rodier, F., Sun, Y., Muñoz, D. P., Goldstein, J., Nelson, P. S., Desprez, P. Y., & Campisi, J. (2008). Senescence-associated secretory phenotypes reveal cell-nonautonomous functions of oncogenic RAS and the p53 tumor suppressor. *PLoS Biology*, *6*(12).

Cordeiro, M. F., Guo, L., Luong, V., Harding, G., Wang, W., Jones, H. E., Moss, S. E., Sillito, A. M., & Fitzke, F. W. (2004). Real-time imaging of single nerve cell apoptosis in retinal neurodegeneration. *Proceedings of the National Academy of Sciences of the United States of America*, *101*(36), 13352–13356.

Cuenca, N., Pinilla, I., Fernández-Sánchez, L., Salinas-Navarro, M., Alarcón-Martínez, L., Avilés-Trigueros, M., de la Villa, P., Miralles de Imperial, J., Villegas-Pérez, M. P., & Vidal-Sanz, M. (2010). Changes in the inner and outer retinal layers after acute increase of the intraocular pressure in adult albino Swiss mice. *Experimental Eye Research*, *91*(2), 273–285.

Cukras, C., Wiley, H. E., Jeffrey, B. G., Sen, H. N., Turriff, A., Zeng, Y., Vijayasarathy, C., Marangoni, D., Ziccardi, L., Kjellstrom, S., Park, T. K., Hiriyanna, S., Wright, J. F., Colosi, P., Wu, Z., Bush, R. A., Wei, L. L., & Sieving, P. A. (2018). Retinal AAV8-RS1 Gene Therapy for X-Linked Retinoschisis: Initial Findings from a Phase I/IIa Trial by Intravitreal Delivery. *Molecular Therapy*, *26*(9), 2282–2294.

Curcio, C. A., Millican, C. L., Allen, K. A., & Kalina, R. E. (1993). Aging of the human photoreceptor mosaic: Evidence for selective vulnerability of rods in central retina. *Investigative Ophthalmology and Visual Science*, *34*(12), 3278–3296.

D. Lukasiewicz, P. (2005). Synaptic mechanisms that shape visual signaling at the inner retina. *Progress in Brain Research*, *147*(SPEC. ISS.), 205–218.

Dana, H., Sun, Y., Mohar, B., Hulse, B. K., Kerlin, A. M., Hasseman, J. P., Tsegaye, G., Tsang, A., Wong, A., Patel, R., Macklin, J. J., Chen, Y., Konnerth, A., Jayaraman, V., Looger, L. L., Schreiter, E. R., Svoboda, K., & Kim, D. S. (2019). High-performance calcium sensors for imaging activity in neuronal populations and microcompartments. *Nature Methods*, *16*(7), 649–657.

Danias, J., Lee, K. C., Zamora, M. F., Chen, B., Shen, F., Filippopoulos, T., Su, Y., Goldblum, D., Podos, S. M., & Mittag, T. (2003a). Quantitative Analysis of Retinal Ganglion Cell (RGC) Loss in Aging DBA/2NNia Glaucomatous Mice: Comparison with RGC Loss in Aging C57/BL6 Mice. *Investigative Ophthalmology and Visual Science*, *44*(12), 5151–5162.

David, R., Zangwill, L., Stone, D., & Yassur, Y. (1987). Epidemiology of intraocular pressure in a population screened for glaucoma. *British Journal of Ophthalmology*, *71*(10), 766–771.

de Leeuw, C. N., Dyka, F. M., Boye, S. L., Laprise, S., Zhou, M., Chou, A. Y., Borretta, L., McInerny, S. C., Banks, K. G., Portales-Casamar, E., Swanson, M. I., D'Souza, C. A., Boye, S. E., Jones, S. J., Holt, R. A., Goldowitz, D., Hauswirth, W. W., Wasserman, W. W., & Simpson, E. M. (2014). Targeted CNS delivery using human MiniPromoters and demonstrated compatibility with adeno-associated viral vectors. *Molecular Therapy - Methods and Clinical Development*, *1*, 5.

Deegan, J. F., & Jacobs, G. H. (1993). On the Identity of the Cone Types of the Rat Retina. *Experimental Eye Research*, *56*(3), 375–377.

Deng, Y., Wang, H., Simms, A. G., Hu, H., Zhang, J., Gameiro, G. R., Rundek, T., Signorile, J. F., Levin, B. E., Yuan, J., Wang, J., & Jiang, H. (2022). Age-related focal thinning of the ganglion cell-inner plexiform layer in a healthy population. *Quantitative Imaging in Medicine and Surgery*, *12*(6), 3034–3048.

Denk, W., Piston, D. W., & Webb, W. W. (1995). Two-Photon Molecular Excitation in Laser-Scanning Microscopy. *Handbook of Biological Confocal Microscopy*, 445–458.

Di Mitri, D., & Alimonti, A. (2016). Non-Cell-Autonomous Regulation of Cellular Senescence in Cancer. *Trends in Cell Biology*, *26*(3), 215–226.

Di Pierdomenico, J., Henderson, D. C. M., Giammaria, S., Smith, V. L., Jamet, A. J., Smith, C. A., Hooper, M. L., & Chauhan, B. C. (2022). Age and intraocular pressure in murine experimental glaucoma. *Progress in Retinal and Eye Research*, *88*.

Di Polo, A., Aigner, L. J., Dunn, R. J., Bray, G. M., & Aguayo, A. J. (1998a). Prolonged delivery of brain-derived neurotrophic factor by adenovirus-infected Müller cells temporarily rescues injured retinal ganglion cells. *Proceedings of the National Academy of Sciences of the United States of America*, *95*(7), 3978–3983.

Di Polo, A., Aigner, L. J., Dunn, R. J., Bray, G. M., & Aguayo, A. J. (1998b). Prolonged delivery of brain-derived neurotrophic factor by adenovirus-infected Müller cells temporarily rescues injured retinal ganglion cells. *Proceedings of the National Academy of Sciences of the United States of America*, *95*(7), 3978–3983.

Dolman, C. L., Mccormick, A. Q., & Drance, S. M. (1980). Aging of the Optic Nerve. *Archives of Ophthalmology*, *98*(11), 2053–2058.

Dong, C. J., Guo, Y., Agey, P., Wheeler, L., & Hare, W. A. (2008). α2 adrenergic modulation of NMDA receptor function as a major mechanism of RGC protection in experimental glaucoma and retinal excitotoxicity. *Investigative Ophthalmology and Visual Science*, *49*(10), 4515–4522.

Dong, L., Hu, Y., Zhou, L., & Cheng, X. (2017). P2X7 receptor antagonist protects retinal ganglion cells by inhibiting microglial activation in a rat chronic ocular hypertension model. *Molecular Medicine Reports*.

Drag, S., Dotiwala, F., & Upadhyay, A. K. (2023). Gene Therapy for Retinal Degenerative Diseases: Progress, Challenges, and Future Directions. *Investigative Opthalmology & Visual Science*, *64*(7), 39.

El-Danaf, R. N., & Huberman, A. D. (2015). Characteristic patterns of dendritic remodeling in early-stage glaucoma: Evidence from genetically identified retinal ganglion cell types. *Journal of Neuroscience*, *35*(6), 2329–2343.

Esquiva, G., Lax, P., Pérez-Santonja, J. J., García-Fernández, J. M., & Cuenca, N. (2017). Loss of melanopsin-expressing ganglion cell subtypes and dendritic degeneration in the aging human retina. *Frontiers in Aging Neuroscience*, *9*(APR).

Feng, G., Mellor, R. H., Bernstein, M., Keller-Peck, C., Nguyen, Q. T., Wallace, M., Nerbonne, J. M., Lichtman, J. W., & Sanes, J. R. (2000). Imaging neuronal subsets in transgenic mice expressing multiple spectral variants of GFP. *Neuron*, *28*(1), 41–51.

Feng, L., Zhao, Y., Yoshida, M., Chen, H., Yang, J. F., Kim, T. S., Cang, J., Troy, J. B., & Liu, X. (2013). Sustained ocular hypertension induces dendritic degeneration of mouse retinal ganglion cells that depends on cell type and location. *Investigative Ophthalmology and Visual Science*, *54*(2), 1106–1117.

Ferdous, S., Liao, K. L., Gefke, I. D., Summers, V. R., Wu, W., Donaldson, K. J., Kim, Y. K., Sellers, J. T., Dixon, J. A., Shelton, D. A., Markand, S., Kim, S. M., Zhang, N., Boatright, J. H., & Nickerson, J. M. (2021). Age-related retinal changes in wild-type C57BL/6J mice between 2 and 32 months. *Investigative Ophthalmology and Visual Science*, *62*(7).

Flach, J., Bakker, S. T., Mohrin, M., Conroy, P. C., Pietras, E. M., Reynaud, D., Alvarez, S., Diolaiti, M. E., Ugarte, F., Forsberg, E. C., Le Beau, M. M., Stohr, B. A., Méndez, J., Morrison, C. G., & Passegué, E. (2014). Replication stress is a potent driver of functional decline in ageing haematopoietic stem cells. *Nature 2014 512:7513*, *512*(7513), 198–202.

Flanary, B. E., Sammons, N. W., Nguyen, C., Walker, D., & Streit, W. J. (2007). Evidence that aging and amyloid promote microglial cell senescence. *Rejuvenation Research*, *10*(1), 61–74.

Fortune, B., Bui, B. V., Morrison, J. C., Johnson, E. C., Dong, J., Cepurna, W. O., Jia, L. J., Barber, S., & Cioffi, G. A. (2004). Selective ganglion cell functional loss in rats with experimental glaucoma. *Investigative Ophthalmology and Visual Science*, *45*(6), 1854–1862.

Fortune, B., Cull, G., Reynaud, J., Wang, L., & Burgoyne, C. F. (2015). Relating retinal ganglion cell function and retinal nerve fiber layer (RNFL) retardance to progressive loss of RNFL thickness and optic nerve axons in experimental glaucoma. *Investigative Ophthalmology and Visual Science*, *56*(6), 3936–3944.

Fried, L. P., Ferrucci, L., Darer, J., Williamson, J. D., & Anderson, G. (2004). Untangling the Concepts of Disability, Frailty, and Comorbidity: Implications for Improved Targeting and Care. *Journals of Gerontology - Series A Biological Sciences and Medical Sciences*, *59*(3), 255–263.

Gaasterland, D. E., Ederer, F., Beck, A., Costarides, A., Leef, D., Closek, J., Banks, J., Jackson, S., Moore, K., Vela, A., Brown, R. H., Lynch, M., Gunsby, J., Lober, K., Marsh, T., Stepka, C., Montgomery, R., Clagett, D., Ashburn, F., … Van Veldhuisen, P. C. (2000). The Advanced Glaucoma Intervention Study (AGIS): 7. The relationship between control of intraocular pressure and visual field deterioration. *American Journal of Ophthalmology*, *130*(4), 429–440.

Galindo-Romero, C., Avilés-Trigueros, M., Jiménez-López, M., Valiente-Soriano, F. J., Salinas-Navarro, M., Nadal-Nicolás, F., Villegas-Pérez, M. P., Vidal-Sanz, M., & Agudo-Barriuso, M. (2011). Axotomy-induced retinal ganglion cell death in adult mice: Quantitative and topographic time course analyses. *Experimental Eye Research*, *92*(5), 377–387.

Gao, H., & Hollyfield, J. G. (1992). Aging of the human retina: Differential loss of neurons and retinal pigment epithelial cells. *Investigative Ophthalmology and Visual Science*, *33*(1), 1–17.

Geng, Y. Q., Guan, J. T., Xu, X. H., & Fu, Y. C. (2010). Senescence-associated beta-galactosidase activity expression in aging hippocampal neurons. *Biochemical and Biophysical Research Communications*, *396*(4), 866–869.

Glasser, A., & C.W. Campbell, M. (1999). Biometric, optical and physical changes in the isolated human crystalline lens with age in relation to presbyopia. *Vision Research*, *39*(11), 1991–2015.

Gresh, J., Goletz, P. W., Crouch, R. K., & Rohrer, B. (2003). Structure-function analysis of rods and cones in juvenile, adult, and aged C57BL/6 and Balb/c mice. *Visual Neuroscience*, *20*(2), 211–220.

Grieger, J. C., & Samulski, R. J. (2005). Packaging Capacity of Adeno-Associated Virus Serotypes: Impact of Larger Genomes on Infectivity and Postentry Steps. *Journal of Virology*, *79*(15), 9933–9944.

Guo, L., Moss, S. E., Alexander, R. A., Ali, R. R., Fitzke, F. W., & Cordeiro, M. F. (2005). Retinal ganglion cell apoptosis in glaucoma is related to intraocular pressure and IOP-induced effects on extracellular matrix. *Investigative Ophthalmology and Visual Science*, *46*(1), 175–182.

Guo, L., Normando, E. M., Nizari, S., Lara, D., & Francesca Cordeiro, M. (2010). Tracking longitudinal retinal changes in experimental ocular hypertension using the cSLO and spectral domain-OCT. *Investigative Ophthalmology and Visual Science*, *51*(12), 6504–6513.

Haas, A., Flammer, J., & Schneider, U. (1986). Influence of age on the visual fields of normal subjects. *American Journal of Ophthalmology*, *101*(2), 199–203.

Halliwell, B. (2006). Oxidative stress and neurodegeneration: Where are we now? *Journal of Neurochemistry*, *97*(6), 1634–1658.

Hanisch, U. K. (2002). Microglia as a source and target of cytokines. *Glia*, *40*(2), 140–155.

Hanlon, K. S., Chadderton, N., Palfi, A., Fernandez, A. B., Humphries, P., Kenna, P. F., Millington-Ward, S., & Farrar, G. J. (2017). A novel retinal ganglion cell promoter for utility in AAV vectors. *Frontiers in Neuroscience*, *11*(SEP).

Hare, W., WoldeMussie, E., Lai, R., Ton, H., Ruiz, G., Feldmann, B., Wijono, M., Chun, T., & Wheeler, L. (2001). Efficacy and safety of memantine, an NMDA-type open-channel blocker, for reduction of retinal injury associated with experimental glaucoma in rat and monkey. *Survey of Ophthalmology*, *45*(6).

Hartsock, M. J., Cho, H., Wu, L., Chen, W. J., Gong, J., & Duh, E. J. (2016). A mouse model of retinal ischemia-reperfusion injury through elevation of intraocular pressure. *Journal of Visualized Experiments*, *2016*(113).

Harvey, A. R., Kamphuis, W., Eggers, R., Symons, N. A., Blits, B., Niclou, S., Boer, G. J., & Verhaagen, J. (2002). Intravitreal injection of adeno-associated viral vectors results in the transduction of different types of retinal neurons in neonatal and adult rats: A comparison with lentiviral vectors. *Molecular and Cellular Neuroscience*, *21*(1), 141–157.

Harwerth, R. S., Wheat, J. L., & Rangaswamy, N. V. (2008). Age-related losses of retinal ganglion cells and axons. *Investigative Ophthalmology and Visual Science*, *49*(10), 4437–4443.

Hashemi, H., Pakzad, R., Yekta, A., Aghamirsalim, M., Pakbin, M., Ramin, S., & Khabazkhoob, M. (2020). Global and regional prevalence of age-related cataract: a comprehensive systematic review and meta-analysis. *Eye (Basingstoke)*, *34*(8), 1357–1370.

Hattar, S., Kumar, M., Park, A., Tong, P., Tung, J., Yau, K. W., & Berson, D. M. (2006). Central projections of melanopsin-expressing retinal ganglion cells in the mouse. *Journal of Comparative Neurology*, *497*(3), 326–349.

Haverkamp, S., & Wässle, H. (2000). Immunocytochemical analysis of the mouse retina. *Journal of Comparative Neurology*, *424*(1), 1–23.

Hayflick, L., & Moorhead, P. S. (1961). The serial cultivation of human diploid cell strains. *Experimental Cell Research*, *25*(3), 585–621.

Heijl, A., Leske, M. C., Bengtsson, B., Hyman, L., Bengtsson, B., & Hussein, M. (2002). Reduction of intraocular pressure and glaucoma progression: Results from the Early Manifest Glaucoma Trial. *Archives of Ophthalmology*, *120*(10), 1268–1279.

Henderson, D. C. M., Vianna, J. R., Gobran, J., Pierdomenico, J. Di, Hooper, M. L., Farrell, S. R. M., & Chauhan, B. C. (2021). Longitudinal in vivo changes in retinal ganglion cell dendritic morphology after acute and chronic optic nerve injury. *Investigative Ophthalmology and Visual Science*, *62*(9).

Hernandez, M. R. (1992). Ultrastructural immunocytochemical analysis of elastin in the human lamina cribrosa: Changes in elastic fibers in primary open-angle glaucoma. *Investigative Ophthalmology and Visual Science*, *33*(10), 2891–2903.

Hernandez-Segura, A., Nehme, J., & Demaria, M. (2018). Hallmarks of Cellular Senescence. *Trends in Cell Biology*, *28*(6), 436–453.

Heys, K. R., Cram, S. L., & Truscott, R. J. W. (2004). Massive increase in the stiffness of the human lens nucleus with age: The basis for presbyopia? *Molecular Vision*, *10*, 956–963.

Hildebrand, C., Remahl, S., & Waxman, S. G. (1985). Axo-glial relations in the retina-optic nerve junction of the adult rat: electron-microscopic observations. *Journal of Neurocytology*, *14*(4), 597–617.

Holz, F. G., Bindewald-Wittich, A., Fleckenstein, M., Dreyhaupt, J., Scholl, H. P. N., & Schmitz-Valckenberg, S. (2007). Progression of Geographic Atrophy and Impact of Fundus Autofluorescence Patterns in Age-related Macular Degeneration. *American Journal of Ophthalmology*, *143*(3).

Howell, G. R., Libby, R. T., Jakobs, T. C., Smith, R. S., Phalan, F. C., Barter, J. W., Barbay, J. M., Marchant, J. K., Mahesh, N., Porciatti, V., Whitmore, A. V., Masland, R. H., & John, S. W. M. (2007). Axons of retinal ganglion cells are insulted in the optic nerve early in DBA/2J glaucoma. *Journal of Cell Biology*, *179*(7), 1523–1537.

Huang, W., Fileta, J. B., Dobberfuhl, A., Filippopolous, T., Guo, Y., Kwon, G., & Grosskreutz, C. L. (2005). Calcineurin cleavage is triggered by elevated intraocular pressure, and calcineurin inhibition blocks retinal ganglion cell death in experimental glaucoma. *Proceedings of the National Academy of Sciences of the United States of America*, *102*(34), 12242–12247.

Huang, W., Fileta, J., Guo, Y., & Grosskreutz, C. L. (2006). Downregulation of Thy1 in retinal ganglion cells in experimental glaucoma. *Current Eye Research*, *31*(3), 265–271.

Huang, W., Fileta, J., Rawe, I., Qu, J., & Grosskreutz, C. L. (2010). Calpain activation in experimental glaucoma. *Investigative Ophthalmology and Visual Science*, *51*(6), 3049–3054.

Ishikawa, M., Izumi, Y., Sato, K., Sato, T., Zorumski, C. F., Kunikata, H., & Nakazawa, T. (2023). Glaucoma and microglia-induced neuroinflammation. *Frontiers in Ophthalmology*, *3*.

Ito, Y. A., Belforte, N., Cueva Vargas, J. L., & di Polo, A. (2016). A magnetic microbead occlusion model to induce ocular hypertension-dependent glaucoma in mice. *Journal of Visualized Experiments*, *2016*(109).

Izzotti, A., Saccà, S. C., Cartiglia, C., & De Flora, S. (2003). Oxidative deoxyribonucleic acid damage in the eyes of glaucoma patients. *American Journal of Medicine*, *114*(8), 638–646.

Jacobs, G. H., Neitz, J., & Deegan, J. F. (1991). Retinal receptors in rodents maximally sensitive to ultraviolet light. *Nature*, *353*(6345), 655–656.

Jaffe, G. J., Alvarado, J. A., & Juster, R. P. (1986). Age-Related Changes of the Normal Visual Field. *Archives of Ophthalmology*, *104*(7), 1021–1025.

Jakobs, T. C., Libby, R. T., Ben, Y., John, S. W. M., & Masland, R. H. (2005a). Retinal ganglion cell degeneration is topological but not cell type specific in DBA/2J mice. *Journal of Cell Biology*, *171*(2), 313–325.

Jeon, C. J., Strettoi, E., & Masland, R. H. (1998). The major cell populations of the mouse retina. *Journal of Neuroscience*, *18*(21), 8936–8946.

John, S. W. M., Hagaman, J. R., MacTaggart, T. E., Peng, L., & Smithes, O. (1997). Intraocular pressure in inbred mouse strains. *Investigative Ophthalmology and Visual Science*, *38*(1), 249–253.

John, S. W. M., Smith, R. S., Savinova, O. V., Hawes, N. L., Chang, B., Turnbull, D., Davisson, M., Roderick, T. H., & Heckenlively, J. R. (1998). Essential iris atrophy, pigment dispersion, and glaucoma in DBA/2J mice. *Investigative Ophthalmology and Visual Science*, *39*(6), 951–962.

Johnson, E. C., Morrison, J. C., Farrell, S., Deppmeier, L., Moore, C. G., & Mcginty, M. R. (1996). The effect of chronically elevated intraocular pressure on the rat optic nerve head extracellular matrix. *Experimental Eye Research*, *62*(6), 663–674.

Johnson, T. V., Bull, N. D., & Martin, K. R. (2011). Neurotrophic factor delivery as a protective treatment for glaucoma. *Experimental Eye Research*, *93*(2), 196–203.

Jurk, D., Wang, C., Miwa, S., Maddick, M., Korolchuk, V., Tsolou, A., Gonos, E. S., Thrasivoulou, C., Jill Saffrey, M., Cameron, K., & von Zglinicki, T. (2012). Postmitotic neurons develop a p21-dependent senescence-like phenotype driven by a DNA damage response. *Aging Cell*, *11*(6), 996–1004.

Kalesnykas, G., Oglesby, E. N., Zack, D. J., Cone, F. E., Steinhart, M. R., Tian, J., Pease, M. E., & Quigley, H. A. (2012). Retinal ganglion cell morphology after optic nerve crush and experimental glaucoma. *Investigative Ophthalmology and Visual Science*, *53*(7), 3847–3857.

Kass, M. A., Heuer, D. K., Higginbotham, E. J., Johnson, C. A., Keltner, J. L., Philip Miller, J., Parrish, R. K., Roy Wilson, M., & Gordon, M. O. (2002). The Ocular Hypertension Treatment Study: A randomized trial determines that topical ocular hypotensive medication delays or prevents the onset of primary open-angle glaucoma. *Archives of Ophthalmology*, *120*(6), 701–713.

Keeler, A. M., & Flotte, T. R. (2019). Recombinant Adeno-Associated Virus Gene Therapy in Light of Luxturna (and Zolgensma and Glybera): Where Are We, and How Did We Get Here? *Annual Review of Virology*, *6*(1), 601–621.

Kessler, P. D., Podsakoff, G. M., Chen, X., McQuiston, S. A., Colosi, P. C., Matelis, L. A., Kurtzman, G. J., & Byrne, B. J. (1996). Gene delivery to skeletal muscle results in sustained expression and systemic delivery of a therapeutic protein. *Proceedings of the National Academy of Sciences of the United States of America*, *93*(24), 14082–14087.

Kim, B. J., Braun, T. A., Wordinger, R. J., & Clark, A. F. (2013). Progressive morphological changes and impaired retinal function associated with temporal regulation of gene expression after retinal ischemia/reperfusion injury in mice. *Molecular Neurodegeneration*, *8*(1).

Kipfer-Kauer, A., McKinnon, S. J., Frueh, B. E., & Goldblum, D. (2010). Distribution of amyloid precursor protein and amyloid-β in ocular hypertensive C57BL/6 mouse eyes. *Current Eye Research*, *35*(9), 828–834.

Klein, R., & Klein, B. E. K. (2013). The prevalence of age-related eye diseases and visual impairment in aging: Current estimates. *Investigative Ophthalmology and Visual Science*, *54*(14).

Ko, M. L., Peng, P. H., Ma, M. C., Ritch, R., & Chen, C. F. (2005). Dynamic changes in reactive oxygen species and antioxidant levels in retinas in experimental glaucoma. *Free Radical Biology and Medicine*, *39*(3), 365–373.

Kolb, H., Nelson, R., Ahnelt, P., & Cuenca, N. (2001a). Cellular organization of the vertebrate retina. *Progress in Brain Research*, *131*, 3–26.

Kong, Y. X., Crowston, J. G., Vingrys, A. J., Trounce, I. A., & Bui, B. V. (2009). Functional changes in the retina during and after acute intraocular pressure elevation in mice. *Investigative Ophthalmology and Visual Science*, *50*(12), 5732–5740.

Kong, Y. X. G., van Bergen, N., Bui, B. V., Chrysostomou, V., Vingrys, A. J., Trounce, I. A., & Crowston, J. G. (2012). Impact of aging and diet restriction on retinal function during and after acute intraocular pressure injury. *Neurobiology of Aging*, *33*(6), 1126.e15-1126.e25.

Kuehn, M. H., Fingert, J. H., & Kwon, Y. H. (2005). Retinal ganglion cell death in glaucoma: Mechanisms and neuroprotective strategies. *Ophthalmology Clinics of North America*, *18*(3), 383–395.

Kwong, J. M. K., Caprioli, J., & Piri, N. (2010). RNA binding protein with multiple splicing: A new marker for retinal ganglion cells. *Investigative Ophthalmology and Visual Science*, *51*(2), 1052–1058.

Kwong, J. M. K., Quan, A., Kyung, H., Piri, N., & Caprioli, J. (2011). Quantitative analysis of retinal ganglion cell survival with rbpms immunolabeling in animal models of optic neuropathies. *Investigative Ophthalmology and Visual Science*, *52*(13), 9694–9702.

Langham, M. (2009). *The Morphology and Hydrodynamics of the Chamber Angle Draining the Aqueous Humor, in Ischemia and Loss of Vascular Autoregulation in Ocular and Cerebral Diseases.* Springer New York.

Lavanya, R., Wong, T. Y., Friedman, D. S., Aung, H. T., Alfred, T., Gao, H., Seah, S. K., Kashiwagi, K., Foster, P. J., & Aung, T. (2008). Determinants of angle closure in older Singaporeans. *Archives of Ophthalmology*, *126*(5), 686–691.

Lee, P. Y., Zhao, D., Wong, V. H. Y., Chrysostomou, V., Crowston, J. G., & Bui, B. V. (2022). The Effect of Aging on Retinal Function and Retinal Ganglion Cell Morphology Following Intraocular Pressure Elevation. *Frontiers in Aging Neuroscience*, *14*.

le Meur, G., Lebranchu, P., Billaud, F., Adjali, O., Schmitt, S., Bézieau, S., Péréon, Y., Valabregue, R., Ivan, C., Darmon, C., Moullier, P., Rolling, F., & Weber, M. (2018). Safety and Long-Term Efficacy of AAV4 Gene Therapy in Patients with RPE65 Leber Congenital Amaurosis. *Molecular Therapy*, *26*(1), 256–268.

Leung, C. K. S., Lindsey, J. D., Crowston, J. G., Ju, W. K., Liu, Q., Bartsch, D. U., & Weinreb, R. N. (2008). In vivo imaging of murine retinal ganglion cells. *Journal of Neuroscience Methods*, *168*(2), 475–478.

Leung, C. K. S., Weinreb, R. N., Li, Z. W., Liu, S., Lindsey, J. D., Choi, N., Liu, L., Cheung, C. Y. lui, Ye, C., Qiu, K., Chen, L. J., Yung, W. H., Crowston, J. G., Pu, M., So, K. F., Pang, C. P., & Lam, D. S. C. (2011a). Long-term in vivo imaging and measurement of dendritic shrinkage of retinal ganglion cells. *Investigative Ophthalmology and Visual Science*, *52*(3), 1539–1547.

Leung, C. K. S., Yu, M., Weinreb, R. N., Ye, C., Liu, S., Lai, G., & Lam, D. S. C. (2012). Retinal nerve fiber layer imaging with spectral-domain optical coherence tomography: A prospective analysis of age-related loss. *Ophthalmology*, *119*(4), 731–737.

Levin, L. A., & Kaufman, P. L. (2011). *Adler's physiology of the eye: clinical application* (11th editi). New York: Saunders/Elsevier.

Li, C., Cheng, M., Yang, H., Peachey, N. S., & Naash, M. I. (2001). Age-related changes in the mouse outer retina. *Optometry and Vision Science*, *78*(6), 425–430.

Li, L., Feng, X., Fang, F., Miller, D. A., Zhang, S., Zhuang, P., Huang, H., Liu, P., Liu, J., Sredar, N., Liu, L., Sun, Y., Duan, X., Goldberg, J. L., Zhang, H. F., & Hu, Y. (2022). Longitudinal in vivo Ca2+ imaging reveals dynamic activity changes of diseased retinal ganglion cells at the single-cell level. *Proceedings of the National Academy of Sciences of the United States of America*, *119*(48).

Li, L., & Song, F. (2020). Biomechanical research into lamina cribrosa in glaucoma. *National Science Review*, *7*(8), 1277–1279.

Li, R. S., Chen, B. Y., Tay, D. K., Chan, H. H. L., Pu, M. L., & So, K. F. (2006). Melanopsin-expressing retinal ganglion cells are more injury-resistant in a chronic ocular hypertension model. *Investigative Ophthalmology and Visual Science*, *47*(7), 2951–2958.

Li, A., Zhang, X., Zheng, D., Ge, J., Laties, A. M., & Mitchell, C. H. (2011). Sustained elevation of extracellular ATP in aqueous humor from humans with primary chronic angle-closure glaucoma. *Experimental Eye Research*, *93*(4), 528–533.

Lichter, P. R., Musch, D. C., Gillespie, B. W., Guire, K. E., Janz, N. K., Wren, P. A., & Mills, M. P. H. R. P. (2001). Interim clinical outcomes in the collaborative initial glaucoma treatment study comparing initial treatment randomized to medications or surgery. *Ophthalmology*, *108*(11), 1943–1953.

Lim, J. K. H., Nguyen, C. T. O., He, Z., Vingrys, A. J., & Bui, B. V. (2014). The effect of ageing on ocular blood flow, oxygen tension and retinal function during and after intraocular pressure elevation. *PLoS ONE*, *9*(5).

Liu, Y., McDowell, C. M., Zhang, Z., Tebow, H. E., Wordinger, R. J., & Clark, A. F. (2014). Monitoring retinal morphologic and functional changes in mice following optic nerve crush. *Investigative Ophthalmology and Visual Science*, *55*(6), 3766–3774.

Lois, N., Owens, S. L., Coco, R., Hopkins, J., Fitzke, F. W., & Bird, A. C. (2002). Fundus autofluorescence in patients with age-related macular degeneration and high risk of visual loss. *American Journal of Ophthalmology*, *133*(3), 341–349.

Lu, W., Hu, H., Sévigny, J., Gabelt, B. T., Kaufman, P. L., Johnson, E. C., Morrison, J. C., Zode, G. S., Sheffield, V. C., Zhang, X., Laties, A. M., & Mitchell, C. H. (2015). Rat, Mouse, and Primate Models of Chronic Glaucoma Show Sustained Elevation of Extracellular ATP and Altered Purinergic Signaling in the Posterior Eye. *Investigative Opthalmology & Visual Science*, *56*(5), 3075.

Martin, K. R. G., Klein, R. L., & Quigley, H. A. (2002). Gene delivery to the eye using adeno-associated viral vectors. *Methods*, *28*(2), 267–275.

Masland, R. H. (2001). The fundamental plan of the retina. *Nature Neuroscience*, *4*(9), 877–886.

May, C. A. (2003). The optic nerve head region of the aged rat: An immunohistochemical investigation. *Current Eye Research*, *26*(6), 347–354.

May, C. A. (2008). Comparative Anatomy of the Optic Nerve Head and Inner Retina in Non-Primate Animal Models Used for Glaucoma Research. *The Open Ophthalmology Journal*, *2*(1), 94–101.

McHugh, D., & Gil, J. (2018). Senescence and aging: Causes, consequences, and therapeutic avenues. *Journal of Cell Biology*, *217*(1), 65–77.

McMenamin, P. G., Lee, W. R., & Aitken, D. A. N. (1986). Age-related Changes in the Human Outflow Apparatus. *Ophthalmology*, *93*(2), 194–209.

Mitnitski, A., Song, X., Skoog, I., Broe, G. A., Cox, J. L., Grunfeld, E., & Rockwood, K. (2005). Relative fitness and frailty of elderly men and women in developed countries and their relationship with mortality. *Journal of the American Geriatrics Society*, *53*(12), 2184–2189.

Miyazaki, M., Segawa, K., & Urakawa, Y. (1987). Age-related changes in the trabecular meshwork of the normal human eye. *Japanese Journal of Ophthalmology*, *31*(4), 558–569.

Mizi, A., Zhang, S., & Papantonis, A. (2020). Genome folding and refolding in differentiation and cellular senescence. *Current Opinion in Cell Biology*, *67*, 56–63.

Morgan, J. E., & Tribble, J. R. (2015). Microbead models in glaucoma. *Experimental Eye Research*, *141*, 9–14.

Morrison, J. C. (2006). Integrins in the optic nerve head: Potential roles in glaucomatous optic neuropathy (an American ophthalmological society thesis). *Transactions of the American Ophthalmological Society*, *104*, 453–477.

Morrison, J. C., Cepurna, W. O., & Johnson, E. C. (2015). Modeling glaucoma in rats by sclerosing aqueous outflow pathways to elevate intraocular pressure. *Experimental Eye Research*, *141*, 23–32.

Morrison, J. C., Dorman Pease, M. E., Dunkelberger, G. R., & Quigley, H. A. (1990). Optic Nerve Head Extracellular Matrix in Primary Optic Atrophy and Experimental Glaucoma. *Archives of Ophthalmology*, *108*(7), 1020–1024.

Morrison, J. C., Jerdan, J. A., Dorman, M. E., & Quigley, H. A. (1989). Structural Proteins of the Neonatal and Adult Lamina Cribrosa. *Archives of Ophthalmology*, *107*(8), 1220–1224.

Morrison, J. C., Moore, C. G., Deppmeier, L. M. H., Gold, B. G., Meshul, C. K., & Johnson, E. C. (1997). A rat model of chronic pressure-induced optic nerve damage. *Experimental Eye Research*, *64*(1), 85–96.

Morrison, J., Farrell, S., Johnson, E., Deppmeier, L., Moore, C. G., & Grossmann, E. (1995). Structure and composition of the rodent lamina cribrosa. *Experimental Eye Research*, *60*(2), 127–135.

Müller, L. P. D. S., Shelley, J., & Weiler, R. (2007). Displaced amacrine cells of the mouse retina. *Journal of Comparative Neurology*, *505*(2), 177–189.

Musi, N., Valentine, J. M., Sickora, K. R., Baeuerle, E., Thompson, C. S., Shen, Q., & Orr, M. E. (2018). Tau protein aggregation is associated with cellular senescence in the brain. *Aging Cell*, *17*(6).

Nadal-Nicolás, F. M., Jiménez-López, M., Sobrado-Calvo, P., Nieto-López, L., Cánovas-Martinez, I., Salinas-Navarro, M., Vidal-Sanz, M., & Agudo, M. (2009). Brn3a as a marker of retinal ganglion cells: Qualitative and quantitative time course studies in naïve and optic nerve-injured retinas. *Investigative Ophthalmology and Visual Science*, *50*(8), 3860–3868.

Nickells, R. W. (2012). The cell and molecular biology of glaucoma: Mechanisms of retinal ganglion cell death. *Investigative Ophthalmology and Visual Science*, *53*(5), 2476–2481.

Nickells, R. W., Schmitt, H. M., Maes, M. E., & Schlamp, C. L. (2017). AAV2-mediated transduction of the mouse retina after optic nerve injury. *Investigative Ophthalmology and Visual Science*, *58*(14), 6091–6104.

Nieuwenhuis, B., Laperrousaz, E., Tribble, J. R., Verhaagen, J., Fawcett, J. W., Martin, K. R., Williams, P. A., & Osborne, A. (2023). Improving adeno-associated viral (AAV) vector-mediated transgene expression in retinal ganglion cells: comparison of five promoters. *Gene Therapy*.

Nongpiur, M. E., Ku, J. Y. F., & Aung, T. (2011). Angle closure glaucoma: A mechanistic review. *Current Opinion in Ophthalmology*, *22*(2), 96–101.

Nuschke, A. C., Farrell, S. R., Levesque, J. M., & Chauhan, B. C. (2015). Assessment of retinal ganglion cell damage in glaucomatous optic neuropathy: Axon transport, injury and soma loss. *Experimental Eye Research*, *141*, 111–124.

Oglesby, E., Quigley, H. A., Zack, D. J., Cone, F. E., Steinhart, M. R., Tian, J., Pease, M. E., & Kalesnykas, G. (2012). Semi-automated, quantitative analysis of retinal ganglion cell morphology in mice selectively expressing yellow fluorescent protein. *Experimental Eye Research*, *96*(1), 107–115.

Osborne, A., Khatib, T. Z., Songra, L., Barber, A. C., Hall, K., Kong, G. Y. X., Widdowson, P. S., & Martin, K. R. (2018). Neuroprotection of retinal ganglion cells by a novel gene therapy construct that achieves sustained enhancement of brain-derived neurotrophic factor/tropomyosin-related kinase receptor-B signaling. *Cell Death and Disease*, *9*(10).

Osborne, A., Wang, A. X. Z., Tassoni, A., Widdowson, P. S., & Martin, K. R. (2018). Design of a Novel Gene Therapy Construct to Achieve Sustained Brain-Derived Neurotrophic Factor Signaling in Neurons. *Human Gene Therapy*, *29*(7), 828–841.

Ota, H., Akishita, M., Akiyoshi, T., Kahyo, T., Setou, M., Ogawa, S., Iijima, K., Eto, M., & Ouchi, Y. (2012). Testosterone deficiency accelerates neuronal and vascular aging of samp8 mice: Protective role of enos and sirt1. *PLoS ONE*, *7*(1).

Park, J. C., Persidina, O., Balasubramanian, G., Nguyen, T., Pradeep, A., Hetling, J. R., & McAnany, J. J. (2023). Effects of normal aging on the mouse retina assessed by full-field flash and flicker electroretinography. *Scientific Reports*, *13*(1).

Pease, M. E., McKinnon, S. J., Quigley, H. A., Kerrigan-Baumrind, L. A., & Zack, D. J. (2000). Obstructed axonal transport of BDNF and its receptor TrkB in experimental glaucoma. *Investigative Ophthalmology and Visual Science*, *41*(3), 764–774.

Polinski, N. K., Gombash, S. E., Manfredsson, F. P., Lipton, J. W., Kemp, C. J., Cole-Strauss, A., Kanaan, N. M., Steece-Collier, K., Kuhn, N. C., Wohlgenant, S. L., & Sortwell, C. E. (2015). Recombinant adenoassociated virus 2/5-mediated gene transfer is reduced in the aged rat midbrain. *Neurobiology of Aging*, *36*(2), 1110–1120.

Polinski, N. K., Manfredsson, F. P., Benskey, M. J., Fischer, D. L., Kemp, C. J., Steece-Collier, K., Sandoval, I. M., Paumier, K. L., & Sortwell, C. E. (2016). Impact of age and vector construct on striatal and nigral transgene expression. *Molecular Therapy - Methods and Clinical Development*, *3*, 16082.

Qin, Z., He, S., Yang, C., Yung, J. S.-Y., Chen, C., Leung, C. K.-S., Liu, K., & Qu, J. Y. (2020). Adaptive optics two-photon microscopy enables near-diffraction-limited and functional retinal imaging in vivo. *Light: Science & Applications*, *9*(1).

Quigley, H. A., Flower, R. W., Addicks, E. M., & McLeod, D. S. (1980). The mechanism of optic nerve damage in experimental acute intraocular pressure elevation. *Investigative Ophthalmology and Visual Science*, *19*(5), 505–517.

Quigley, H. A., McKinnon, S. J., Zack, D. J., Pease, M. E., Kerrigan-Baumrind, L. A., Kerrigan, D. F., & Mitchell, R. S. (2000). Retrograde axonal transport of BDNF in retinal ganglion cells is blocked by acute IOP elevation in rats. *Investigative Ophthalmology and Visual Science*, *41*(11), 3460–3466.

Quigley, H., & Broman, A. T. (2006). The number of people with glaucoma worldwide in 2010 and 2020. *British Journal of Ophthalmology*, *90*(3), 262–267.

Quigley, H., & RM, H. (1983). Laser energy levels for trabecular meshwork damage in the primate eye. *Investigative Ophthalmology & Visual Science*, *24*(9), 1305–1307.

Quina, L. A., Pak, W., Lanier, J., Banwait, P., Gratwick, K., Liu, Y., Velasquez, T., O'Leary, D. D. M., Goulding, M., & Turner, E. E. (2005). Brn3a-expressing retinal ganglion cells project specifically to thalamocortical and collicular visual pathways. *Journal of Neuroscience*, *25*(50), 11595–11604.

Risner, M. L., Pasini, S., Cooper, M. L., Lambert, W. S., & Calkins, D. J. (2018). Axogenic mechanism enhances retinal ganglion cell excitability during early progression in glaucoma. *Proceedings of the National Academy of Sciences of the United States of America*, *115*(10), E2393–E2402.

Rocha, L. R., Nguyen Huu, V. A., Palomino La Torre, C., Xu, Q., Jabari, M., Krawczyk, M., Weinreb, R. N., & Skowronska-Krawczyk, D. (2020). Early removal of senescent cells protects retinal ganglion cells loss in experimental ocular hypertension. *Aging Cell*, *19*(2).

Rockwood, K., Awalt, E., Carver, D., & MacKnight, C. (2000). Feasibility and measurement properties of the Functional Reach and the Timed Up and Go tests in the Canadian Study of Health and Aging. *Journals of Gerontology - Series A Biological Sciences and Medical Sciences*, *55*(2).

Rockwood, K., Blodgett, J. M., Theou, O., Sun, M. H., Feridooni, H. A., Mitnitski, A., Rose, R. A., Godin, J., Gregson, E., & Howlett, S. E. (2017). A Frailty Index Based on Deficit Accumulation Quantifies Mortality Risk in Humans and in Mice. *Scientific Reports*, *7*.

Rockwood, K., & Mitnitski, A. (2007). Frailty in relation to the accumulation of deficits. *Journals of Gerontology - Series A Biological Sciences and Medical Sciences*, *62*(7), 722–727.

Rodrigues-Neves, A. C., Aires, I. D., Vindeirinho, J., Boia, R., Madeira, M. H., Gonçalves, F. Q., Cunha, R. A., Santos, P. F., Ambrósio, A. F., & Santiago, A. R. (2018). Elevated Pressure Changes the Purinergic System of Microglial Cells. *Frontiers in Pharmacology*, *9*.

Rodriguez, A. R., de Sevilla Müller, L. P., & Brecha, N. C. (2014). The RNA binding protein RBPMS is a selective marker of ganglion cells in the mammalian retina. *Journal of Comparative Neurology*, *522*(6), 1411–1443.

Romano, G. L., Amato, R., Lazzara, F., Porciatti, V., Chou, T.-H., Drago, F., & Bucolo, C. (2020). P2X7 receptor antagonism preserves retinal ganglion cells in glaucomatous mice. *Biochemical Pharmacology*, *180*, 114199.

Russell, S., Bennett, J., Wellman, J. A., Chung, D. C., Yu, Z.-F., Tillman, A., Wittes, J., Pappas, J., Elci, O., McCague, S., Cross, D., Marshall, K. A., Walshire, J., Kehoe, T. L., Reichert, H., Davis, M., Raffini, L., George, L. A., Hudson, F. P., … Maguire, A. M. (2017). Efficacy and safety of voretigene neparvovec (AAV2-hRPE65v2) in patients with RPE65 -mediated inherited retinal dystrophy: a randomised, controlled, open-label, phase 3 trial. *The Lancet*, *390*(10097), 849–860.

Sakai, H., Morine-Shinjyo, S., Shinzato, M., Nakamura, Y., Sakai, M., & Sawaguchi, S. (2005). Uveal effusion in primary angle-closure glaucoma. *Ophthalmology*, *112*(3), 413–419.

Sakamoto, K., Endo, K., Suzuki, T., Fujimura, K., Kurauchi, Y., Mori, A., Nakahara, T., & Ishii, K. (2015). P2X7 receptor antagonists protect against N-methyl-d-aspartic acid-induced neuronal injury in the rat retina. *European Journal of Pharmacology*, *756*, 52–58.

Salinas-Navarro, M., Jiménez-López, M., Valiente-Soriano, F. J., Alarcón-Martínez, L., Avilés-Trigueros, M., Mayor, S., Holmes, T., Lund, R. D., Villegas-Pérez, M. P., & Vidal-Sanz, M. (2009). Retinal ganglion cell population in adult albino and pigmented mice: A computerized analysis of the entire population and its spatial distribution. *Vision Research*, *49*(6), 637–647.

Salminen, A., Ojala, J., Kaarniranta, K., Haapasalo, A., Hiltunen, M., & Soininen, H. (2011). Astrocytes in the aging brain express characteristics of senescence-associated secretory phenotype. *European Journal of Neuroscience*, *34*(1), 3–11.

Samsel, P. A., Kisiswa, L., Erichsen, J. T., Cross, S. D., & Morgan, J. E. (2011). A novel method for the induction of experimental glaucoma using magnetic microspheres. *Investigative Ophthalmology and Visual Science*, *52*(3), 1671–1675.

Samuel, M. A., Zhang, Y., Meister, M., & Sanes, J. R. (2011). Age-related alterations in neurons of the mouse retina. *Journal of Neuroscience*, *31*(44), 16033–16044.

Sánchez-Farías, N., & Candal, E. (2015). Doublecortin is widely expressed in the developing and adult retina of sharks. *Experimental Eye Research*, *134*, 90–100.

Sánchez-Migallón, M. C., Valiente-Soriano, F. J., Nadal-Nicolás, F. M., Di Pierdomenico, J., Vidal-Sanz, M., & Agudo-Barriuso, M. (2018). Survival of melanopsin expressing

retinal ganglion cells long term after optic nerve trauma in mice. *Experimental Eye Research*, *174*, 93–97.

Sanes, J. R., & Zipursky, S. L. (2010). Design Principles of Insect and Vertebrate Visual Systems. *Neuron*, *66*(1), 15–36.

Sappington, R. M., Carlson, B. J., Crish, S. D., & Calkins, D. J. (2010). The microbead occlusion model: A paradigm for induced ocular hypertension in rats and mice. *Investigative Ophthalmology and Visual Science*, *51*(1), 207–216.

Savinova, O. V., Sugiyama, F., Martin, J. E., Tomarev, S. I., Paigen, B. J., Smith, R. S., & John, S. W. M. (2001). Intraocular pressure in genetically distinct mice: An update and strain survey. *BMC Genetics*, *2*.

Schaub, J. A., Kimball, E. C., Steinhart, M. R., Nguyen, C., Pease, M. E., Oglesby, E. N., Jefferys, J. L., & Quigley, H. A. (2017). Regional retinal ganglion cell axon loss in a Murine glaucoma model. *Investigative Ophthalmology and Visual Science*, *58*(5), 2765–2773.

Schlamp, C. L., Li, Y., Dietz, J. A., Janssen, K. T., & Nickells, R. W. (2006a). Progressive ganglion cell loss and optic nerve degeneration in DBA/2J mice is variable and asymmetric. *BMC Neuroscience*, *7*.

Schneider, C. A., Rasband, W. S., & Eliceiri, K. W. (2012). NIH Image to ImageJ: 25 years of image analysis. *Nature Methods*, *9*(7), 671–675.

Scholz, M., Buder, T., Seeber, S., Adamek, E., Becker, C. M., & Lütjen-Drecoll, E. (2008). Dependency of intraocular pressure elevation and glaucomatous changes in DBA/2J and DBA/2J-Rj Mice. *Investigative Ophthalmology and Visual Science*, *49*(2), 613–621.

Schuettauf, F., Quinto, K., Naskar, R., & Zurakowski, D. (2002). Effects of anti-glaucoma medications on gangion cell survival: The DBA/2J mouse model. *Vision Research*, *42*(20), 2333–2337.

Schuettauf, F., Rejdak, R., Walski, M., Frontczak-Baniewicz, M., Voelker, M., Blatsios, G., Shinoda, K., Zagorski, Z., Zrenner, E., & Grieb, P. (2004). Retinal neurodegeneration

in the DBA/2J mouse - A model for ocular hypertension. *Acta Neuropathologica*, *107*(4), 352–358.

Schuman, J. S. (2008). Spectral domain optical coherence tomography for glaucoma (an AOS thesis). *Transactions of the American Ophthalmological Society*, *106*, 426–458.

Seitz, R., Ohlmann, A., & Tamm, E. R. (2013). The role of Müller glia and microglia in glaucoma. *Cell and Tissue Research*, *353*(2), 339–345.

Seki, M., & Lipton, S. A. (2008). Targeting excitotoxic/free radical signaling pathways for therapeutic intervention in glaucoma. *Progress in Brain Research*, *173*, 495–510.

Sharma, R., Yin, L., Geng, Y., Merigan, W. H., Palczewska, G., Palczewski, K., Williams, D. R., & Hunter, J. J. (2013). In vivo two-photon imaging of the mouse retina. *Biomedical Optics Express*, *4*(8), 1285.

Si, Z., Sun, L., & Wang, X. (2021). Evidence and perspectives of cell senescence in neurodegenerative diseases. *Biomedicine and Pharmacotherapy*, *137*.

Sieving, P. A. (1991). Retinal ganglion cell loss does not abolish the scotopic threshold response (STR) of the cat and human ERG. *Clinical Vision Sciences*, *6*(2), 149–158.

Skowronska-Krawczyk, D., Zhao, L., Zhu, J., Weinreb, R. N., Cao, G., Luo, J., Flagg, K., Patel, S., Wen, C., Krupa, M., Luo, H., Ouyang, H., Lin, D., Wang, W., Li, G., Xu, Y., Li, O., Chung, C., Yeh, E., … Zh, K. (2015). P16INK4a Upregulation Mediated by SIX6 Defines Retinal Ganglion Cell Pathogenesis in Glaucoma. *Molecular Cell*, *59*(6), 931–940.

Smith, B. J., Wang, X., Chauhan, B. C., Côté, P. D., & Tremblay, F. (2014). Contribution of retinal ganglion cells to the mouse electroretinogram. *Documenta Ophthalmologica*, *128*(3), 155–168.

Smith, C. A., & Chauhan, B. C. (2015). Imaging retinal ganglion cells: Enabling experimental technology for clinical application. *Progress in Retinal and Eye Research*, *44*, 1–14.

Smith, C. A., & Chauhan, B. C. (2018). In vivo imaging of adeno-associated viral vector labelled retinal ganglion cells. *Scientific Reports*, *8*(1).

Spry, P. G. D., & Johnson, C. A. (2001). Senescent changes of the normal visual field: An age-old problem. *Optometry and Vision Science*, *78*(6), 436–441.

Stowell, C., Arbogast, B., Cioffi, G., Burgoyne, C., & Zhou, A. (2011). Retinal proteomic changes following unilateral optic nerve transection and early experimental glaucoma in non-human primate eyes. *Experimental Eye Research*, *93*(1), 13–28.

Sun, M., McDonald, S. J., Brady, R. D., Collins-Praino, L., Yamakawa, G. R., Monif, M., O'Brien, T. J., Cloud, G. C., Sobey, C. G., Mychasiuk, R., Loane, D. J., & Shultz, S. R. (2020). The need to incorporate aged animals into the preclinical modeling of neurological conditions. *Neuroscience and Biobehavioral Reviews*, *109*, 114–128.

Takano, Y., Shi, D., Shimizu, A., Funayama, T., Mashima, Y., Yasuda, N., Fukuchi, T., Abe, H., Ideta, H., Zheng, X., Shiraishi, A., Ohashi, Y., Nishida, K., Nakazawa, T., & Fuse, N. (2012). Association of Toll-like Receptor 4 Gene Polymorphisms in Japanese Subjects With Primary Open-Angle, Normal-Tension, and Exfoliation Glaucoma. *American Journal of Ophthalmology*, *154*(5), 825-832.e1.

Taylor, D. L., Jones, F., Chen Seho Kubota, E. S. F., & Pocock, J. M. (2005). Stimulation of microglial metabotropic glutamate receptor mGlu2 triggers tumor necrosis factor α-induced neurotoxicity in concert with microglial-derived Fas ligand. *Journal of Neuroscience*, *25*(11), 2952–2964.

Tezel, G., Chauhan, B. C., LeBlanc, R. P., & Wax, M. B. (2003). Immunohistochemical assessment of the glial mitogen-activated protein kinase activation in glaucoma. *Investigative Ophthalmology and Visual Science*, *44*(7), 3025–3033.

Tezel, G., Li, L. Y., Patil, R. V., & Wax, M. B. (2001). TNF-α and TNF-α receptor-1 in the retina of normal and glaucomatous eyes. *Investigative Ophthalmology and Visual Science*, *42*(8), 1787–1794.

Tezel, G., & Wax, M. B. (2000). Increased production of tumor necrosis factor-α by glial cells exposed to simulated ischemia or elevated hydrostatic pressure induces apoptosis in cocultured retinal ganglion cells. *Journal of Neuroscience*, *20*(23), 8693–8700.

Tezel, G., & Yang, X. (2004). Caspase-independent component of retinal ganglion cell death, in vitro. *Investigative Ophthalmology and Visual Science*, *45*(11), 4049–4059.

Tezel, G., Yang, X., & Cai, J. (2005). Proteomic identification of oxidatively modified retinal proteins in a chronic pressure-induced rat model of glaucoma. *Investigative Ophthalmology and Visual Science*, *46*(9), 3177–3187.

Tham, Y. C., Li, X., Wong, T. Y., Quigley, H. A., Aung, T., & Cheng, C. Y. (2014). Global prevalence of glaucoma and projections of glaucoma burden through 2040: A systematic review and meta-analysis. *Ophthalmology*, *121*(11), 2081–2090.

Turner, A. J., Vander Wall, R., Gupta, V., Klistorner, A., & Graham, S. L. (2017). DBA/2J mouse model for experimental glaucoma: pitfalls and problems. *Clinical and Experimental Ophthalmology*, *45*(9), 911–922.

Urcola, J. H., Hernández, M., & Vecino, E. (2006). Three experimental glaucoma models in rats: Comparison of the effects of intraocular pressure elevation on retinal ganglion cell size and death. *Experimental Eye Research*, *83*(2), 429–437.

Valiente-Soriano, F. J., Salinas-Navarro, M., Jiménez-López, M., Alarcón-Martínez, L., Ortín-Martínez, A., Bernal-Garro, J. M., Avilés-Trigueros, M., Agudo-Barriuso, M., Villegas-Pérez, M. P., & Vidal-Sanz, M. (2015). Effects of ocular hypertension in the visual system of pigmented mice. *PLoS ONE*, *10*(3).

Van Deursen, J. M. (2014). The role of senescent cells in ageing. *Nature*, *509*(7501), 439–446.

Vannas, S., & Teir, H. (1960). OBSERVATIONS ON STRUCTURES AND AGE CHANGES IN THE HUMAN SCLERA. *Acta Ophthalmologica*, *38*(3), 268–279.

Vaupel, J. W., Manton, K. G., & Stallard, E. (1979). The impact of heterogeneity in individual frailty on the dynamics of mortality. *Demography*, *16*(3), 439–454.

Vianna, J. R., Danthurebandara, V. M., Sharpe, G. P., Hutchison, D. M., Belliveau, A. C., Shuba, L. M., Nicolela, M. T., & Chauhan, B. C. (2015). Importance of normal aging in estimating the rate of glaucomatous neuroretinal rim and retinal nerve fiber layer loss. *Ophthalmology*, *122*(12), 2392–2398.

Vidal-Sanz, M., Galindo-Romero, C., Valiente-Soriano, F. J., Nadal-Nicolás, F. M., Ortin-Martinez, A., Rovere, G., Salinas-Navarro, M., Lucas-Ruiz, F., Sanchez-Migallon, M. C., Sobrado-Calvo, P., Aviles-Trigueros, M., Villegas-Pérez, M. P., & Agudo-Barriuso, M. (2017). Shared and differential retinal responses against optic nerve injury and ocular hypertension. *Frontiers in Neuroscience*, *11*(APR).

Vidal-Sanz, M., Salinas-Navarro, M., Nadal-Nicolás, F. M., Alarcón-Martínez, L., Valiente-Soriano, F. J., Miralles de Imperial, J., Avilés-Trigueros, M., Agudo-Barriuso, M., & Villegas-Pérez, M. P. (2012). Understanding glaucomatous damage: Anatomical and functional data from ocular hypertensive rodent retinas. *Progress in Retinal and Eye Research*, *31*(1), 1–27.

Wang, J., Struebing, F. L., & Geisert, E. E. (2021). Commonalities of optic nerve injury and glaucoma-induced neurodegeneration: Insights from transcriptome-wide studies. *Experimental Eye Research*, *207*.

Wang, S. W., Mu, X., Bowers, W. J., Kim, D. S., Plas, D. J., Crair, M. C., Federoff, H. J., Gan, L., & Klein, W. H. (2002). Brn3b/Brn3c double knockout mice reveal an unsuspected role for Brn3c in retinal ganglion cell axon outgrowth. *Development*, *129*(2), 467–477.

Wang, X., Archibald, M. L., Stevens, K., Baldridge, W. H., & Chauhan, B. C. (2010). Cyan fluorescent protein (CFP) expressing cells in the retina of Thy1-CFP transgenic mice before and after optic nerve injury. *Neuroscience Letters*, *468*(2), 110–114.

Webb, R. H., Hughes, G. W., & Delori, F. C. (1987). Confocal scanning laser ophthalmoscope. *Applied Optics*, *26*(8), 1492.

Weber, A. J., Kaufman, P. L., & Hubbard, W. C. (1998). Morphology of single ganglion cells in the glaucomatous primate retina. *Investigative Ophthalmology and Visual Science*, *39*(12), 2304–2320.

Wei, X., Yu, Z., Cho, K. S., Chen, H., Malik, M. T. A., Chen, X., Lo, E. H., Wang, X., & Chen, D. F. (2011). Neuroglobin is an endogenous neuroprotectant for retinal ganglion cells against glaucomatous damage. *American Journal of Pathology*, *179*(6), 2788–2797.

Weinreb, R. N., Aung, T., & Medeiros, F. A. (2014). The pathophysiology and treatment of glaucoma: A review. *Jama*, *311*(18), 1901–1911.

Weinreb, R. N., & Tee Khaw, P. (2004a). Primary open-angle glaucoma. *Lancet*, *363*(9422), 1711–1720.

Weitz, A. C., Behrend, M. R., Lee, N. S., Klein, R. L., Chiodo, V. A., Hauswirth, W. W., Humayun, M. S., Weiland, J. D., & Chow, R. H. (2013). Imaging the response of the retina to electrical stimulation with genetically encoded calcium indicators. *Journal of Neurophysiology*, *109*(7), 1979–1988.

Williams, G. A., & Jacobs, G. H. (2007). Cone-based vision in the aging mouse. *Vision Research*, *47*(15), 2037–2046.

Winkler, B. S., Boulton, M. E., Gottsch, J. D., & Sternberg, P. (1999). Oxidative damage and age-related macular degeneration. *Molecular Vision*, *5*, 32.

Wojtkowski, M., Srinivasan, V., Fujimoto, J. G., Ko, T., Schuman, J. S., Kowalczyk, A., & Duker, J. S. (2005). Three-dimensional retinal imaging with high-speed ultrahigh-resolution optical coherence tomography. *Ophthalmology*, *112*(10), 1734–1746.

Wolf, D. E. (2013). Fundamentals of fluorescence and fluorescence microscopy. *Methods in Cell Biology*, *114*, 69–97.

Wong, T. T., Wong, T. Y., Foster, P. J., Crowston, J. G., Fong, C. W., & Aung, T. (2009). The relationship of intraocular pressure with age, systolic blood pressure, and central corneal thickness in an Asian population. *Investigative Ophthalmology and Visual Science*, *50*(9), 4097–4102.

Wu, K., Meyers, C. A., Guerra, N. K., King, M. A., & Meyer, E. M. (2004). The effects of rAAV2-mediated NGF gene delivery in adult and aged rats. *Molecular Therapy*, *9*(2), 262–269.

Xiao, X., Li, J., & Samulski, R. J. (1996). Efficient long-term gene transfer into muscle tissue of immunocompetent mice by adeno-associated virus vector. *Journal of Virology*, *70*(11), 8098–8108.

Yang, Z., Quigley, H. A., Pease, M. E., Yang, Y., Qian, J., Valenta, D., & Zack, D. J. (2007). Changes in gene expression in experimental glaucoma and optic nerve transection: The equilibrium between protective and detrimental mechanisms. *Investigative Ophthalmology and Visual Science*, *48*(12), 5539–5548.

Ye, L., Haroon, M. A., Salinas, A., & Paukert, M. (2017). Comparison of GCaMP3 and GCaMP6f for studying astrocyte Ca2+ dynamics in the awake mouse brain. *PLoS ONE*, *12*(7).

Yerramothu, P., Vijay, A. K., & Willcox, M. D. P. (2018). Inflammasomes, the eye and anti-inflammasome therapy. *Eye*, *32*(3), 491–505.

Yin, L., Masella, B., Dalkara, D., Zhang, J., Flannery, J. G., Schaffer, D. V., Williams, D. R., & Merigan, W. H. (2014). Imaging light responses of foveal ganglion cells in the living macaque eye. *Journal of Neuroscience*, *34*(19), 6596–6605.

Yu, H. M., Zhao, Y. M., Luo, X. G., Feng, Y., Ren, Y., Shang, H., He, Z. Y., Luo, X. M., Chen, S. Di, & Wang, X. Y. (2012). Repeated lipopolysaccharide stimulation induces cellular senescence in BV2 cells. *NeuroImmunoModulation*, *19*(2), 131–136.

Yuan, L., & Neufeld, A. H. (2000). Tumor necrosis factor-α: A potentially neurodestructive cytokine produced by glia in the human glaucomatous optic nerve head. *Glia*, *32*(1), 42–50.

Zhang, Y., Rózsa, M., Liang, Y., Bushey, D., Wei, Z., Zheng, J., Reep, D., Broussard, G. J., Tsang, A., Tsegaye, G., Narayan, S., Obara, C. J., Lim, J. X., Patel, R., Zhang, R., Ahrens, M. B., Turner, G. C., Wang, S. S. H., Korff, W. L., … Looger, L. L. (2023). Fast and sensitive GCaMP calcium indicators for imaging neural populations. *Nature*, *615*(7954), 884–891.

Zincarelli, C., Soltys, S., Rengo, G., & Rabinowitz, J. E. (2008). Analysis of AAV serotypes 1-9 mediated gene expression and tropism in mice after systemic injection. *Molecular Therapy*, *16*(6), 1073–1080.